POLITECNICO DI TORINO

Master of Science in Energy and Nuclear Engineering

Master's Degree Thesis

Silicon carbide paste development for the extrusion based 3D printing of a heat exchanger employed in concentrated solar power applications

Supervisors:
Prof. Monica Ferraris
Prof. Dr.-Ing. Dietmar Koch
Prof. Dr.-Ing. Suelen Barg

Candidate:
Gabriele Londero

Scientific Assistant:
Michéle Scholl

Academic Year 2021–2022

Acknowledgements

This thesis was supported by Politecnico di Torino and University of Augsburg (Germany, EU) at the chair of Material Resource Management. I wish to thank Michéle Scholl for the scientific counseling and all the general help she gave me during the whole research period.

Abstract

The next-generation concentrated solar power (CSP) applications consider the use of heat exchangers characterised by outstanding corrosion and oxidation resistances. These chemical and physical features are essential when using molten salts and supercritical CO_2 as heat transfer fluids into a Brayton power cycle. To improve the heat exchange, the contact surface in between the working fluids have to be enhanced, implying the utilization of a more complex geometry. Due to common production technology limits, the Additive Manufacturing (AM) via Direct Ink Writing (DIW) has been considered as an alternative. In this context the control of rheological properties of the produced inks represents a crucial step for the printing. A suitable material able to build a heat exchanger for CSP applications is SiC. In this thesis the formulation of an innovative hydrogel based SiC ink has been developed, considering a greater solid amount than the usual receipts present in similar recent studies. The rheological properties of various ink formulations have been studied in terms of printability and possible improvements. The key rheological parameters were identified and linked to the printability aspects. Different production technologies have been compared to understand the best ink production. To perform the rheological studies four algorithms were developed. Temperature Ramp algorithm allowed to understand the thermal reversible behaviour of the hydrogel. Shear Rate algorithm showed the correlation in between the shear rate of the screw used to print and the viscosity of the paste. Shear Stress and Frequency Sweep algorithm were implemented as further studies useful to understand the behaviour of the ink when subjected to a change in shear stress and frequency acted by the printing device. The pritability characteristics have been tested in a 3D printer, demonstrating the possibility of printing a ceramic structure in a complex geometry. To print with DIW an off-the-shelf printer for polymer filaments has been used. The printer was modified to be able to print pastes, implying some structural changes as well as programming manipulations. Scanning electron microscope has been used to analyse the microstructure and see the material distribution.

Contents

List of Figures

List of Tables

INTRODUCTION

Heat exchangers are fundamental for the operation of a Concentrated Solar Power (CSP) plant in order to allow an efficient operation and power production. A general Brayton cycle is used as scheme for the CSP power conversion using supercritical Carbon Dioxide (sCO_2) as working fluid. The heat is conducted through the heat exchanger by the molten salts, which are the main heat transfer fluid used for the CSP applications, working in between the operating temperature of the solar collectors (700°C) and the power block working fluid (sCO_2) temperature [1]. The heat exchangers used nowadays imply the use of metal alloys able to withstand high temperatures [2]. However, metals undergo corrosion and oxidation due to the contact with molten salts. The sCO_2 needs high pressures that involves high stresses on the structures and high temperatures that cause the material degradation. A key point for the development of the next generation CSP plants is the development of new heat exchanger structures, able to be reliable at high temperatures [1, 3, 4]. The heat exchanger effectiveness affects the cycle efficiency of the sCO_2. Some still existing technology limitations such as large working space, high manufacturing expenditures, leakage and reliability affect the final performances of the designed structures. In this context, the utilization of 3D printing technologies plays a fundamental role, allowing the printing of more complex geometries and decreasing the manufacturing costs. The use of geometrically complex structures allows to abate technological limits that affects the limiting efficiencies of nowadays technologies [5].

To solve the material problem related to the degradation of the materials, high temperatures involved and high pressures due to the working fluids, advanced ceramics have emerged to be the best alternative. Silicon Carbide (SiC) represents one of the materials mostly used in the engineering field, such as aerospace, nuclear, energy and electronics [1, 3, 6]. The wide range of usabilty of SiC comes from its outstanding attributes, thermophysical properties, resistance to wear and lightweight. As a consequence, SiC ceramics are the most suitable for heat exchanger construction [3]. The SiC utilization in many different fields is because of its extraordinary mechanical, thermal and chemical properties, making it one of the most attractive for industry and energy applications. High temperature applications are the most suitable for its utilization [7].

SiC structures are commonly produced by powder agglomeration techniques and their manufacturing process through innovative techniques is of fundamental importance for many applications [8]. Binder jetting (Chapter 2) represents one the most used 3D printing technology used to print with ceramics due to its easy utilization and scalability, presenting however the drawback of high expenditures [7]. The most challenging development of the 3D printing with SiC is represented by its use in robocasting, also called Direct Ink Writing (DIW). Robocasting represents a possibility for the implementation of ceramic paste and their direct extrusion through a nozzle. The DIW utilization has been achieved directly to take advantage of the colloidal processing of ceramics [8]. For the printing, a ceramic filament is extruded through the nozzle and it is deposited on the printing bed, creating a layer by layer structure after which the final 3D geometry takes form [9].

Moreover, the use of Additive Manufacturing (AM), such as a ceramic printed via a paste produced previously, allows to abate obstacles such as impossibility in reaching complex geometries due to technological limitations. In this meaning, an optimal ink formulation is fundamental to avoid premature ink drying during the production procedure. The rheological properties should be sufficient to let the ink flowing through the printer nozzle and allow the subsequent deposition, avoiding presence of imperfections after the deposition process [7]. The general deposition process starts with the extrusion of a large amount of material to build the first layer. The first stage represents a crucial

process since all the consequent layers must stay attached one to the other to print the final structure, avoiding presence of structural break. Moreover, a larger first layer allows to increase the structural mechanical stability [9].

A porous structure is one of the main drawbacks of a ceramic printed structure for energy applications due to the poor thermal and physical properties [10]. Considering the ink formulation, a greater solid fraction gives the possibility to obtain a stronger structure filling all the empty spaces. In this consideration the increase in the solid content is followed by a challenging production process due to an increase in viscosity.

DIW can help in improving the final heat exchange efficiency by considering different printable geometries. Ceramic structures made with current manufacturing technologies cannot implement complex architectures due to the nonexistent elastic behaviour and hard machining attitude. As a consequence, the manufacturing production of ceramics produces simple structures that cannot be implemented in heat exchangers for CSP applications. Metal pipes and special metal alloys are used as a substitution, presenting the already mentioned issues. By using robocasting, every geometry can be printed. The no limit in shape architecture can allow the achievement of greater efficiencies in the heat exchange between the working fluids by adopting an innovative structure.

In this thesis, various ink formulations involving SiC were considered. The rheological behaviour of each were tested and compared in order to find the best alternative that allows a DIW process. By considering the best ink alternatives, printing tries were done in order to testify the printing process. The final aim to print an innovative heat exchanger structure has been followed.

STATE OF THE ART

The current state of technology and constant greater demand in innovation requires an even greater advance in materials. Considering the energy field, certain advances can be achieved only through the study of new materials and ways to produce them. Among all the others, ceramics represent one of the most suitable for the energy components improvement concerning thermodynamic applications.

The ceramics as material class are known from the ancient times but they still represent a fascinating area of study. One of the most advanced and young material belonging to this advanced class is SiC due to its extraordinary properties.

SiC is corrosion and chemical erosion resistant, as well as stable above very high temperatures. It implies that it is seriously useful as a substitution of the common heat exchanger components, enlarging the temperature range application and the fluids selection [11]. The temperature limitations deal with the decomposition temperature of the SiC stated at 2500°C. It has been recently reported by Somiya et al. that the SiC decomposition starts at 2000°C, therefore working below the limit temperature allows to work risk free [11, 12]. As a direct consequence, SiC represents the best choice for applications implying severe environments such as: rockets, jet engines, depositions and components inside gas turbines, space vehicles heat shields and fusion reactor walls [11].

AM branches out in binder jetting, direct energy deposition, material extrusion, materials jetting and many others [13]. This improvement can overcome some actual restrictions that characterise binder jetting, which is the 3D printing technology commonly used to print ceramics [14]. Binder jetting uses a liquid binding agent that is selectively deposited on a bed layer of powder in order to joint the powder particles. It has the ability to print large objects made with a wide variety of materials, from metals to ceramics, to polymers or hybrid. However, it presents material waste and huge costs related to the expenditures for machineries and material used [13]. A well-known technology thoroughly studied and developed is the ink deposition through a robotic assisted procedure, called Robocasting. This technique is achieved by controlling the rheological properties of the inks produced, while the printing is based on a continuous ink deposition. For this reason the rheological properties of the inks have to be deeply investigated [15]. One of the main difficulties in robocasting is that an aqueous ceramic paste or a solvent with a low organic content has to be used, with fine rheological properties that have to allow the controlled flow during the extrusion process, enabling shape retention and avoiding crack formation [9]. Considering the common production technologies like extrusion, slip casting and tape casting, the main limit is related to the shape production. Depending on the production technology only certain shapes can be obtained. By considering the ceramic field, the paste preparation and consequent sintering allows the shaping through extrusion before reaching the green structure. Ceramics are fragile, therefore a handling after the sintering process is not possible. A possibility to overcome this limit comes from 3D printing, since by the use of a paste and the use of robotic assisted design, any possible shape can be produced. 3D printing take the name of AM, which implies the printing through addition of material. For sake of research for AM of ceramics, SiC represents one of the the primary material of application for the preparation of a paste able to print structures for the high temperature energy field trough a 3D printer. This procedure would give an alternative to the current technology limits that imply a relevant material waste. Therefore, this paper gives a possibility to a 3D printer using an extrusion head in a robotic assisted procedure, allowing the printing of complex geometries using a machine commercially available and cheaper than the other printing technologies.

A crucial step for the ceramic ink preparation is represented by the maximization of the solid content in order to obtain a high density and avoid crack formation. However, by increasing the solid content, some rheological parameters called storage modulus and yield stress increase. The yield stress represents a shear stress that implies the change in behaviour between solid and liquid state. The storage modulus is the ability to absorb energy while being loaded by a stress. This change in the two moduli could prevent paste extrusion and yield poor strut merging in the case of monolithic parts, implying an almost impossible printability [16].

Densification through sintering and infiltration allows to increase thermal and mechanical properties [1]. Some techniques have been proven to reduce porosity in the green body SiC ceramics including liquid silicon infiltration, sintering and utilization of a mixed powder [17, 18, 19, 20, 21, 22, 23].

Liquid Silicon Infiltration (LSI) is a fast and low cost manufacturing process that uses carbon (C) and SiC composites. It is divided into three main steps: the formation of a ceramic or carbon fiber reinforced polymer and fibers, the pyrolisis of the polymer chains to obtain only carbon and subsequent densification by liquid silicon infiltration done at 1650°C [24].

By considering the AM as main producing technology, the materials used has to be in powder form. This allows the production of a paste to be used in robocasting or the layer deposition for the binder jetting [13].
Considering the utilization of mixed material powders, depending on their chemistry the possibility to create new bonding allows to create stronger structures. Moreover, by using different dimensions of the grains, the voids left into a structures can be filled by the smaller particles, obtaining a greater density. It is therefore a chemical and physical process.

Commonly the liquid infiltration is preferred since it is easier to be processed compared to the other techniques, such as Polymer Integration and Pyrolisis, Chemical Vapour Infiltration or Reactive Melt Infiltration. As a consequence, liquid silicon can represent the best used material for liquid infiltration. Moreover, it involves lower operating temperatures and shorter times than the other technologies, being definitely the best alternative for densification involving AM, decreasing the overall working times and reducing the costs [10]. Moreover LSI is not largely used in AM therefore its development has still to come. Mechanical properties of this densification are reported by Cramer et al. [7]. As an additional possible advantage, since the structure is produced by an organic binder and SiC, after the pyrolisis process the organic part vaporizes and the carbon molecules at high temperature may interact with Silicon (Si) infiltrated producing new SiC inside the structure already formed. For this happening it is crucial to have an inert atmosphere or vacuum to avoid presence of other chemicals that may interact with the final structure. The pyrolisis avoids the presence of oxygen, therefore the C molecules do not burn.

One evidence of the structural densification usefulness comes from the geothermal field. Energy piles have been largely used in the energy field, especially in geothermal applications where they have been strongly adopted into many Europeans buildings. Several studies have been conducted to improve their energy exchange efficiency and optimization of the design, using material mixtures and comparing their characteristics. A comparison among energy piles made of graphite concrete and SiC concrete has been made. It has been discovered that with addition of graphite over 15vol.% the heat exchange coefficient increased, lowering however the compressive strength. By increasing the SiC content the thermal conductivity increased, increasing also the compressive strength [25]. Similarly to the concrete piles, a heat exchanger made of SiC represents best alternative for enhancing thermal properties. Moreover, since the porosity might be a problem after the drying process, additional silicon infiltration may fill these pores improving therefore the thermal conductivity.

There are different utilizations of SiC into the energy field, and considering the applications that come from the 3D printing they represent a huge fraction which is open to innovation and development. From the geothermal field to the exhaust fumes after-treatment and cathalization, from the nuclear fusion reactor design and heat exchanger main components, SiC finds its main utilizations. The design and study of how to print several technologies through 3D printing is therefore crucial for the development of new technologies, implying easier manufacturing and more complex geometries.

The application of a SiC ceramic as a heat exchanger infiltrated with liquid silicon may represent also the possibility to be used as a exhaust gas after treatment at the engine outlet. A honeycomb structure is generally used to increase the contact surface to enhance heat exchange and particles trapping. The complex geometry is hard to obtain with common industrial technologies, but it can be obtained easily with a 3D printer, allowing to preserve chemical characteristic of the SiC contained without requiring material combinations or substitutions. As a heat exchanger the system serves also as a second heat source for the refrigerant fluid of the filter, taking heat from the exhaust gases and warming up the second fluid [4]. A general honeycomb like heat exchanger structure is reported into the paper proposed by Fend et al. and it is represented into the Figure 2.1 [4].

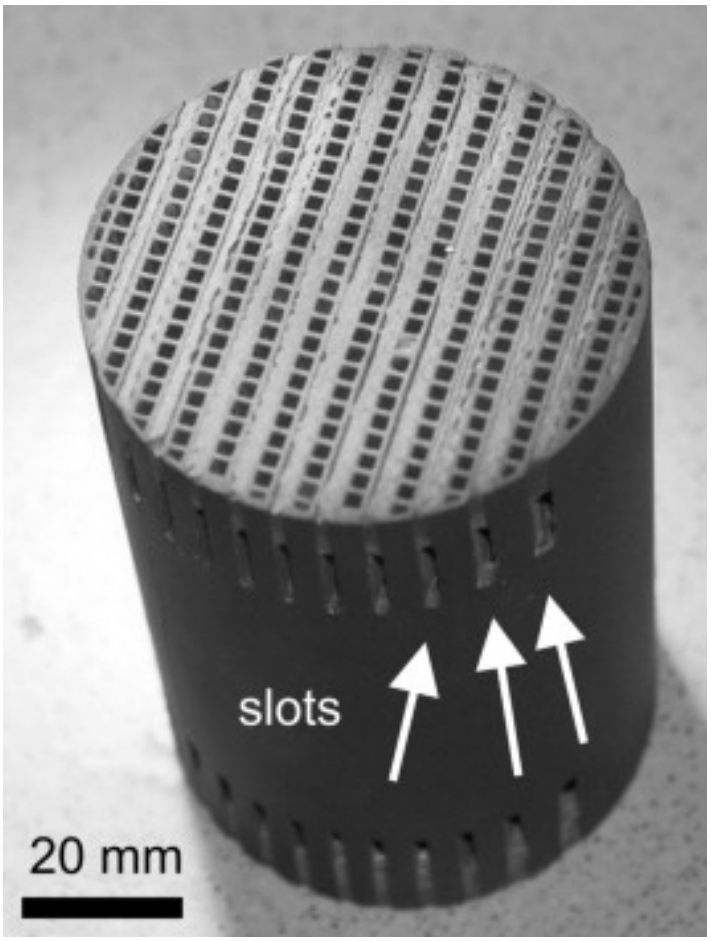

Figure 2.1: Honeycomb structure using extruded SiC, the slots shown by the arrows have been obtained and filled with ceramic material. The cutting has allowed to produce the separated channels system inside which the thermal fluids flow [4].

The honeycomb structure is generally used for the particle filter treatment, in order to allow the physical and chemical block of the particles that run out of the engine and may be toxic and polluting. The main advantage of the honeycomb structure comes from the contact surface increase and the use of the SiC structure itself to capture polluting particles contained into the fumes. The design enhances the contact area and the structure compactness. As reported into the paper presented by Fend et al., to increase the density and allow the exhaust gases after-treatment, some metallic silicon is infiltrated [4]. The sintering with metallic silicon, together with liquid silicon infiltration and carbon dispersed into the matrix, allows to obtain SiC bondings in between SiC grains. Moreover, by using the metallic silicon, a fully dense Si-SiC composite is obtained. [4]

By considering an energy application as the one considered by Du et al., it shows a heat exchanger for CSP application obtained by a 3D printing via binder jetting [1]. The CSP case study is composed by a Brayton Cycle, a thermal-to-shaft power cycle that consists of five basic components: compressor,

turbine, heat input, heat rejection, and recuperation. The Brayton power cycle is considered as a high efficient power generation cycle that can be integrated with solar receivers for the next generation CSP Plants [2]. In the subsequent picture, the general scheme of a Brayton Cycle is represented. Figure 2.2 was taken form a paper by Lavric et al. [26].

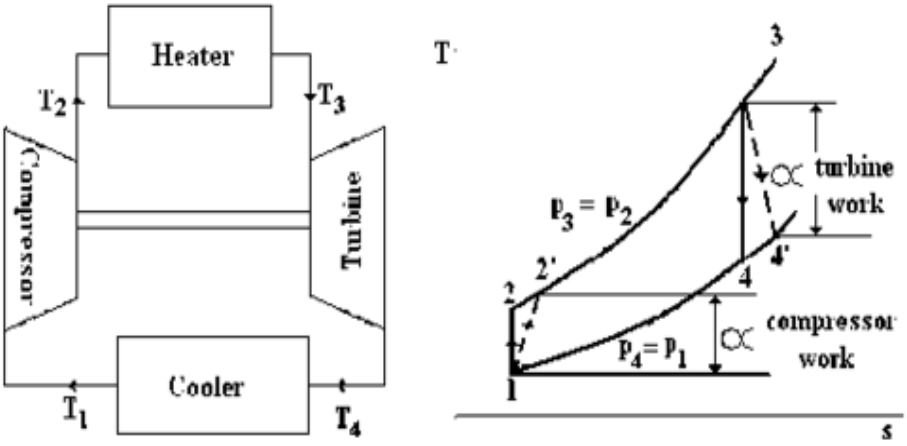

Figure 2.2: General closed Brayton Cycle scheme represented as a cycle composed by a first compressor stage, a heat exchanger, a turbine to produce the electric power and the final cooler to reproduce the original starting temperature conditions of the working fluid [26]

In Figure 2.2 it is possible to see the general thermodynamic scheme. The thermodynamic path is composed by: a first compression (T_1 and T_2), an isobaric heating (T_2 and T_3), an expansion (T_3 and T_4) and a final isobaric cooling (T_4 and T_1). The compression and expansion stages are ideally represented as adiabatics since no heat should be exchanged. However, due to the inevitable losses into any thermodynamic process and the second law of thermodynamic, a loss due to entropy increase is always present [26].

The fluid flowing inside the Brayton Cycle power block is sCO_2 while the molten salts are generally used as heat transfer fluids (HTF) from solar collectors to the power block working fluid, which are however a highly corrosive and stressing fluid on the mechanical parts of all the heat exchangers [2]. A corrosive environment could be detrimental for the reliability to the metal-based heat exchanger [3]. The molten salts are used due to their volumetric heat capacity and heat conductivity. Examples of such operating fluids could be fluoride molten salts, conventional nickel alloys and austenitic stainless steel [2]. sCO_2 refers to a super-critical state of the Carbon Dioxide (CO_2) when kept above its critical level of temperature and pressure, having the density of a fluid even if it behaves as a gas. CO_2 usually behaves as a gas in air at standard temperature and pressure (STP), or as a solid called dry ice when frozen. If the temperature and pressure are both increased from STP to be at or above the CO_2 critical point, it can adopt properties midway between a gas and a liquid. At this state, sCO_2 can be used efficiently throughout the entire Brayton cycle since it is addressed by a gas flowing behaviour and liquid thermal characteristic [2]. This behaviour together with the dependence on density and temperature make this working fluid as perfect for the energy production [27].

The molten salts are considered as primary coolant and heat transfer media for nuclear energy systems and CSP applications. They are characterised by a high boiling point as well as high volumetric heat capacity and heat conductivity. An example could be fluoride salts. However, it has to be considered that these materials are corrosive at high temperatures [28]. An important drawback to consider is that the molten salts are moisture or oxygen sensitive, condition that may lead to a

premature oxydation [6]. Moreover, the CSP working fluid must be kept at liquid state in order to deliver the heat. The molten state is reached at high temperature, thermal condition that may impact the cycle working conditions, implying a minimum working temperature greater than the maximum solidification temperature [1, 3, 6]. In this consideration, an inert material should be used for the heat exchanger construction. It is already known that the ceramics above all the others are the most stable materials for both thermal and chemical perspectives. Advanced ceramics are the new frontier of these category, considering as examples Alumina (Al_2O_3) and SiC. This last one has already been deeply investigated for lots of applications, such as in nuclear fusion reactors, depositions inside gas turbines and many other applications [1, 3, 6].

The temperatures involved inside a Brayton cycle are generally greater than 700°C. The sCO_2 considered as working fluid causes stress problems due to the high pressures involved and material degradation due to the high operating temperatures. Normal operating conditions are in the order of 20MPa and 700°C. Such harsh conditions could cause creep and fouling. As a consequence a reliable heat exchanger able to work in these conditions into a sCO_2 Brayton power cycle is an attractive and ambitious point of arrival. There is a huge need of structural parts working under extremely high temperatures. Mechanical, chemical and physical properties should be maintained constant for all the working period. Among the other advanced ceramic materials, SiC stands out due to its extraordinary corrosion and oxidation resistance. Furthermore, SiC is characterised by an easy synthetization and possibility to be used in AM. Printing technologies are not far from ceramic utilizations as already mentioned but binder jetting represents the most used. For the densification of the green structure of the heat exchanger, liquid polymer infiltrations and pyrolysis is used [1]. As main consequence SiC is the perfect material due to its mechanical, tribological, chemical and physical properties, which can be all maintained during the CSP operation time at standard operating conditions [29]. It has already been used but still with simple geometries, limit that will be overcome in the next years by the constant increase in the printing technology utilization.

Firstly, a 3D printed ceramic heat exchanger done by robocasting could increase the heat exchange through a more complex geometry, reducing the production costs being made with a commercial technology. Secondly, SiC can enhance the current operating limit conditions. An advanced structure obtained via binder jetting is reported by Thomas et al., in which the heat exchange has been increased by adopting the design proposed [3]. By using a 50μm SiC powder a density up to 55vol.% of the green body has been obtained, requiring a liquid silicon infiltration to increase the density reaching values in the range of 85-95% in the final sintered structure [7]. The final structure was suitable for the heat exchanger characteristics, having mechanical and thermal properties deeply investigated, as well as the microstructural characterization, by [3]. By using a finer powder the green density should be greater than the one already reported, requiring a lower amount of infiltration, creating an even better heat exchanger structure.

It has to be considered that due to the dimensions of the sintering machine used, a complete heat exchanger structure would not be possible to be built. As a consequence, the final comparison among the different properties will be conducted on a sample, requiring shorter times for the printing and being simpler to be designed.

The design proposed by Du et al. considers the utilization of crossed pipes in which heating fluid and refrigerant fluid flow. The Figure 2.3 represents the main structure [1].

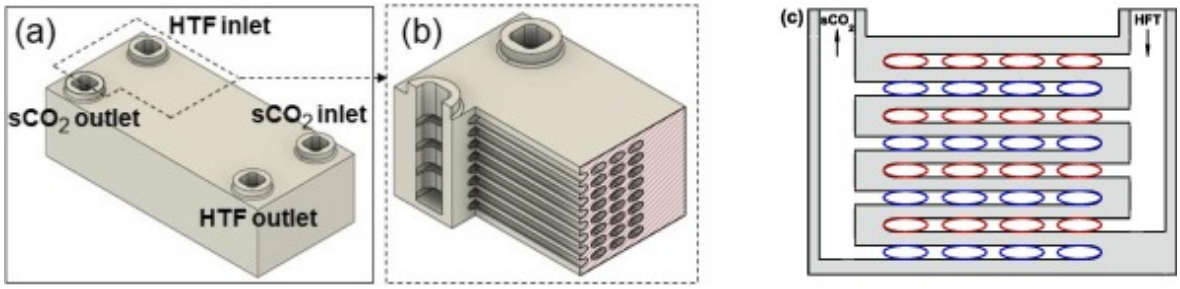

Figure 2.3: Heat Exchanger that considers two separated channel systems for the HTF. HTFs enter vertically through the header channels and than flow through the horizontal header channels. HTF fluid flows in the HTF flow channels while the cold sCO_2 in the sCO_2 flow channels [1].

Du et al. reported the main achievements obtained through AM. In fact the structure represents a design not achievable through common production technologies. It allows to integrate fluid headers with the Heat Exchanger channels as well as introducing inlet fluid restrictions. The heat carriers enter into the structure by the vertical channels and flow through the horizontal headers to reach the elliptical flow channels. At the outlet, the fluids flow through the last vertical connection. In the figure, the red elliptical shapes represents the flow channels in which the hot fluid flows. The cold flow happens through the blue elliptical channels [1].

As densification step, a similar to Polymer Integration and Pyrolysis (PIP) process has been used. As a consequence, it has been seen that after the pyrolisis a restricted shrinkage was caused [1].

As a post printing treatment, the shape has been treated with a particle remove technology by using compressed air. In this way the remaining powder in the header and flow channels can be removed. At the end, a comparison among weights in between the theoretical result and the actual one has allowed to estimate if the remaining imperfections were acceptable or not. On the first try bubbles were detected while on the second time the sealing was completed without causing any other bubble formation [1].

To test the flowability through the channels, compressed air with a flow indicator has been used. Moreover, the water submersion leakage process has been performed by using a compressed gas flowing through one of the two channels. By increasing the gas pressure, the sealing could be tested. By analysing the bubble formation, it was possible to investigate if the channels created were sufficiently sealed, demonstrating the isolation of the pipes [1].

Thermal analysis has been performed by using air flowing in both the ducts, using hot air at 250°C while the cold one at ambient temperature. The counter flow configuration was used.

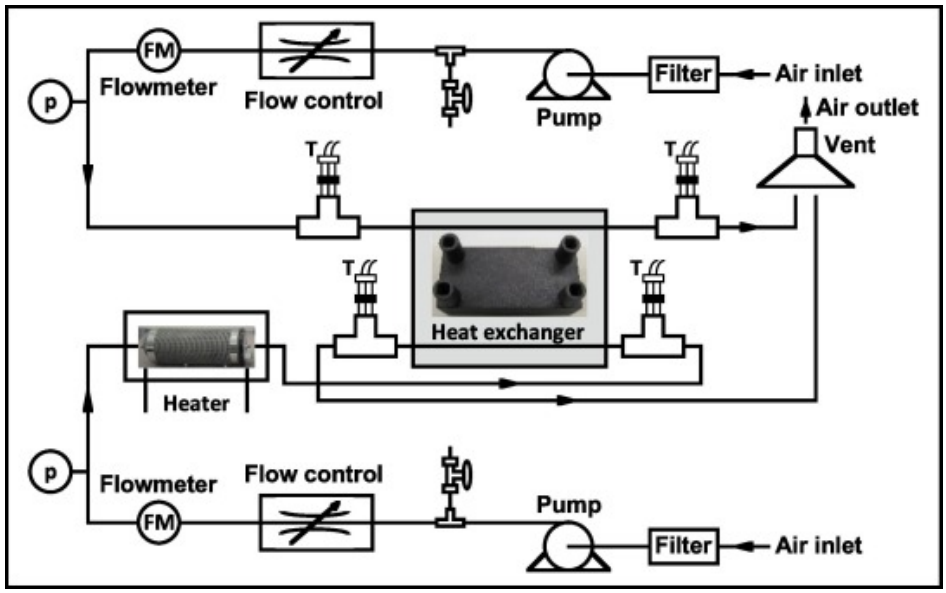

Figure 2.4: Thermal testing cycle for the counter flow configuration of the printed heat exchanger. Hot air is pumped by an air pump through a flow-control device, flow-meter and air heater, it enters than into the heat exchanger air inlet at 250°C. Symmetrically the cold air is inserted in the cycle [1].

As expressed in the conclusions by Du et al. the results demonstrated reasonable heat exchange in between the flows, increasing trend in the heat flow rates and reasonable agreement in between tested and simulated results [1].

A similar study is the one done by Thomas et al. in which the densification process followed the Phenolic Binder Integration (PBI) and LSI, since the printed specimen porosity was around 55vol.% [3]. A pyrolisis process was used to eliminate the PBI inside the structure leaving only C molecules inside the printed structure. A final LSI has been done [3].

The heat exchanger design proposed by Thomas et al. represents a similar structure to the one proposed by Du et al., implying similar physical characteristics [1, 3]. As a consequence, a further comparison among the results may be useful to understand the main differences in between the various technologies considered.

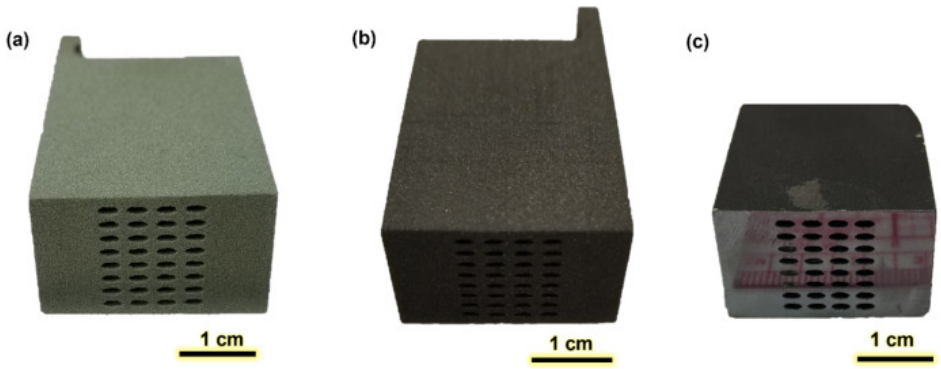

Figure 2.5: Heat exchanger printed by Thomas et al. by binder jetting [3].

As main outcome represented, the Scanning Electron Microscope (SEM) images represent the final chemical structure. Moreover, the residuals can be highlighted. The residuals principally shown are C and Si molecules dispersed into the main SiC matrix. In the next figure from the same paper by Thomas et al. the various elements are detected [3].

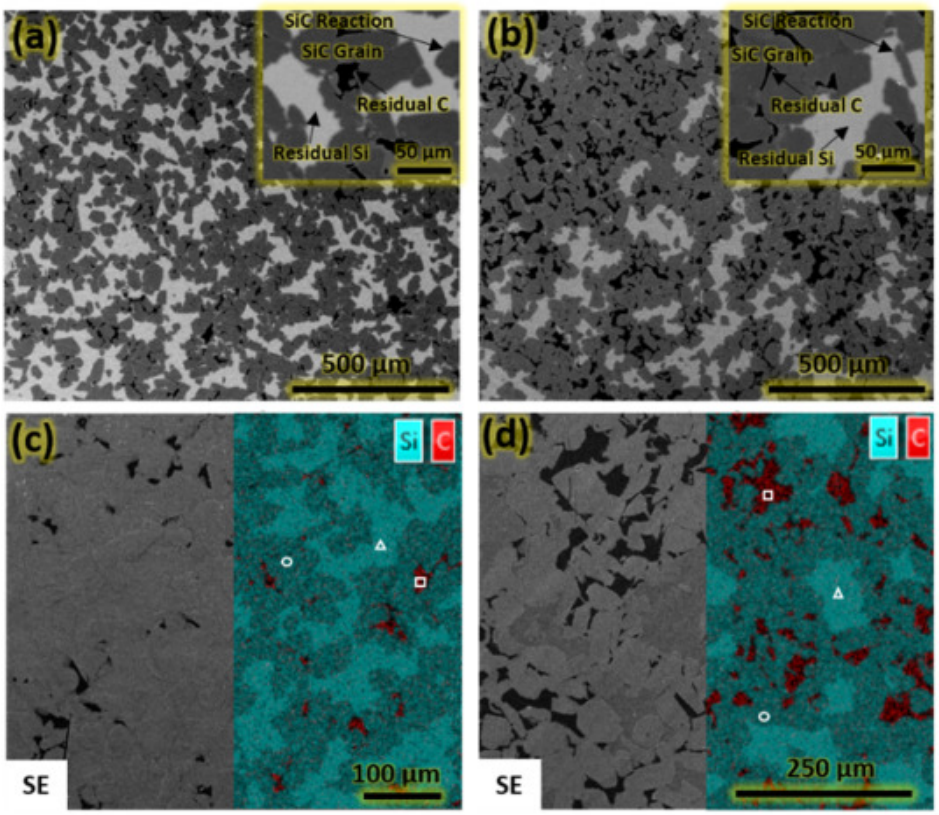

Figure 2.6: SEM charcaterization done by Thomas et al. tht considers the differenciation of the different materials in the microstructure. By considering Figure a) and Figure b) the material agglomerations can be distinguished, differentiating SiC grains from the C grains. In Figure c) and Figure d) Si and C are coloured [3].

By considering Figure 2.6a), the SiC reacted grains can be differentiated from the other present structures. Moreover, thanks to the Energy Dispersive X-ray spectroscopy (EDS) the differentiation among C and Si granuli can be made. By increasing the focus the created structures can be seen in more detail. Agglomerations of C particles can be distinguished as well as the Si structures.

MATERIALS AND METHODS

The most common ceramic suspension preparation for the 3D printing deals with phenolic resins [3]. However, recent studies, which are focused on a second ink preparation, are based on an emulsion able to gelify and to produce a printable paste [30]. Among the different binder alternatives, Pluronic F-127 stands out due to its easy availability and possibility to be mixed with SiC. Several are the studies that propose a paste made by SiC and Pluronic, using some stabilizers in order to allow a proper viscosity.

Phenolic resin has been largely used due to its easy availability and easy connection with SiC, even if presenting some detrimental effects harming health and polluting the environment. The main drawbacks of this production technology are related to the formation of residual Si, non reacted C and SiC grains [10]. On the other hand, structures created with these resins were characterised by a green body with a strong architecture, while through the pyrolysis the dangerous components evaporate compromising atmosphere and health due to toxic emissions [3]. Phenolic resins are obtained from a step growth polymerization of difunctional monomers [31]. This synthetic resin represents one of the most used chemicals in industry, characterised by outstanding chemical and physical properties: hardness, heat withstanding, electrical and chemical resistance [32]. Such characteristics allows the resin to be used in several areas, from thermal and electrical insulators to adhesives [33, 34]. However, it has to be considered that phenolic resins are made via a non renewable petroleum based phenol and formaldehyde, causing important impact on the human health and on the environment itself [34, 35, 36].

Pluronic F-127 (generally called Pluronic) is a bio-organic material that, together with water, works as binder for ceramic particles, as an example SiC particles. It represents a good solution for the production of an ink, since it does not imply any risk for the human health and the environmental risk is limited. Pluronic binding with water allows the production of a gel that does not require special care due to a simple production process. Pluronic is not toxic and it has been deeply used in the biochemical and biomedical field [37]. The crucial part concerning Pluronic is represented by the final production step due to a non-simple expiration. This can be solved by the pyrolisis process conducted in an inert atmosphere in which the production of secondary products that may contaminate the final structure is avoided. With high temperatures, water evaporates and organic components are pyrolyzed, so the carbon can react with the infiltrated liquid Si to produce new SiC and densify the final structure.

The constant increase of ceramic utilization from the ancient times followed by the will to recreate the behaviour of clay to build new structures if mixed with water, being therefore addressed by naturally incomparable properties, has driven to a continuous study. In recent times, the most advanced techniques take the name of colloidal processing [38, 39].

Colloidal processing stands for a wet process that involves a liquid solution in which ceramic particles are suspended. It is a method to consolidate particles which have a high density and homogeneous microstructure by controlling inter-particle interactions in a suspension. A crucial point is represented by the control of the particle stability in the solution. Particles are loaded in the solvent, and therefore it is essential to understand the particle characteristic in the solvent. Ceramic particles are charged into the solvent due to the particle surface and solvent. The ζ-potential represents the best approximation of the particle surface potential [40]. Moreover, the ζ-potential controls the particle dispersion [41].

A homogeneous structure and a good packing of the powders at consolidation stage of the green body can improve the sintering and final properties of the ceramic body. During all the production steps, rheological properties must be controlled [42]. Normally to control the dispersion of the ceramic particles in an aqueous solution and avoid agglomerations the surface charge potential is kept under control. More in detail, the production procedure of the SiC particles is fundamental since some alterations on the particle surface layer may alter the particle stability in aqueous suspension [43]. In the example reported by Tartaj et al. due to the production of SiC nanopowder via inductively coupled plasma an accumulation of C molecules on the particle outer layers causes the formation of an hydrophobic layer. To solve the hydrophobic layer formation and increase the particle stability, a thermal treatment is sufficient to substitute the carbon layer with a SiO_2. The new SiO_2 outer layer represent an hydrophilic layer that can be further removed by the use of chemicals [43]. The powder surface potential has emerged as main controller of the flow properties and powder dispersion characteristics. In this extent, the control of the pH has become more crucial. However, the identification of the correct pH or dispersing agent becomes more difficult [44].

The ζ-potential can be defined as the difference in potential between particle and its ionic atmosphere. In this extent the ζ-potential is useful to control the colloidal suspension stability [41]. It must be said that there are no direct ways for its direct measurement. Due to its correlation to the particle mobility, the ζ-potential evaluation can be performed through theoretical methods or through the electrophoretic mobilty [45].

However, for sake of simplicity and wide availability of results, no studies related to particle energy and interaction have been made. Everything is related to researches and measurements accomplished in the most recent times. All the suspensions are replications of the previous works done by different groups, that have been used as starting point for the new inks developed [30, 46, 47].

The gel-embedded suspensions have been developed as an alternative to colloidal suspensions for the 3D printing pastes involving ceramics, since the particle-particle interactions are not the only reason of the rheological properties. They depend mainly on the gelation agent in which the ceramic particles are dispersed. An easy manipulation and low volatility of the water based solutions are the main characteristics of the most used chemicals: Pluronic F-127 and Cellulose [30]. Cellulose represented the main alternative for an hydrogel based ink, being soluble in water at any temperature. However, it was not considered since generally more expensive, even in its main utilization as Carbomethylcellulose. Carbomethylcellulose represents a cellulose derivative which is soluble in water. As a consequence its utilization might be similar to the Pluronic one. Moreover, this natural binder is characterised by a fast hydration. Rapid hydration may cause severe agglomeration, making the production of a ceramic ink harder [48]. Pluronic works as dispersant, plasticizer and coagulant agent, therefore the use of a Pluronic based hydrogel represents a huge advantage in producing a ceramic paste [49, 50].

Without the accumulation attitude related to the action of the particle surface chemistry on the gel-embedded suspensions, any ceramic powder may be compatible for a final ink production with Pluronic F-127 [51].

There are two main strategies proposed by M'barki et al. for a ceramic ink production [52]. The first approach proposes an ink preparation that has a gelation behaviour after printing, so that a sufficient strength is developed to resist deformation after printing. Another approach involves the control of ink rheological properties, in order to obtain a viscoelastic ceramic ink with a sufficient yield strength to support consequent layer deposition and being able to construct complex geometries. A viscoelastic material combines a viscosity characteristic of a liquid, being deformable if a stress is applied, and the elastic term, so the recover of the deformation once the stress is removed [53].

3.1 PLURONIC F-127

Pluronic F-127 powder (BioReagent, Non-ionic Surfactant, Sigma-Aldricht, US.) is characterised by a density of 1.06 g/cm^3 given by the producer.

Pluronic represents the commercial name of a synthetic-organic material used frequently in biomedical application, generally named as Poloxamer 407. It belongs to the synthetic polymers and it is thermoreversible in aqueous solution, meaning that the gelation behaviour is completely reversible with the temperature evolution [54]. The gelation temperature stands for the transition temperature in which the change in viscosity happens. In several studies this temperature has been detected in between 15°C and 17°C [46, 55]. Pluronic is composed by a hydrophilic ethylene oxide and a hydrophobic propylene oxide in a ratio of 2:1. The next figure represents the 3D structure of the Pluronic chain [56].

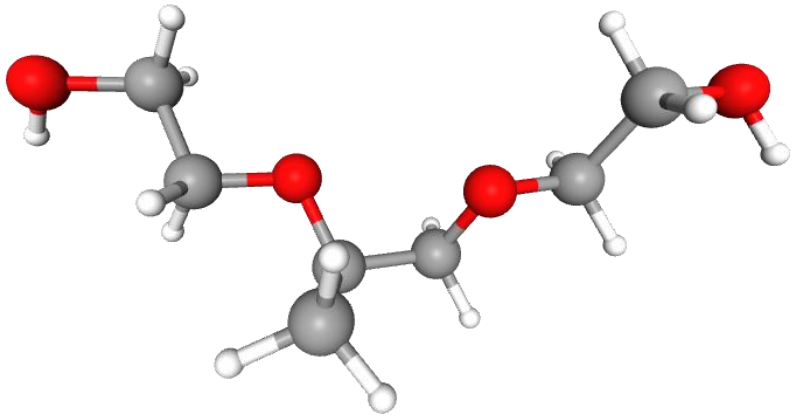

Figure 3.1: Pluronic F-127 structure: red blocks represent the Oxygen (O), the gray ones C while the small ones the Hydrogen (H) [56].

It is composed by a chain structure with 101 repeated units. The monomer can be written like this: $C_7H_{16}O_4$. This molecular structure takes the IUPAC name of 2-[2-(2-hydroxyethoxy)propoxy]ethanol [56]. As represented by the name itself, the chains are composed by two main components: hydroxyethoxy and propoxyethanol. These two components give the Pluronic an amphilic structure, therefore a polar and water-soluble group is connected to a nonpolar water-insoluble hydrocarbon chain. The amphilic block copolymer molecules autonomously combine into micelles in aqueous solution, which are temperature dependent structures that affect the degradation properties of the material [57].

Figure 3.1, presented by National Centre for Biotechnology Information, shows the main Pluronic structure that is composed as, the chemical formula says, by four O atoms, 16 H atoms and seven C atoms. Respectively, red blocks represent the O, the gray ones the C while the white ones the H.

The gelation behaviour is a consequence of the thermoreversible behaviour of the aqueous solutions mainly related to the variations in enthalpy and entropy of the solution molecules. At low temperatures there is a local higher order of water molecules around hydrophobic units of the polymer in solutions. By increasing the temperature, the interaction in between polymer hydrophobic molecules squeezes out the ordered water molecules creating the bulk solution characterised by a lower order. Endothermic heat changes are the main reason why there is a change in the hydrophobic molecules interaction. As a consequence, gelation happens [57].

By increasing the temperature the hydrogen bonds of the poly(propilene oxide) (PPO) are broken increasing the hydrophobicity. Poly(etilene oxyde) remain unchanged in their hydrophilic state. Once

the micellization is achieved, the micelle aggregate again into a crystalline structure at a different temperature [58].

The thermal process is reversible as demonstrated by Pradines et al. Micelle were in equilibrium at any temperature and their structure changes reversibly. The thermal analysis has been conducted with a paste composed of 20wt.% of Pluronic into deionized water. The results shown the phase transition temperature at 20°C due to the lower binder content. By analysing the rheological thermal analysis, two distinct peaks are found in the Pluronic evolution. The first stands for the gelation temperature, at which the micelle aggregate losing the order and forming a disordered structure. The second peak is related to a second greater temperature related to the cristallization phase, therefore the assembly of more ordered structures due to the micelle re-aggregation. The endothermic peak has been addressed as the micellization of the Pluronic unimers [58].

Pluronic can be stored in ambient temperature in solid form. Furnished as a powder, Pluronic can form agglomerates. If it is used to produce a mixture with water, depending on the temperature different structures may create. When temperature is greater than 17°C, the solution gets a gel-like structure. When the temperature is lower, the viscosity decreases, increasing the flowing behaviour and looking like a liquid solution [55]. As it can be seen in the next figure, if the solution is stored at 4°C it gets a completely liquid structure, having therefore a good homogeneity [55]. In addition, it can be detected that by increasing the Pluronic content the viscosity rapidly increases as soon as the ambient temperature is approached. The process is thermally reversible, without serious degradation in behaviour if the process is done cyclically [58].

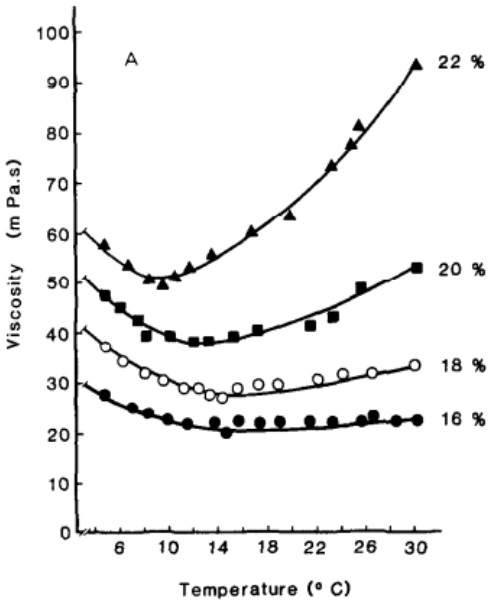

Figure 3.2: Pluronic F-127 temperature dependent viscosity. By increasing the Pluronic concentration the viscosity decreases [55].

Hydrogels such as Pluronic F-127 and cellulose are the most used since they have a easy manipulation. Most of them rely on the liquid to solid transition through solvent evaporation after filament deposition [30]. Hydrogels refer to long polymer chains 3D assembly [59]. These long chains are held together as water-swollen gels by several interactions or their combinations. Some of these may be listed as: primary covalent cross-links, ionic forces, hydrogen bonds, affinity or bio-recognition interactions and many others [60]. Generally, hydrogels are not soluble in water due to their chemical or physical crosslinks and/or chain entanglements. They are present in nature or they can be made synthetically. As a general characteristics list it can be named the sensibility to pH and temperature changes [60]. The first studies on hydrogels are dated back in the 1930s in Germany, focused on kinetics and cross-linked polymers. In mid 1940s, noble prize Paul Flory lead to the fundamental un-

derstanding of hydrogels' cross-linked structure, swelling/syneresis characteristics and their behaviour in water. From that time, different efforts have been made on studying characteristics, preparation and structure. Several books have addressed the preparation, structure, characterization and application of the hydrogels [60].

Some hydrogels, like Pluronic F-127 in water undergo a gelation behaviour which implies strong viscosity changes. Below the gelation temperature, water works as a good solvent for the polyethylene oxide, but as soon as the temperature increases the hydrophobicity of the polypropylene oxide increases, decreasing therefore its solubility and causing the formation of micelle [61].

Hydrogels are polymer chains arranged in 3D networks that can capture large amount of water as well as release it due to thermal treatments. This main characteristic of water storage implies a reversible effect. Due to this incredible characteristic, its utilization goes from the biomedical field to the engineering one [59].

General Pluronic concentrations in water are in between 20wt.% to 30wt.% varying its concentration also according with the kind of ceramic used [55]. Several studies have been made on the rheological characterization of this solution, finding as degrees of freedom both temperature and concentration [46]. As reported in the vast majority of the papers cited that deal with a production of a SiC ink, the concentration of Pluronic mostly used is 25wt.% solved in water. 2000 rpm was used in a vortex mixer (heidolph Reax Top, US) as initial mixing speed. Intermittent ice bath was performed to cool down the solution in order to preserve the liquid like structure. Due to this inefficient preparation methodology, bubbles were created due to the excessive agitation making the final steps more complicated. To avoid such problem a magnetic stirrer (heidolph MR Hei-Tec, US) must be used, using slower speeds and increasing the required mixing time but also enhancing the homogeneity.

In order to keep the liquid like structure of the Pluronic solution, it has to be kept at 4°C. It is also useful to avoid problems as increased viscosity and heterogeneity. This procedure allows to have a simpler mixing process. Therefore, a subsequent stay for 24h of the Pluronic into a refrigerator is necessary. This allows the mixing defects to dissipate [62].

As a summery, Pluronic-127 is an additive that works as a carrier for the ceramic powder [49, 63]. Its thermal reversible characteristic as hydrogel make it a suitable actor for the ceramic ink formation. In addition, being completely usable into the biomedical applications, make it a possible choice for a sustainable application of materials for large scale applications, without causing pollution and toxicity.

3.2 SILICON CARBIDE

SiC provided by Nanoparticles/ Nanopowder (SiC, 99.0+%, 40nm, beta) by SkySpring Nanomaterials, Inc. (ssnano.com, US) with characteristics of 40nm as main diameter, 15-35 m^2/g as specific surface area and 3.126 g/m^3 as true density. SiC crystalline structure is shown sequently in a Figure by Almashhadani et al. [64].

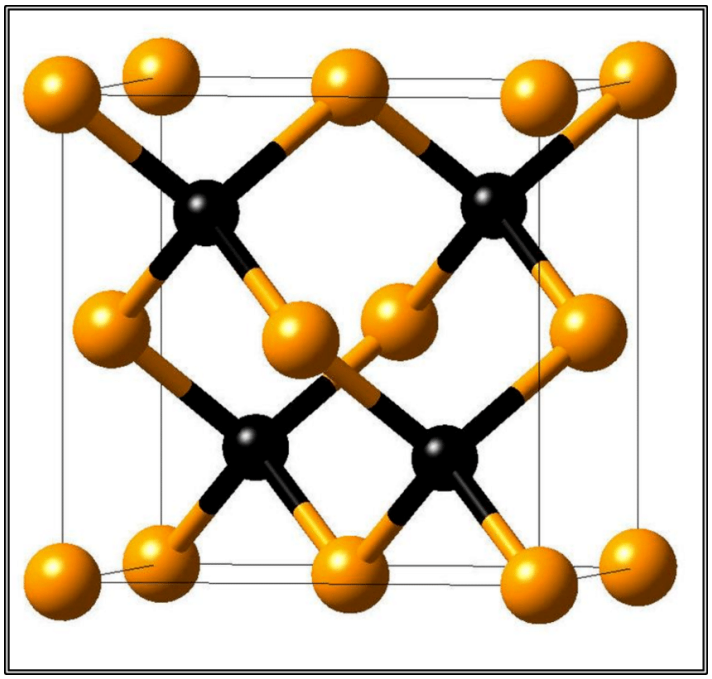

Figure 3.3: SiC crystal structure by Almashhadani et al. with black particles as C atoms and orange particles as Si atoms [64].

SiC is one of the ceramics with a unique set of physical-chemical properties. It is characterised by a high hardness (600-3800 [MPa] [65]) and mechanical stability at high temperatures, excellent thermal conductivity (3.8-20.7 [W/mK] [65, 66]) and low thermal expansion coefficient (7.9-11 [$10^{-6}/K$] [65, 67]). Moreover it has a high resistance to corrosion and oxidation, characteristics that are fundamental to work in harsh conditions such as into a Brayton Cycle [68].

The SiC fabrication requires manufacturing techniques able to satisfy a good architectural control at micro and macro level. The structures should be strong and stable [47].

Due to its extraordinary thermal and electrical properties, SiC becomes suitable for high temperature, high power and high frequency applications. This unique combinations make this ceramic material one of the best constituents for the actual and future energy applications [69].

SiC is characterised by a nanoarchitecture that is dimensional dependent. The one-dimensional disorder leads to the possibility of having many structures with different stacking sequences. The one-dimensional disorder refers to the fact that the different crystal structures (called polytypes) are differentiated in one of the three dimensions even if having the same chemical structure. Depending on the conditions, SiC has different structures. The different polytypes let this material to be used in several applications. The structures vary from 3C, 2H up to 14H, 15R and 19R, 24R, 20H and 21H. C refers to the cubic structure while R to the rhombohedral and H to the hexagonal crystallographic group, the numbers refer to the stacking sequence [70, 71]. The most common structure is represented by the α-SiC which takes form at 1700°C and it is characterised by an hexagonal crystal structure. The β-SiC is a modification that happens below 1700°C but it has a diamond structure. These two crystal structure are the ones used during the study experimental process.

Considering the tetrahedral bonding between Si and C with Si atoms on the corners of the tetrahedral structure forming concise bonds length give the bases for very high hardness and higher chemical and mechanical stability. Such configuration allows this material to have excellent density (3.23g/ml) for mechanical and energy applications, high strength and extraordinary thermomechanical properties. Considering the elastic modulus, it reaches values of 424GPa, low friction coefficient (0.17) and hardness of 45.8MPa. SiC is therefore one of the most suitable materials to work in energy applications [72].

Like all the materials, some defects are present in the structure. The most important are the

dislocations, stacking faults and low angle grain boundaries. A possibility is also the interaction of different defects that may cause the device performances collapse. Pre-existing defects may grow together with the growth of the structure and inclusion of impurities may happen with temperature and pressure evolutions causing immense shear stress [73, 74]. To avoid presence of defects, densification into an inert atmosphere could avoid presence of cracks and inclusion of alien molecules [37]. It must be said that a complete absence of defects is impossible.

Due to its extraordinary combination of thermal, physical and mechanical properties, SiC is the material of choice for several different industrial and energy applications. One of the most demanding applications regarding harsh environments and high temperatures are the heat exchangers [75]. Commonly the use of SiC is limited to technologies that use a ceramic powder and lead to simple shapes. Considering the use of AM, ceramic powders can be used and they have been already demonstrated to be successful for paste production and printing objects with complex shapes.

3.3 CERAMIC PRINTING TECHNOLOGIES

Binder jetting is the most used printing technology for ceramics nowadays due to its easy utilization and well green structure characteristics, such as good structure mechanical stability [7, 76, 77]. A large material waste accompanies the binder jetting production procedure, since the protocol requires deposition of layers of ceramic powder over which an adhesive ink is sprayed drawing the final shape. The material not used and that has been in contact with the binder is wasted or needs an energy consumed procedure to be recycled. The final structure is obtained by subsequent layer deposition, allowing the overall substainment of the green structure. As main drawback, all the material not directly touched by the binder is sequently wasted [14]. However, one disadvantage is the use of large diameter particles ($>5\mu$m) that may cause a poor dense structure. To solve the density problem a Polymer Integration and Pyrolysis (PIP) using ceramic polymer precursor may help the agglomeration of the paste, as well as Chemical Vapour Infiltration (CVI) or Reactive Melt Infiltration (RMI) [7]. PIP is the most used techniques for the Ceramic Matrix Composites (CMC) using a SiC matrix. This technique permits to prevent fiber damage being performed at low temperatures and to have a good control of the microstructure even if requiring long times for the manufacture [78]. Fibers come from the burning of the polymer chains involved in the production procedure; the only material left are the SiC fibers. PIP involves the use of a SiC precusor that is pyrolyzed on the surface generating a weak native surface. By infiltrating a low viscosity polymer and consequently pyrolyzing it, the polymer is converted into the ceramic by burning the hydrocarbon chains leaving only the ceramic structures due to their high temperature resistance [79]. The process is done cyclically, producing a final gain in increase density by reducing the porosity, increase the flexural strength and the Young's Modulus [80]. CVI is used commonly to deposit debonding and protective coatings on the reinforced fiber structures. However, it my also be used to produce a porous ceramic preform, which can be subsequently infiltrated by liquid silicon [78]. The most used CVI process uses a isobaric-isothermic thermal treatment, in which the preform is kept at uniform temperature while the reactant gasses are supplied to preform at constant pressure. Several are the other options, involving temperature and pressure gradients, controlling therefore physically the gas deposition through the pressure or temperature gradient. By the use of CVI it is possible to control the crystal orientation and morphology getting the most effective process to obtain CMCs [81]. As main drawbacks, CVI causes high expenditures for large volume productions and the structures present some final open porosities [82]. RMI has been extensively used to produce a range of composite structures. The chemical composition of the preform is made altering by the reaction with the melt Si-Metal or directly infiltrating a refractory metal into the carbon-containing matrix. The matrix composition is dependent on the chemical species present, their affinity to carbon, composite porosity and time available for the reaction [83].

Considering the densities obtained in the various papers, the most common ranges are in the order of 85-95%, via binder jetting, being time intensive and resource expensive. Porosity detected is still at 8% [7].

Robocasting is a technology related to AM that was developed in the 1980s. It is a fabrication technique based on a layer wise deposition of colloidal slurries containing ceramics [84]. It has been used mainly for the production of monolithic bodies and periodic lattices. For the structure printing,

a paste is extruded from the tip of a nozzle and let rest on a surface [85]. In the following, the general robocasting technology is shown in Figure 3.4 by Munch et al. [86]. There are different alternatives of nozzle (Figure 3.8) that may be used, implying different loads on the ink.

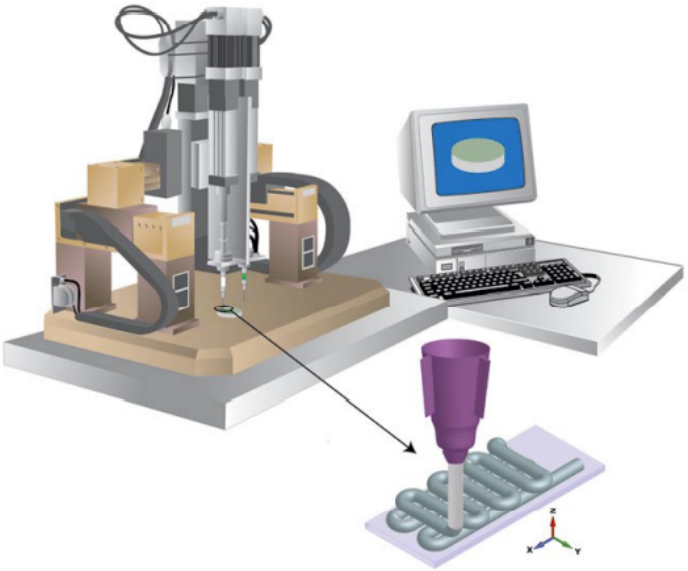

Figure 3.4: Robocasting technology [30]

The additive manufacturing follows a path programmed by a Computer Aided Design (CAD) file, obtained from a computer. From the CAD file, a G-Code is obtained. The G-code represents the most used programming language of numerical control machine, that produces a sequence of steps needed by the machine to complete a determined action [87]. This programming language is also used by other machineries such as milling machines. The G-code consists of lines of text that represent a specific action, regulated by the ISO 6983 [88].

The main advantage of robocasting is related to the mechanical properties attributed to the printed materials through the printing process (such as toughness, hardness etc.) due to the ink deposition technique itself and the mechanical unaffected ink structure. Moreover, robocasting is characterised by the flexbility of using different material inks to print [46].

The ink rheological properties are considered the most important in robocasting. There is the need to avoid disomogeneities and air bubbles, to have a high-volume fraction of ceramic powder and correct flow properties. As major characteristic the ink must be highly shear thinning in order to be extruded from the printing head. Strength and stiffness have to be at a sufficient level to be self-supporting after the printing. Aqueous inks are generally preferred to the other ink alternatives due to their simplicity, low cost, low toxicity and low drying. The low concentration of organics, in this case represented by Pluronic F-127 25wt.% in an aqueous solution allows to have a fast burnout and a high density [46].

Rheology of the suspensions has to be adjusted to fit specific techniques like ink deposition through a nozzle [89]. In Section 3.5 the basic rheological properties will be explained. In Chapter 4 the rheology characterization of the ink prepared will be explained in details.

3.4 TETRAMETHYLAMMONIUM HYDROXYDE

Tetramethylammonium hydroxide (TMAH) aqueous solution has been provided by Sigma-Aldrich, US. The solution considers 25wt.% of TMAH in water.

TMAH has been chosen as ink stabilizer. TMAH has a chemical structure represented as $(CH)_4N(OH)$ and it is an ammonium salt, in our case dissolved in water. Figure 3.5 reports the TMAH structure proposed by [90].

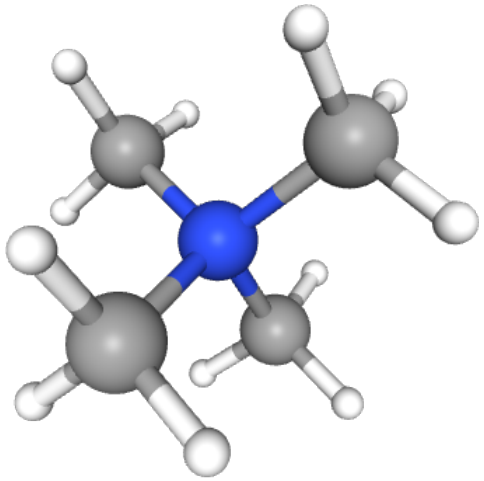

Figure 3.5: TMAH structure: blue blocks represent the Nitrogen (N) atoms, grey blocks represent the C atoms and the white ones the H atoms [90].

TMAH solution is a base, as the pH value is 13. It is a recent material, introduced the first time in 1991 by Tabata et al [91]. The TMAH behaviour with a SiC ceramic ink allows to reduce the viscosity even with high concentrations of SiC, increasing the maximum solid fraction usable making easier the printing process. It is used commonly in industry for the developing of the photosynthesis pattern or as an etching agent for SiC [92].

Figure 3.5 shows the TMAH structure assembled by blue, grey and white blocks. The blue one represents the N atoms, while grey and white represent C molecules and H ones as already explained for the Pluronic.

It has been proved by Oliveira et al. that there is a relationship in between stability and ζ-potential of the ceramic powders. A high ζ-potential is associated to a higher stability than a low ζ-potential [93]. In Li et al. paper the effect of TMAH on SiC suspension has been demonstrated [44].

The influence of pH on rheological properties of the suspension is significant. It has been reported by Li et al. that the viscosity decreases by increasing the pH. Values around 9.5 and 9.8 are addressed as the ones with lower viscosity than the previously measured ones with a lower pH value [44]. It has been demonstrated that the interparticle interaction forces differences are associated to a change in the ζ-potential. Strong repulsive forces are detected at high and low pH values. The relationship in between rheological properties and amount of dispersant added is explained by the correlation in between shear rate and viscosity, varying the TMAH concentration. In this study a solid loading of 48wt.% has been used and 0.6wt.% of TMAH has reached the lowest values of viscosity. Therefore, this TMAH concentration has been proposed as the best to disperse the ceramic particles and the maximum ζ-potential. Moreover, a better particle order has been proven to be present with 0.6% of dispersant if compared to lower values [44]. Figure 3.6 shows the study done by Li et al. on the solution compactness by setting the TMAH amount to 0wt.%, 0.3wt.% and 0.6wt.% respectively [44].

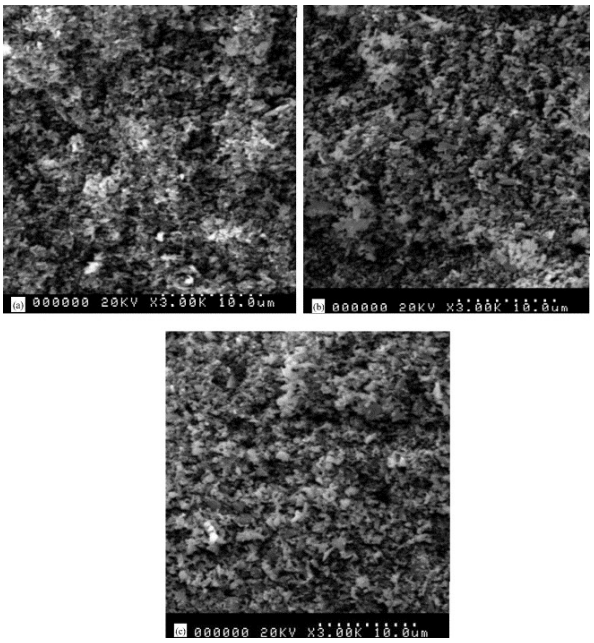

Figure 3.6: TMAH addition to a SiC paste [44]

As a consequence the dependency in between dispersant concentration and green density is an obvious conclusion [44]. In Figure 3.7 it can be seen the trend reported by Li et al. concerning the relationship in between the dispersant (TMAH) content with respect to the green density of the SiC final structure [44]. The green density tends to increase by increasing the dispersant, reaching the maximum value around 0.6wt% and than decreasing again.

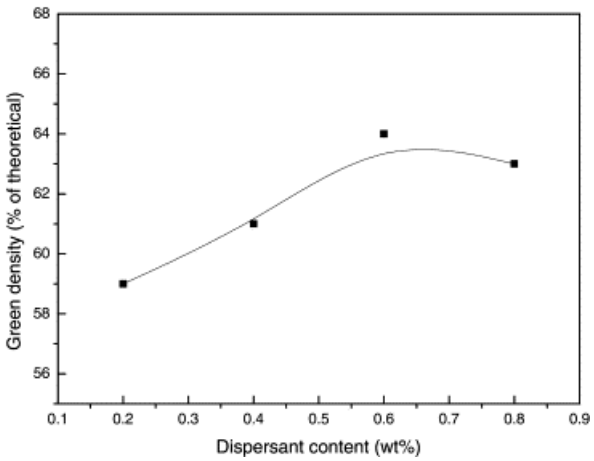

Figure 3.7: TMAH addition trend. Proportionality in between Green density and Dispersant content up to 0.6wt%.

As an outcome, it can be said that the repulsion forces act to enhance the colloidal stability. In this context, repulsion forces should be comparable to the attractive forces. The addition of TMAH enhances the presence of negative charges, improving the dissociation of silanol groups (chemical name SiOH) [44].

The ink surface in contact with the air is generally agreed to form an oxyde film. The silanol group represents the major functional group of SiC, and it is related to a connectivity of Si-O-H. Silanol groups are generally present on the surface of silica and represent the adsorption sites [94]. In water solution, the silanol group dissociates into [95]:

$$[SiOH2]^{+} \leftarrow H^{+}[SiOH] \rightarrow OH^{-}[SiO]^{-} + H2O \tag{3.1}$$

The silanol group dissociation can be boosted by the consequent addition of TMAH. As a result the addition of stabilizer changes the ζ-potential of the ceramic paste increasing the dispersion and decreasing the viscosity [41].

It must be said that TMAH is considered as a toxic material. If it is inhaled, ingested, or it comes in contact with skin it may cause several injury and death. Its inhalation may cause lung inflammation. Its burning may cause irritating, corrosive and toxic gases. Its dilution in water or fire might be corrosive and/or toxic and cause environmental contamination. If this material is heated, the vapours might form explosive mixtures with air. Environmental contamination could be caused by its fire runoff and water dilution. It can burn even if it does not ignite readily. If heated the vapours originated could be the beginning point for explosive mixtures with air [56]. Although being diluted, the TMAH aqueous solution should be handled with care to avoid any further health risk.

In solution with water its danger is limited. Swallowing or skin contact have to be avoided. It can cause skin burns and eye burns, damage the central nervous system or damage to the organs if subjected to a prolonged skin contact. It is toxic for the aquatic life having a long lasting effect. As reported into the safety datasheet, TMAH has to be handed with eye protection, gloves and facial protection [96].

3.5 RHEOLOGY INTRODUCTION

Rheology is a science that studies the correlation between thermophysical-chemical conditions of the pastes and loadings acting on the ink structure [97]. It can be summarized as the study of deformation and flow of matter. The two main aspects to consider while doing rheological analysis are the viscosity and the yield shear stress [98].

The ink is forced to flow through a nozzle under the action of an applied stress. Several are the types of extruder (as shown in Figure 3.8, from Lamnini et al. [9]), each one is characterised by the application of a certain stress. Using a screw as main stress application, the flow is caused only by a shear stress. As a consequence the rheological properties are of paramount importance for the extrusion process behaviour and filament after extrusion behaviour [30].

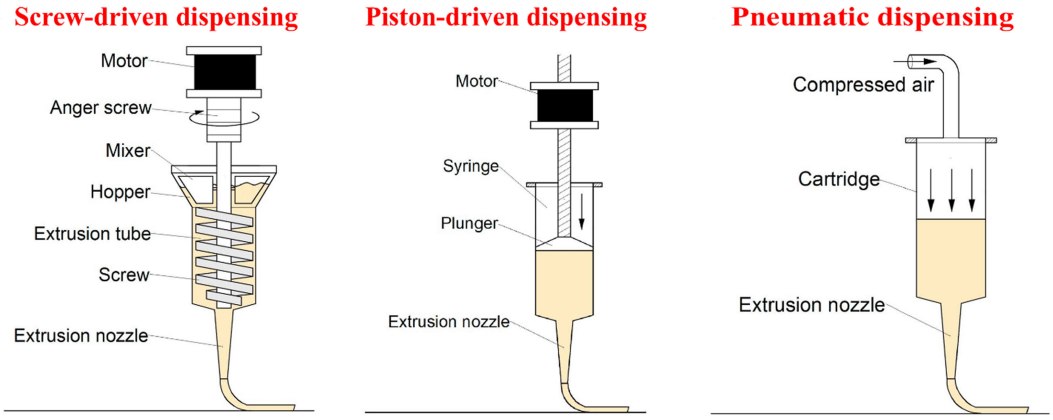

Figure 3.8: Different extrusion mechanisms. **Screw-driven process** represents the extrusion process via a shear stress applied to the ink, implying a change in viscosity and the subsequent ink deposition. **Piston-driven dispensing** represents the action of a piston that pushes the ink out of the nozzle; the main stress applied is a normal stress caused by a motor. **Pneumatic dispensing** uses a similar approach to the Piston-driven dispensing, however the pressure that extrudes the ink is generated by the action of compressed air forced to flow into the cartridge [30].

For the printing technology it is fundamental that the printing paste flows through a nozzle of a certain diameter when a stress is applied. In our case there will be no normal stress applied by external pressure, as depicted in Figure 3.8 but a screw will apply a shear stress and by tuning the speed, the flowrate will be affected. As a consequence the physico-chemical properties that allow the ink flow are fundamental to determine the extrusion process and filament behaviour after the extrusion.

The Pluronic based ink belongs to the viscoplastic material family, therefore its structure is a trade-off in between solid and liquid structure. A solid is characterised by a deformation which can be plastic or elastic due to the inter-atomic bonds, while liquid molecules are not ordered and they can flow when a shear stress is applied [99]. The viscosity can be defined as the ability of a fluid to resist the flowing behaviour. In the next section, viscosity represents one of the main characteristics useful for the rheological analysis.

The fluid behaviour can be defined by the Oswald-de Waele power law [30, 99]:

$$\tau = k * \dot{\gamma} \tag{3.2}$$

in which the shear stress (τ) is defined as the product of a constant (k) and shear rate ($\dot{\gamma}$), k represents the flow consistency.

$\dot{\gamma}$ is the first variable that impacts the apparent viscosity (η), which is useful to define and evaluate the shear stress. In the following equation n represents the flow behaviour. Generally, the apparent viscosity is dependent on the shear rate [30, 99].

$$\eta = k * (\dot{\gamma})^{n-1}. \tag{3.3}$$

The shear rate can be subsequently evaluated by:

$$\tau = k * \dot{\gamma}^{n-1} * \dot{\gamma} = \eta * \dot{\gamma}. \tag{3.4}$$

This last formula can be also written in the Hershel-Bulkley model in which it refers to the yield stress (τ_y) [100]:

$$\tau = \tau_y + K * \dot{\gamma}^n. \tag{3.5}$$

The yield stress stands for the stress at which the Storage modulus and the Loss modulus are overlapped, meaning that there is a phase change in which solid and liquid are coexisting. K stands for the viscosity parameter while n is the shear thinning coefficient.

Viscous materials can be classified according to the n parameter: Newtonian n=1 meaning that viscosity is constant and not dependent from the shear rate, $0< n <1$ is for pseudoplastic materials, dilatant materials are characterised by n>1. In pseudoplastics, viscosity and shear rate have opposite behaviour. As an example, by increasing the shear rate, the viscosity will decreases. This shear rate/viscosity correlation takes the name of shearthinning behaviour. Shear rate is the only factor that can be manipulated form the outside since viscosity is an intrinsic property of the material that can be varied indirectly.

If the materials used were dilatant fluids, the behaviour would have been the opposite. For an increase in shear rate, the viscosity undergoes a directly proportional trend [101].

The ink undergoes a mechanical deformation. In this prospect it is fundamental to introduce the Storage modulus G' which represents the amount of energy stored during the shearing and it represents an indicator of the material stiffness [102]. G" represents the Loss modulus, so the amount of energy dissipated due to the flow motion.

G' and G" can be represented by the use of a single parameter called G* [62]. The complex modulus G* is the result of the stress divided by the strain:

$$G^* = \frac{\tau}{\dot{\gamma}} \tag{3.6}$$

G^* can be decomposed in Storage modulus G' and Loss modulus G" [30]:

$$G' = G^* cos(\delta) \tag{3.7}$$

$$G" = G^* sin(\delta) \tag{3.8}$$

depending on the amplitude of the phase angle (δ). δ assumes a value of 0° for purely elastic materials and 90° for purely plastic materials.

Considering the value of these two parameters, when G'>G" the paste behaves as a solid like material, while if G">G' the material behaves like a liquid [30]. If the ink behaves as a liquid, it may be moved by the application of a shear stress, being therefore addressed by the possibility of being extruded through a 3D printer nozzle.

During the printing process the material undergoes a shear stress that increases by flowing through the nozzle, where a fast acceleration happens and a higher shear rate is reached [30]. The ink flows with an increasing acceleration towards the nozzle, reaching the maximum speed when the outlet is approached and the ink is extruded. After the deposition the ink should stay still, without being subjected to any other movement or change in the structure [103].

The ink flow through a cylindrical nozzle in case of a Newtonian fluid can be represented by the Hagen-Poiseuille law, leading to a parabolic velocity profile [30].

$$v = 2\bar{v}(1 - \left(\frac{r}{R}\right)^2) \tag{3.9}$$

$\bar{v}$ represents the average extrusion velocity, R is the nozzle diameter, r is the radial position of the particle to which the velocity relate varies according to the position: r=0 means maximum velocity, r=R means no velocity at all [104]. A general pseudoplastic ink can be represented by the same law even if not being fully described by the general Newtonian fluid characteristics.

It is generally agreed that in order to print in DIW a high G' is needed as well as a τ_y around 200 Pa [105]. High G' and τ_y values are also needed to ensure a good shape retention and structural integrity of the extruded ink filaments [106]. The high G' implies a structurally stable solid characteristic that could allow the extruded ink to keep its shape. The low τ_y implies the early crossing of G' over G", causing the sequent solid like behaviour. The addition of additives as Pluronic is of fundamental importance for the particle dispersion and viscosity adjustment, while the solid loading affects G' and G" [16]. The hydrogels affects the ζ-potential as well as the primary viscosity to allow the solid particle dispersion and avoid agglomeration. G' and G" are affected by the solid loading

since it is the only alteration in the hydrogel particle mobility.

The ink ability of flowing through small nozzle openings is related to the shear thinning behaviour, since viscosity has a reverse proportionality with shear rate for pseudoplastic. This means that by flowing down, the ink should undergo a drastic viscosity decrease while experiencing a high increase in shear rate [9].

3.5.1 Rheological measurements

For the rheological analysis an Anton Paar Modular Compact Rheometer MCR 302 (Anton Paar GmbH, Austria) has been used.

The rheometer is a rotational rheological machine, represented by very high measurement precision. It is characterised by a huge variability of configurations, By the control of specific geometrical configurations and environmental conditions it allows different measuring techniques. The modulable setup allows to measure different materials belonging to liquid, solid, viscoelastic material families. The configurations mostly used are concentric cylinders, cone-plate or parallel plate, in which the upper part is moving while the second one is held by the rheometer.

The proper configuration for a viscoelastic material such as a general ink needs the utilization of a planar upper plate. Therefore, the configuration used is a Parallel Plate (P-P) configuration. This mechanical assembling allows the plates to remain parallel during the whole measurement, keeping a constant distance of 1mm between the two surfaces. The ceramic inks has been assumed as viskoelastic materials, even if its behaviour changes strongly with temperature altering the viscosity feature due to the temperature dependent behaviour of Pluronic hydrogel. The upper plate represents the only moving part of the instrument, being also the main measuring part. A long list of sensors provided by Anton Paar allow the exact measurement of all the parameter required. The bottom plate is the dish on which the paste has to be deposited. This last surface remains perfectly still during the whole measuring process by means of tight screws. Moreover, the atmosphere can be manipulated, injecting air, N or some other gases in order to modify the behaviour of the materials tested. Moreover, a prior temperature control is required in order to permit consistent measurements. For the experiments, the parameter controlled are the temperature (fixing it as initial value to the ambient level), the upper plate spinning frequency and the loads acting on the paste. The tests have been conducted in order to set the atmospheric conditions as similar to the normal operation atmosphere as possible.

As exposed by del Manzo et al., the test can be performed in both oscillatory and rotationally mode, using the algorithms sequently explained [30].

1. **Temperature Ramp** represents the most useful algorithm for viscosity measurements. Moreover, many studies were focused on its measurements [30, 46, 55]. It gives informations concerning the viscosity, G' and G". Since the pastes are water based, and since the viscosity is strictly related to the Pluronic and ceramic powder inside, the plots will show a significant change in slope around the gelation temperature, depending on the fractions of ceramic and binder that are contained. It has been conducted in both increasing temperature and decreasing temperature, from 4°C to 23°C. It is expected that in all the plots it is possible to detect a drastic change in behaviour around 17°C, which is the standard temperature of gelation of the Pluronic. This transition temperature can slightly vary due to different concentrations of SiC in the overall amount. A starting plateau in which G">G' is the first path, than at 17°C G' becomes greater than G". This means that after 17°C the paste becomes printable since it is characterised by a solid like structure being however characterised by a liquid flowing behaviour. After a first ramp up around a temperature level of 18°C, the plateau is again obtained with G'>G". A comparison in the later mentioned results can be observed in papers like Feilden et al. in which the main behaviour evolution follows a determined path, in a final hysteresis like plot [46].

   For the Temperature Ramp results, viscosity is strongly affected by the temperature variation due to its close link to molecular motion. Considering the use of Pluronic as a binder, due to

its temperature dependent structural characteristic the ink rheological properties are severely changing.

As one of the main outputs, if G´>G" the ink has a solid like behaviour, while if G">G' it behaves as a fluid. Even if the gelation behaviour induces a liquid-like to solid-like transition into the hydrogel, the ceramic paste has a solid-like behaviour over the whole temperature range. As main consequence, the ink should be printed above the gelation temperature in order to take advantage of the viscoelastic behaviour of the hydrogel at low shear rates, maximizing shape retention ability and self-supporting capacity [30]. Some similar tests are reported into other inks (using commonly Al_2O_3) used for DIW using Pluronic as binder. These are reported into: Goyos-Ball et al. and Feilden et al. [46, 107].

The gelation behaviour can be approximated around 17°C as it can be seen in the following chapters. Above 23°C the viscosity remains almost unchanged, presenting the highest values as soon as the ambient temperature is reached. As a consequence, all the studies done are referred to the ambient temperature as 23°C [46].

2. **Shear Rate** uses a shear rate profile set by the user. For the study a 1-100 1/s variability of the shear rate been considered. The deformation caused by the spinning plate affects the complete sample. No condition of normal force absence is imposed since the main actor that produces the results is the shear stress caused by the friction created by the contact in between plate and sample.

   The study implies a rotational test which applies an increasing shear rate. As an outcome, the viscosity evolution is measured. By increasing the shear rate it is expected, due to the pseudoplastic main behaviour characteristic, that the viscosity decreases at higher shear rates [46, 49, 108, 109, 110].

   As a result, the viscosity is calculated by the rheometer generating a shear rate-viscosity plot. The relation between viscosity and shear rate is therefore highlighted. A decrease in viscosity at increasing shear rate would imply a decrease in extrusion pressure and so would facilitate the extrusion through a small nozzle [52].

3. **Shear Stress algorithm** considers the application of a shear stress on the upper paste layer and by considering the analysis conducted it gives viscosity (μ), G' and G" as outcomes. The spinning caused to the samples does not consider a twist of 360° but an oscillation of a fraction of the sample. The Shear Stress algorithm represents a useful test since according to the shear stress applied to the specimen it gives the exact values of G' and G".These values are the ones useful in order to understand which ink could be used to print the final 3D architecture. The shear stress diagram expresses the relationship between the dynamic moduli (G' and G") and the shear stress (τ) [106]. It shows the yielding behaviour of the gel. For a general stress increases, G" increases being greater than G'. When G'=G" the gel yield stress is reached, indicating that the ink is printable [46].

   The ratio in between G' and G" represented by:

$$\frac{G'}{G''} = tan(\delta) \tag{3.10}$$

   gives info about the characteristics of the ceramic ink [111].

   The yield stress τ_y is changed by the dispersion and composition of the ceramic powder. In colloidal inks τ_y can be varied by tuning the surface interactions [112]. However since the ink is not a colloidal but a hydrogel, the strength comes mainly from the Pluronic paste that works

as a particle carrier [46]. The increase in τ_y followed by the increase in ceramic powder content can be attributed to the particles shared load, requiring a larger shear stress to move the paste. This effect can be demonstrated by the Krieger-Dougherty model [113]:

$$\frac{\tau_y}{\tau_{yP}} = \left(1 - \frac{\varphi}{\varphi_m}\right)^{-2.5\varphi_m} \tag{3.11}$$

φ_m represents the volume fraction corresponding to the ideally maximum value of yield stress, it indicates the ceramic loading limit. φ represents the actual volume fraction used. τ_{yP} is the Pluronic yield stress.

By increasing the shear strain from 10Pa to 10000Pa at constant frequency of 1Hz, G' and G" have been evaluated [62].

4. **Frequency sweep** measures the material response to changes in the applied stress frequency, detecting changes in the shear rate caused and viscosity. The deformation of the sample is kept constant, fixing it at 1% of deformation, measured as a circular motion of the sample. the upper plate spinning frequency is varied between 100Hz and 0.1Hz. During the whole application of the test, the shear stress applied is kept constant. To avoid other stress applied, a boundary condition of no normal force has been imposed. As a secondary control boundary, the temperature has been fixed at 25°C. This study was investigated in order to understand the frequency up to which the screw could be spinning in order to print structures. This test can demonstrate the dependency in between screw spinning frequencies and ink printability, representing a degree of freedom to obtain an easier extrusion process [62].

   Printability (P) can be defined as the area obtained on the plate divided by the theoretical area printed ($A_t h$)[52]:

$$P = \mathrm{A}/\mathrm{A_{th}} \tag{3.12}$$

The P-P configuration used has been performed with a plate diameter of 40mm, as cited in the previous mentioned papers [46]. The distance between the plates has been set to 1 mm and the temperature to 23°C as ambient temperature since no great changes on viscosity happen later on. In temperature sweep the temperature behaviour has been tested from 4°C to 23°C. In order to do the rheological measurements of the temperature dependent parameters such as viscosity, the machine temperature has to be set as the initial temperature of the test. However, due to excessive strength in the thickness of some compositions, it has been necessary to tune the temperature in order to take advantage of the temperature dependent properties of the Pluronic, decreasing the viscosity allowing to reduce viscosity and reaching always 1mm thickness in between the two plates.

Differently than papers, no solvent trap has been used in order to keep test conditions as close as possible to the operating conditions, since the ink will work in ambient conditions, isolated by the action of the printing head.

3.5.2 Theoretical Rheological Results

As a main comparison, literature tests can be used as a reference for the ink rheological results. It is expected to obtain results similar to the ones shown by the majority of papers, considering small variations due to experimental inaccuracies.

Concerning the **Temperature ramp algorithm**, Figure 3.9 from del Manzo et al. shows the general trend of an ink formed by 30wt.% of Pluronic in an aqueous solution and 65wt.% of β-tricalcium

phosphate (β-TCP) particles [30].

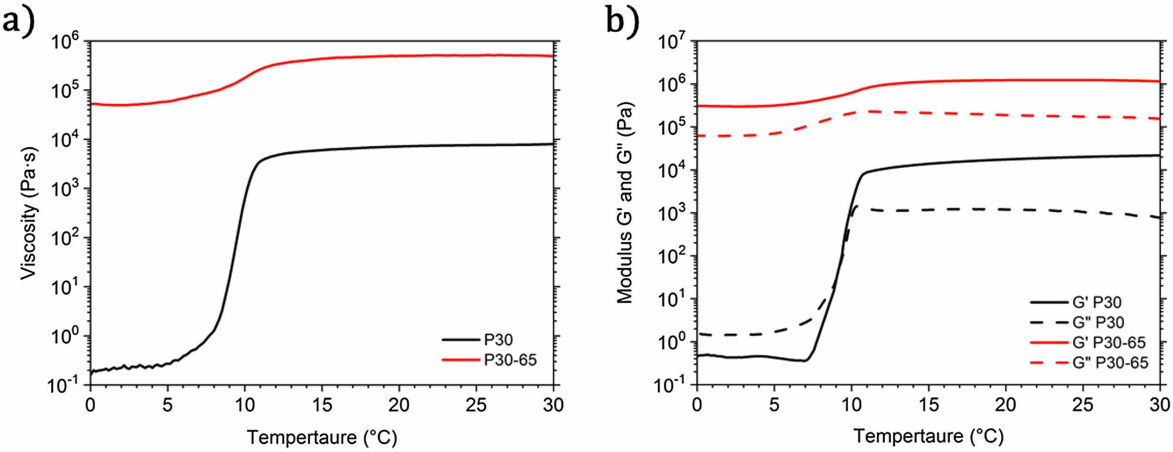

Figure 3.9: Temperature ramp algorithm comparing the pure Pluronic solution labelled as P30 with the ceramic paste in Pluronic solution P30-65 [30].

The plots represent the two main results of the temperature ramp algorithm: a viscosity dependency on temperature variation and the variation of G' and G" with temperature. As a general consideration, the plots are characterised by a similar trend, approaching a rising as soon as the transition temperature is reached. This behaviour demonstrates the theoretical behaviour of the Pluronic with respect to temperature, changing its structure from a liquid state (G">G') to a solid like state (G"<G'). P30 refers to the pure Pluronic solution. P30-65 refers to the ink formed by the Pluronic solution and ceramic particles. The red graph shows behaviour of ceramic particles embedded into the solution. By adding a ceramic powder the action of the gelation temperature is not expired but mitigated, decreasing the difference in behaviour before and after the transition temperature.

In Figure 3.9a) the viscosity trend is shown with respect to a temperature variation from 0°C to 30°C. The Pluronic solution viscosity trend (P30) approaches a gelation temperature close to 10°C, as demonstrated by Lenaerts et al., the change in state is dependent on the amount of binder added to the aqueous solution [55]. The ramp up lasts until the maximum viscosity is reached, after which a plateau represents the constant state of the solution in solid state. The ink viscosity trend (P30-65) is concretely different than the P30 trend by one order of magnitude of 1. The effect of solid particles into the hydrogel make the viscosity trend change, achieving a quasi constant state. In fact, the viscosity change across the transition temperature experiences a rise by one order of magnitude. Moreover, before the state change the P30-65 viscosity is five orders of magnitude greater than P30 while after 10°C the difference is just of one order of magnitude [30].

In Figure 3.9b) the storage and loss modulus trends are represented. In both the solutions the G' trend behaves similarly to the viscosity trend. Slightly different is the G" trend that is characterised by an attenuated variation in modulus. P30 plot of G' and G" shows a s-shaped trend in which G" crosses G' when the transition temperature of 10°C is reached. This situation demonstrates the hydrogel behaviour: before 10°C G'<G" causing a liquid behaviour, after 10°C G'>G" causing Pluronic to behave as a solid. As in figure 3.9a), the general increase in modulous due to the addition of SiC is respected. Moreover, it can be observed that by considering the final ink receipt G" does not behave as in the pure hydrogel, crossing at halfway the G' trend. In fact ink G" is distinguished by an average difference of half order of magnitude from the ink G', implying a constant progress of G"<G' [30].

The **shear rate algorithm** is shown in the next plot by del Manzo et al [30].

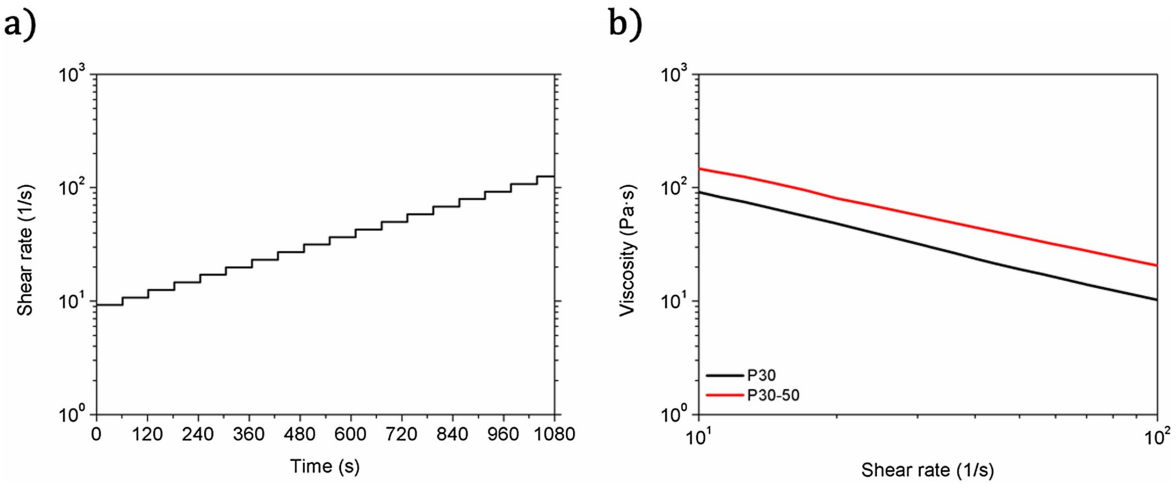

Figure 3.10: Shear Rate algorithm by Del Manzo et al. [30].

Figure 3.10a) represents the shear rate change in time applied to the ink. Each shear rate step refers to a time interval of 60s to completely detect the change in behaviour of the paste. The shear rate is changed in time by a step-wise increasing trend. In Figure 3.10b) the ink viscosity response is represented. By increasing the shear rate, as a general trend the viscosity experiences a linear decrease. The main explanation of the decrease in viscosity is related to the decrease in the inter-particle interaction due to a constant increase in shear rate. As a consequence, the final micro-structure is completely altered if compared to the original one [30].

The Pluronic viscosity response to a shear rate change behaves as a linear descending trend. By applying no shear rate the viscosity starts from its first original value, considering its original value (around 100Pa*s [30]) depending on the Pluronic paste concentration, to the final value around 10Pa*s when the shear rate reaches its maximum value of 100 1/s.

By considering the addition of the $\beta-$TCP to the Pluronic paste, the viscosity behaviour slightly decreases, following an almost parallel trend to the pure Pluronic solution. The effect of the solid volumetric percentage is seen from the beginning, causing an higher viscosity than the pure solution initial value. The plot tendency continues with a lower inclination. Consequently, the difference in between the two plots enlarges, causing an even higher ink final viscosity.

Moreover, a plot concerning the shear rate algorithm altered by the addition of stabilizer is represented [46].

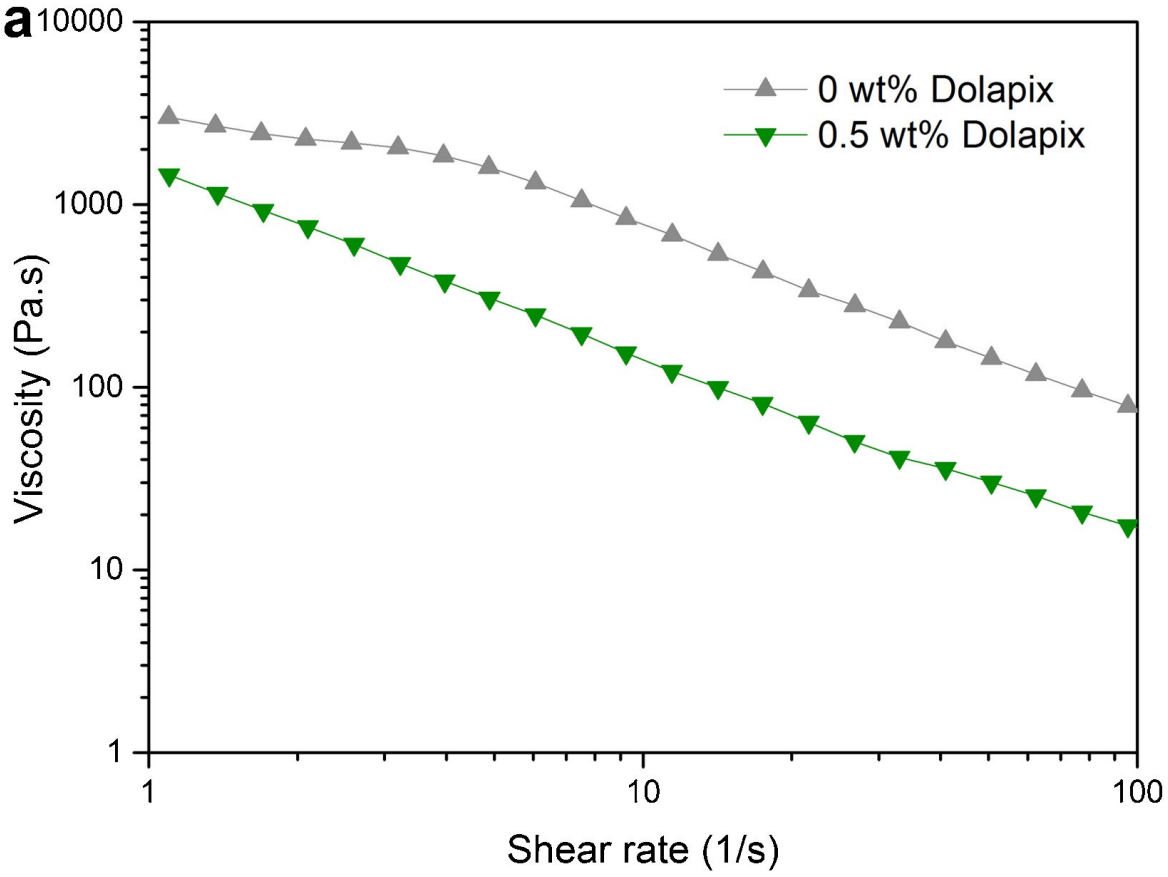

Figure 3.11: Shear Rate algorithm by Feilden et al. reporting the viscosity behaviour comparison during the Shear rate algorithm after the addition of Dolapix as ink stabilizer. The obtained plot is compared to the initial ink composition made of Al_2O_3 [46].

The stabilizer used by Feilden et al. for the Al_2O_3 ink is Dolapix with final aim of simplifying the mixing and avoiding agglomerations [46]. However, as already explained for the TMAH, the general effect of a stabilizer is to alterate the microstructure.

The receipt followed by Feilden et al. uses a Pluronic concentration of 25wt.% into an aqueous solution. The subsequent ceramic addition considers the addition of 37.5vol.% of Al_2O_3. The Dolapix has been added sequently into a second ink alternative [46].

The general decreasing rate of the shear rate plot has been newly demonstrated. However, by adding 0.5wt.% of Dolapix causes a decrease in the viscosity behaviour. The small initial plateau present in the original ink disappears by adding the binder, causing an almost linear behaviour. Moreover, the viscosity response to a shear rate change detects lower values if compared to the original ink [46].

Two examples concerning the **Shear Stress** algorithm are represented in the following. The first plot is from Alvaréz et al paper [62].

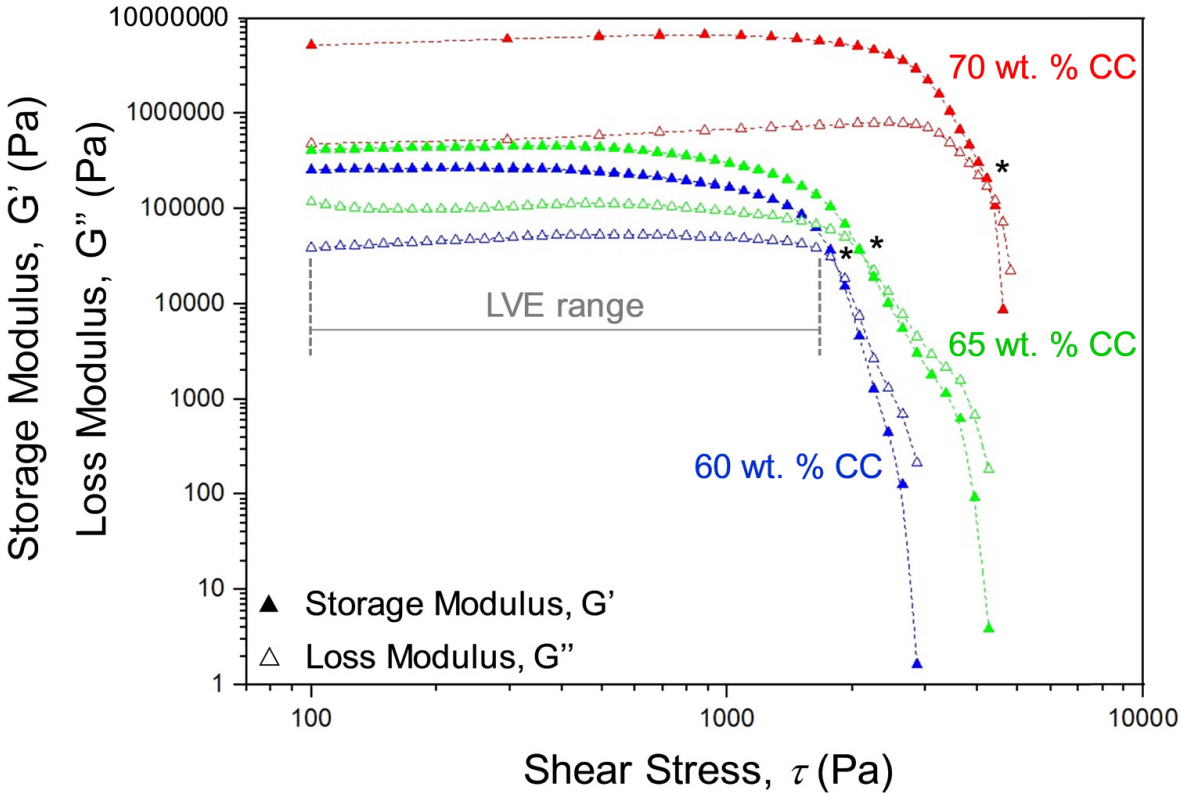

Figure 3.12: Shear Stress algorithm showing the first Linear Visco-Elastic (LVE) behaviour up to 1000Pa of shear stress. During the LVE the structure undergoes an elastic deformation that can completely recovered after the stress removal. by crossing 1000Pa the initial structure is broken causing the different trend of G' and G" [62].

Figure 3.12 represents the shear stress algorithm with different Ceramic Charges (CC) up to 70wt.% The inks used involve the solution production from an aqueous solution in which Pluronic is added. To obtain the final ceramic ink a Al_2O_3 powder is added [62].

As a primary observation, it can be seen that by varying the CC from 60wt.% to 65wt.% and 70wt.% the Storage and Loss modulus increase. The increasing behaviour of the moduli does not follow a linear increase. In fact, the largest difference in magnitude is achieved by increasing the CC from 65wt.% to 70wt.% In all the ink alternatives the crossing of the G' and G" plots happens in correspondence of the dynamic moduli decrease [62].

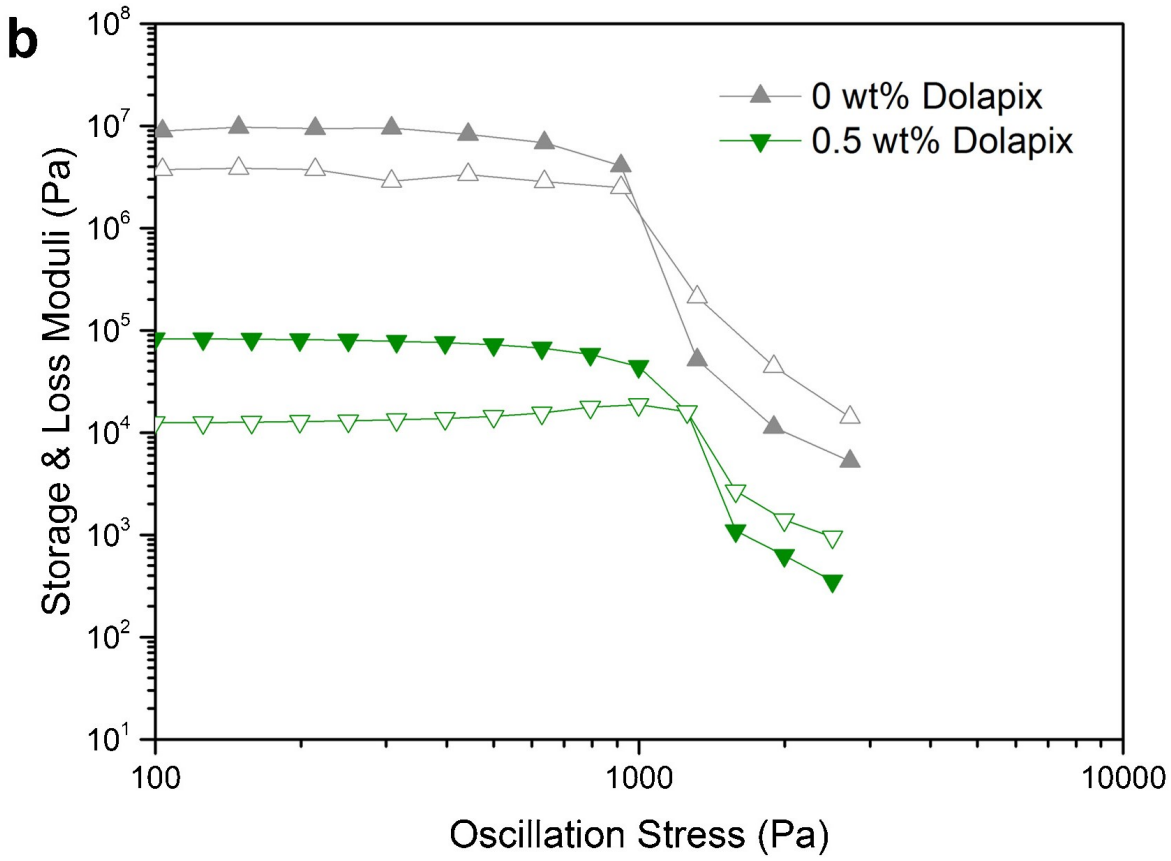

Figure 3.13: Shear Stress algorithm after Dolapix addition to the $\beta-$TCP ink [46].

The second plot refers to the study done by Feilden et al. considering the same ink formulation already cited in the shear rate algorithm: Pluronic powder is added to the aqueous solution to be used as binder, the $\beta-$TCP is added to form the ceramic ink. Dolapix has been used as ink stabilizer by Feilden et al. causing the change in G' and G" behaviour during the shear stress algorithm [46]. The plot shows that by the addition of Dolapix the oscillation stress behaviour is completely altered. By considering the general behaviour undergoing a shear stress, the $\beta-$TCP ink G' and G" decrease by feeling a logarithmic increase in shear stress [46]. The crossing of the dynamic moduli happens as already explained in the previous section. By adding the stabilizer a significant fall in the values of the two moduli happens. Two orders of magnitude are lost by the Dolapix addition of 0.5wt.% However, the general trend is respected.

The moduli crossing happens around a shear stress value of 1000Pa in both the ink alternatives. By increasing the shear stress the two ink plots are no longer addressed by a difference of two orders of magnitude but they become closer, approaching a distance of 1000Pa.

3.6 INK PREPARATION

In order to produce a paste, a binder material is needed. Pluronic F-127 has been chosen as main binder of the ceramic ink due to its versatility and easy utilization (Chapter 3.1). Pluronic is a material soluble in water at low temperatures and it allows the dispersion of ceramic particles when temperature is kept low. By controlling the amount of SiC and Pluronic it is possible to tune the suspension properties for the printing process. Viscosity is the first parameter affected by the addition of SiC particles while the Pluronic affects the thermal reversible behaviour of the hydrogel. Moreover, it has been seen that Pluronic enhances the volume of micro-porosity. The Pluronic content can be tuned to control the micro-porosity, in order to obtain the highest density and a more dense structure [86]. As demonstrated by literature, Pluronic solutions are liquid at temperatures below 17°C. In the previous examples (Figure 3.9) the transition temperature was at 10°C instead of 17°C due to a greater amount of Pluronic powder int aqueous solution, a comparison of the different amount of Pluronic can be seen in Figure 3.2.

Pluronic F-127 and SiC powders with 10μm and 40nm diameter represent the main ink components (Chapters 3.1 and 3.2). The SiC particle dimension has been chosen smaller than the commonly used in literature. This choice has been done to follow the Ferraro et al. [47]. Moreover, this procedure could increase the density and decrease porosity during the sintering process [7].

By using high temperature sintering process to sinter the ceramic structure, the TMAH undergoes a burning process being then processed by an aftertreatment. The fumes produced might have an impact on the environment and must be treated with a suitable after-treatment [114]. In this prospect, the oven and fumehood are equipped with after-treatments and filters. In our utilizations the sintering process will be conducted in controlled atmosphere with argon environment so to avoid presence of the air [90].

3.6.1 Pluronic F-127 solution preparation

For the Pluronic solution preparation the receipt followed is the one presented by the majority of the papers such as [46]. It needs deionized water 75wt.% and Pluronic F-127 powder 25wt.%.

Deionized water has to be injected into the flask in the correct amount. The addition of Pluronic to water must be done step-wise to obtain the highest homogeneity possible. Moreover, the step-wise addition of powder allows the powder agglomerates to be solubilized, and the mixing process becomes more efficient [46]. To allow the dissolution and avoid the gelation behaviour of Pluronic in water (Chapter 3.2), it is useful to work in an ice-bath. The cooling process can be obtained with ice cubes contained in a beaker. The beaker must have dimensions to completely contain the sample and the ice, including water for a complete contact between the ice and the sample. As a consequence, the solution maximum volume is limited by the maximum dimension of the bowl.

As reported in Feilden paper a greater quality is obtained by performing the Pluronic addition steps several times. Performing powder addition of some mg the mixing becomes immediately homogeneous avoiding agglomerations [46] .

Inside the beaker the samples can be stored by keeping the ice bath. The lowest temperatures can be lower than 4°C which is the temperature given by Leanerts et al. at which the Pluronic solution is assumed to be completely fluidized, so to completely avoid formation of solid like structures as well as keep the liquid structure so to obtain the best mixing efficiency possible [55].

The solution mixing must be performed by a mixer. The sample must be mounted on the mixer during the whole process to avoid further movements, compromising the mixing efficiency.

During every addition process the sample has to be kept in the ice bath to allow a cooling down and keep the temperature around acceptable values for viscosity. Since the powder addition has to be performed in episodes, the mixing process has to be subsequent to every addition process.

The production process is completed with a final cooling, to 4°C for 24h. This step permits the solution to become completely homogenized, without formation of agglomerations and bubbles. Moreover, the low temperatures permit the surface bubbles to expire, liquifying them [63]. This step has been highlighted by several papers, being fundamental to avoid ink imperfections [30, 46, 63].

For the experimental production phase, several production technologies have been followed: using a vortex mixer (heidolph Reax Top, US), using the immersion mixer (IKA Dispersers T25 easy clean digital ULTRA-TURRAX, Germany) and the last one using the magnetic stirrer (heidolph MR Hei-Tec, US).

The vortex mixer has been used to produce the firsts Pluronic samples. Only small samples are possible to be produced, each with an overall quantity of some millilitres due to instrument limitations. The immersion mixer has been used in order to obtain the highest solution amount possible (400g of overall solution). Due to the limited dimensions of the flask that can be mounted on the mixer, after the mixing process some agglomerations are present. In these two firsts steps the ice bath was not used since the production process was fast enough to avoid the gelation process.

Several other attempts have been performed in the vortex mixer with 3200rpm using also some cooling steps in an ice bath in between each mixing process, leaving the sample sufficiently long to be liquified again. In these attempts it has been noticed that by using an excessive speed some bubbles may be created. The bubbles may affect the quality and worsen the preparation since a complete liquified solution cannot be obtained as well as difficulty in mixing [62].

The last production procedure analysed is through the magnetic stirrer. This production technology allows to reach the best quality even if being more time demanding. Due to the geometrical impedances, the maximum speed was limited to 600rpm. The limited speed was related to instabilities of the magnetic stirrer, that occur crossing this limit causing unstable spinning of the magnets and damage of the sample due to the magnets hitting the glass walls. Even if the main working diameter is wider than the sample, the usable depths are shorter. Therefore, the obtainable quantities are smaller. An overall quantity of 160 ml has been produced. It has been discovered that slow spinning and low temperature allow to reach the highest quality.

No controls on the pH are required. Pluronic keeps its structure independently from the acidity of the solution and the concentration of H ions are not important for the formulation of a pseudo-plastic paste. Generally, no additives are needed, and the preparation should be easier than the one in colloidal inks [46]. TMAH has been added after the final ink preparation to stabilize the ceramic particles in the solution, increasing the final usable solid fraction.

The ice bath has been used for the final Pluronic production step while a direct cooling in a refrigerator has been used as standard final production step, keeping the solution in liquid state.

The final Pluronic paste production has been performed with a speed mixer (Hauschild Speedmixer, SMART DAC 400.4 VAC-P LR), limiting time expenditures and simplifying the preparation process. The speed mixer works similarly to the vortex mixer but it is completely automatic and involves only one revolutionary axis. It can be programmed to mix at a certain speed and for a certain time. Moreover, as a main drawback, the mixer cannot implement an ice filling volume. The ice-bath has to be performed separately to avoid agglomerations.

3.6.2 SiC paste preparation

In literature many ink alternatives are present. The binder-ceramic powder (Pluronic with SiC or Dolapix with Al_2O_3) relation has been already discussed in the previous sections, implying the prior importance of the rheological properties. The flowing behaviour of the paste has to be kept sufficient for the paste to be printable. In this context, the Pluronic use as a binder is the most recent and innovative [9, 62].

36vol.% of SiC is the volumetric solid load of the ink proposed by Feilden et al. [46]. In this

consideration, 25wt.% of Pluronic is used to produce the liquid binder (Section 3.5.1).

Ferraro et al. used a solid loading of 33.5vol.% of SiC by following a receipt involving different binders [47] . In this context, the paste has been made with two different powders: 70wt.% with 450nm diameter and specific area of 23-26 m^2/g and 30wt.% of SiC nanoparticles with 40nm diameter and >80m^2/g specific area (SkySpring Na-nomaterials, USA) even if the vast majority of experiments have been conducted with the 450nm SiC powder. This powder has been added to the multifunctional copolymer surfactant and sequently added to a water solution with a pH of 12 adjusted with NaOH 1M. As sintering aids, boron, Al_2O_3 and yttria has been used. TMAH has been used as stabilizer without specifying the correct amount. The chosen shaping method in Ferraro et al. paper was ice-templating, therefore ice-shaping agents such as PVA and Surcose [47].

As a rule, printable ceramics should be characterised by a quantity from 30vol.% to 45vol.% of ceramic powder into the gel. Below 30vol.% implies a difficult densification during sintering, mainly due to low green densities and drying cracks. Volume fraction above 45vol.% exhibited prohibitively high viscosity and poor printability [46]. However, it has been demonstrated that the rheological properties content can be tested from 0vol.% to 48vol.% of SiC [30].

As mentioned by Cai et al., geometrically complex ceramic 3D structures were produced by robo-casting using a SiC paste with a solid loading of 44vol.%. The printed paste was an aqueous colloidal ink in a dilute polymer solution characterised by high molecular weight polyethyleneimine (H-PEI), low molecular weight polyethyleneimine (L-PEI), methylcellulose and ammonium polyacrylate. This composition allowed to obtain 97% of theoretical density and 22.8% of linear shrinkage [8].

In Feilden et al.'s paper the SiC powder is added to the Pluronic solution in a step-wise manner to prepare inks with various solid loadings. Three steps are said to be sufficient for an appropriate powder distribution, followed by mixing steps at 2000 rpm for 1min, followed by a consequent cooling at 0°C in order to break agglomerates and to obtain a smooth and homogeneous structure [46].

For the final ink production, a trade-off between the various alternative has been chosen as best option. Various ink alternatives have been considered as equally usable. A solid fraction from 10vol.% to 50vol.% has been chosen as solid content range. Since the powder quantity is expressed in vol.% the usual density of SiC has to be considered to perform the calculations.

$$V = M/\rho \tag{3.13}$$

In the previous equation, V stands for the volume, M for the mass and ρ for the density. The used density value is 3.126 g/m^3 as provided by the producer. The Pluronic represents the most suitable binder for a renewable ceramic ink production. To avoid excessive viscosity related to a greater solid fraction, TMAH has been used as stabilizer.

As a first step, the Pluronic solution produced as described in Chapter 3.6.1 has to be taken by a syringe in the amount expressed in vol.% and injected in the flask. To maintain the liquid state, it should be stored in an ice bath to keep sufficient fluidity to allow the mixing. The ceramic powder addition must be done step-wise to avoid accumulation of powder in some regions of the solutions. This may impact the whole process requiring a more prolonged mixing. SiC has to be added during the freezing of the solution. For the mixing process, the vortex mixer has been used since no parts are immersed and no solution loss would be caused. The intermittent ice-bath allows to keep the solution liquid during the whole solid addition. The ceramic tends to increase the temperature of the solution due to its specific heat coefficient and different temperature, so a suitable cooling is crucial for a successful ink preparation. By adding an amount of SiC greater than 36vol.% the mixing becomes harder due to formation of solid balls. A cooling down in the refrigerator to 4°C has been proven to be useful to decrease the viscosity thanks to the thermoreversible behaviour of the binder.

In Table 3.1 the various ink formulations are reported. A volumetric fraction range from 10% to 50% has been considered. A greater solid amount has been avoided in order to respect the limits reported by [46].

Table 3.1: SiC ink receipts: 0a 0b 0c 0d represent the first experimental ink in which the production procedure was not sufficiently clever to consider them as possible to be analyzed; the subsequent numeration follows the constant increasing solid loading.

name	SiC [vol.%]	Pluronic and H_2O [vol.%]
0a	10	90
0b	15	85
0c	20	80
0d	25	75
1	30	70
2	36	64
3	40	60
4	45	55
5	48	52
6	50	50

For the printing experiments, SiC inks with an amount of 36vol.% and 45vol.% have been done. For these last receipts the speed mixer has been used. The obtained amounts with 150ml of Pluronic each required more time for the cooling in the ice bath. The mixing process started with 1800rpm, which was consequently reduced due to mixer limits. The reduction in mixing speed caused longer mixing steps in order to obtain a similar paste quality.

3.6.3 Stabilizer addition

The addition of a stabilizer represents the most dangerous and crucial step. The TMAH has been used as stabilizer [115] due to its utilization mentioned by Ferraro et al. [47]. Using a stabilizer makes the use of a greater solid content possible, increasing the SiC percentage to 45vol.% representing the maximum usable by literature. The solid content increase is followed by a consequent increase in viscosity that affects the mixing process by reducing the mixing efficiency. TMAH is necessary to decrease the viscosity of the paste admissible levels.

Pastes with TMAH content up to 13.75vol.% have been produced. However, for sake of safety the content of TMAH has been kept constant at 9.625vol.% and SiC up to 45vol.%, in order to be in line with the ink properties reported in the many papers investigated. The increase of stabilizer helps to increase the solid content keeping sufficient fluidity levels. The fixed quantities utilization has been done to limit the paste toxicity and to avoid too low SiC content that would cause structural problems due to scarcity of volumetric solid fraction [116].

The addition of the correct amount of stabilizer plays a crucial role since it strongly affects the rheological properties. It has been found that the change in suspension viscosity affects the thickness and uniformity of the top paste layer [117].

A volumetric solid fraction of 45vol.% has been chosen as representing the maximum solid fraction to allow the ink extrusion. TMAH has to be added by an appropriate pipette. The addition has been done with syringes of: 5μl, 10μl, 50μl, 100μl, 500μl, 1000μl. The final ink composition considers quantities of TMAH of: 700μl, 800μl, 900μl, corresponding to (Table 3.2) 9.625, 11 and 12.375 μl. In Table 3.1 the TMAH additions to the final ink composition have been summarised.

Table 3.2: Final ink composition considering the different TMAH contents: by increasing the stabilizer amount a letter from the alphabet has been used to name the ink. 4 stands for the ink containing 45vol.% of SiC. After f the labels report ccedd, deddd and edd due to the previous ink naming, considering "e" as 500μl pipette, "c" as 50μl pipette and "d" as 100μl pipette

name	SiC [vol.%]	Pluronic and H_2O [vol.%]	TMAH [vol.%]
4a	45	55	0.06875
4b	45	55	0.1375
4c	45	55	0.6875
4d	45	55	1.375
4e	45	55	6.875
4f	45	55	13.75
4ccedd	45	55	11
4deddd	45	55	12.375
4edd	45	55	9.625

Table 3.1 and Table 3.2 represent the inks on which rheological studies have been performed. All the four rheology algorithms have been used and the comparison with literature has been conducted.

3.7 3D PRINTER SETTINGS

To print the produced paste, a commercial 3D printer PRUSA MK3S (Prusa Research, Czeck Republic) has been used. It is a 3D printer for additive manufacturing which uses fused filament fabrication. It is a layer-by-layer technique to print a complete object, extruding the paste through a small nozzle [46]. PRUSA MK3S belongs to robocasting printing technologies in which polymer filament is used, reducing the material waste and simplifying the printing process. The main printing issue is related to the ink rheological characteristics and printability. All the rheological parameters have to be taken into account.

As many other commercial 3D printers, PRUSA printing technologies use a nozzle able to extrude plastic filaments thanks to a combination of extrusion and high temperatures. Temperatures are necessary to decrease the viscosity of organic compositions allowing the melting of the thermoplastic polymer. At the end the ink is deposited onto a printing bed, in this case a coated-metal surface. Some of the regular polymers require a heated bed to allow the adhesion of the printed material. Adhesion behaviour of a ceramic paste is attributed by the ink itself; a heated bed is therefore not needed.

The PRUSA MK3S is not able to print with different materials than the thermoplastic polymers, therefore an alteration in the assembly is needed. The printing head represents the first modification to be done in order to print with ceramics into aqueous solution. The regular PRUSA extruder involves temperatures up to 200°C, allow the melting of the thermoplastic polymers and the subsequent extrusion through the nozzle. Ceramic paste flowing through the nozzle is due to rheological properties. Moreover, the technology chosen for the ceramic paste extrusion is a screw extruder, as shown in Figure 3.14: PUREDYNE KIT B by PUREDYNE (ViscoTec Pumpen - u. Dosiertechnik, Germany). Puredyne kit B requires a maximum current level in the motor of 250mA, therefore modifications into the G-Code is needed [118]. Usually PRUSA printers work at 960mA, levels that could block the screw spinning while the fuses prevent damage in the printing head. To change the current levels, a possibility is represented by the modification of the printer firmware, implying a new coding of the main commands. The firmware modification however can lead to consistent errors related to the programming; therefore it is preferable to work with the G-Code. By testing, it was found out that the current should be set to 150mA in order to prevent a possible extrusion interruption. As a consequence, a continuous printing process is permitted.

Figure 3.14: PureDyne KIT B by Viscotec with the plastic cartridge in which the ink is stored and the red motor that makes the screw [118].

Figure 3.15 represents the 3D PRUSA i3 MK3S used to print the ceramic pastes. It is represented as given by the producer with the standard features. It mounts a plastic filament for the printing via filament melting. The three axis of movement allow the extruded motion by means of controlled screw, while the LED screen allow the direct control on the printer settings [119].

Figure 3.15: PRUSA i3 MK3S by Joseph Prusa assembly with plastic filaments mounted [119].

3.7.1 Interface design

To allow a correct printing head attachment to the main printer structure and the correct relative motion of all the axis, an adaptor has been designed and printed in PETG (FORM FUTURA, HD glass, 1.75mm diameter) with a custom made Tumaker NX PRO 3D printer. The design has been performed entirely with Solid Edge (Siemens PLM, Germany). The material choice is not crucial for the realization of the final architecture since no significant temperature variations are present nor structural loads. By using a thermoplastic polymer it was possible to insert a thread for the screw holding by using its low temperature melting property.

A correct design of the adapter involves also the support of the Prusa INDuction Autoleveling sensor (PINDA) mounted on the PRUSA printer. PINDA sensor is a vital component that allows the calibration of the PRUSA printers [120]. By keeping the sensor mounted it is possible to skip the manual calibration at each printing start, allowing the usual automatic calibration of the printer. Moreover, the interface part permits the mounting of the new printing head to the printer by means of three screws, reducing the vibrations and possible motion of the parts. The boundary conditions to be considered were the screw holes, the various geometrical intrusions due to non-planar mounting structure, height of the new nozzle and assembly of the PINDA sensor. As it can be seen in Figure 3.16 three smaller holes are present on the bottom part of the structure allowing the mounting on the printer support. The upper three holes allow the mounting of the Puredyne nozzle. Moreover, these last three holes are larger than the previous three and excavated, in order to allow the assembly of the PINDA sensor mounting structure and the use of longer screws.

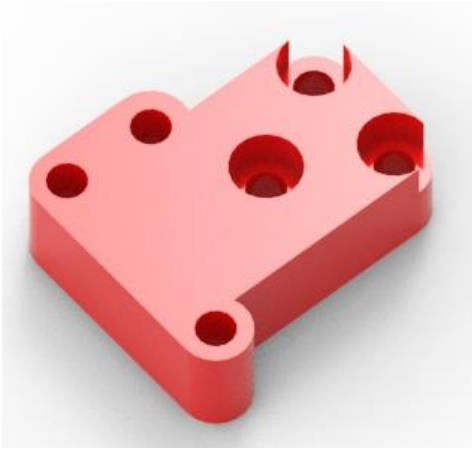

Figure 3.16: Final support structure edited with Keyshot (Siemens PLM, Germany).

3.7.2 G-Code

A second G-Code modification deals with relative positioning of sensor and printer nozzle. In fact a different relative position is caused by the printer head change, implying different settings and possible damage of the structure in case of automatic calibration. The relative distance between the new nozzle and the sensor is 1.5cm. The G-Code should be modified in order to avoid possible collisions of the new nozzle with the printing bed.

Other G-code modifications have to deal with the temperatures required by the printer to work. Generally PRUSA printers are programmed to work with thermoplastic polymers therefore a minimum bed heating is necessary to allow the printed parts to stick on the printed bed. Ceramic pastes do not need an heated bed since no melting can be obtained at low temperatures. As a consequence the G-code could be handed to avoid the nozzle heating and bed heating.

The G-Code used is subsequently reported:

```
    M350 E4 % set the micro stepping for the E0 stepper driver;
M92 E80 % used to set the steps per unit of one or more axis, referred in this case to
```

```
the E axis;
M201 E50 % set max acceleration for one or more axis;
M302 P1 % set minimum extrusion temperature, P0 disables cold extrusion checking;
M907 E150 % set motor current of the stepper;
M83 % used instead of G90 (absolute positioning) in order to put the E-axis into independent
relative motion to the other axis;
M115 U3.0.7 % use the latest firmware version;
G28 W % brings to home position all axes without mesh bed leveling;
G80 % run mesh bed leveling routine;
G0 Z22.4 % go up to nozzle position;
G4 S30 % set a timer for waiting 30 seconds;
G1 E400 F20000 % used to fill the nozzle allowing a fast extrusion;
G1 E400 F20000;
G1 E400 F20000;
G1 E400 F20000;
G1 E400 F20000;
G1 E400 F20000;
G1 E400 F20000;
G1 E400 F20000;
G1 E400 F20000;
G4 S5 % set a timer for waiting 5 seconds in order to allow the manual cleaning of the
nozzle;
G1 Y-3.0 F1000.0 % prepare to prime.
```
[121]

The current setting to 150mA instead of 250mA which is the maximum that the extruder head can withstand is due to the fact that by increasing the current over this limit the screw stopped to spin after some turns.

A compressed air supply is needed by PUREDYNE KIT B to permit the complete void filling of the nozzles by the ink in case of high viscous materials like the ceramic pastes analysed. A 4mm diameter tube can be directly inserted on the head top and the compressed air flowing has to be modulated without compromising the nozzle-head detachment due to high pressures. A limit of 0.5bar has to be respected.

To prevent oxidation and excessive solidification of the paste in the printer head, N has been used instead of the compressed air. In fact, by using this gas the oxidation reaction reported in the previous chapters can be reduced.

The multiplier setting parameter represents the factor needed to tune the spinning of the screw inside the printing head. It is a crucial parameter since the extrusion is strictly related to the shear rate imposed to the paste. In Chapter 4 the dependency of printing behaviour and rheological properties will be explained.

Due to the collision with the already printed ink, an accumulation of ink occurred on the nozzle tip. To avoid such problem, some controls similar to the already mentioned are used to move up and clean the nozzle. In this way it is possible to avoid further collision in between the already printed parts and the nozzle itself while printing.

The consequent commands are used:

```
G0 Z60 % go up of 6cm from where the nozzle is in that moment while printing;
G4 S10 % set a timer for waiting 10 seconds.
G0 Z[zlayer] % used to bring back the nozzle tip to the previous z position
```
[121]

The final codes are used to bring back to a certain position the extruder head and set all the temperatures to 0:

```
    M104 S0 % turn off temperature
G28 X0 % brings the extruder to the home X value
M84 % disable all motors.
```
[121]

3.7.3 PrusaSlicer Settings

The software used to do the G-Code extraction form the .stl file is PrusaSlicer, Prusa Research. An .stl file represents a file format native to the stereolithography CAD software created by 3D systems, the acronym stands for Standard Triangle Language (stl) [122]. PrusaSlicer is a software that takes the 3D models as .stl files or other extensions and it converts them into G-Code instructions for FFF printers or Portable Network Graphics (PNG) layers for Modified Stereolitographie Apparatus (mLSA) 3D printers [123]. By tuning the software settings it is possible to find the best configurations to allow a proper printing. Two parameters have been highlighted as most impacting on the printing performances: extrusion multiplier and layer height.

The extrusion multiplier changes the amount of flow extruded proportionally to other settings such as printer acceleration and velocity along x-axis and y-axis, layer width and layer height. By tuning the extrusion multiplier the paste printing head spins faster or slower and as a consequence the amount of ink extruded changes. By correlating these settings to the rheological analysis results explained in Chapter 4, the most suitable spinning speed of the screw can be obtained.

Layer height refers to the first layer height and layer height generally. The first layer is fundamental to work as base for the following layers, as a consequence it allows the final structure a sufficient structural integrity. A suitable height of the first layer allows to have the most structurally withstanding architecture. The other layers thickness allows to obtain a sufficient structure quality by printing, since by reducing the layer height the accuracy with which the printer produces the structure increases. The nozzle positioning is crucial for the printing process. A too low positioning blocks the extrusion process while a too high positioning does not allow a proper precision while printing. For this reason, before any printing the nozzle has to be calibrated.

3.8 MICROSTRUCTURAL CHARACTERIZATION

To complete the SiC characterization, the microstructural analysis has been conducted. The SEM has been used to detect the material distribution and the microstructure. This step has been conducted without the sintering process, as a consequence no SiC grains can be seen. The green structures however presents already the final distribution of the material, with the water evaporated and the TMAH and SiC already reacted following the chemical reactions (Eq. 3.1) presented at Chapter 3.4.

The SEM is generally used as a technique for the surface visualization and characterization [124]. SEM is one of the preferred practices to study the morphology and dimensional property of the material surfaces. The general SEM process uses high-energy beam of electrons that scan the sample surface in a raster scan pattern. A high vacuum is needed to let the primary electron beam to be scanned across the surface of a specimen. By striking the specimen a variation in the signal is generated, producing the image [125].

The utilization of electron beams implies the conductivity of the material as necessary to reproduce an image. SiC presents a not sufficient level of conductivity therefore it has been coated with Platinum (Pt) through Sputtering in Physical Vapour Deposition (PVD). The PVD is a process that exposes the specimen (called generally substrate) to some physical precursors that deposit on the substrate surface to produce a thin film deposit [126]. This deposition method allows to obtain high-quality solid materials under vacuum. It does not involve chemical reactions between the organometallic and gases [127].

For the SEM images characterization a Prisma E SEM, ThermoFisher - US, has been used.

RESULTS

In this chapter the main results are presented and explained. Moreover the results are referred to the most useful experiments conducted by considering the most probable correct results based on literature. Many samples have been tested, and the experience gathered have allowed to develop some assumptions. These hypothesis have permitted to obtain the final inks.

As a general overlook, in Section 4.1 the results concerning the Pluronic paste can be found. In Subsection 4.1.1 a comparison of the different Pluronic pastes rheological characteristic have been done. Similarly, in Section 4.2 the main SiC ink production outcomes are reported, followed by the subsequent rheological characteristics analysis in Subsection 4.2.1. As a third and last step concerning ink preparation, the TMAH addition results are reported in Section 4.3. The final rheological properties obtained after the addition have been investigated in Subsection 4.3.1.

4.1 PLURONIC F-127 PASTE

The Pluronic F-127 production process has been done as already explained in chapter 3.5.1. By following the main production recipe, 25wt.% has been added to deionized water. The solution preparation has been developed by using the three kind of mixers reported in chapter 3.5.1. All the samples have been stored at 4°C in a refrigerator for 24h after the final mixing process. The prolonged cooling has proved to be useful to eliminate impurities and agglomerations and increase the homogeneity.

The first try has been conducted by the use of a vortex mixer. The paste was produced by 3g of Pluronic and 12g of deionized water. The powder addition has been done directly at the beginning without a step-wise process, adding subsequently the dionized water. The gelation behaviour of the paste has been ignored. As a consequence, as the viscosity increased the mixing process became harder, until reaching of a maximum viscosity and mixing interruption. The mixer has been set to 3200rpm, to follow the production procedure reported in the papers and allow a proper mixing.

The subsequent picture shows the gelation behaviour of the first Pluronic paste after the 24h of storing at 4°C and sequent warming at room temperature.

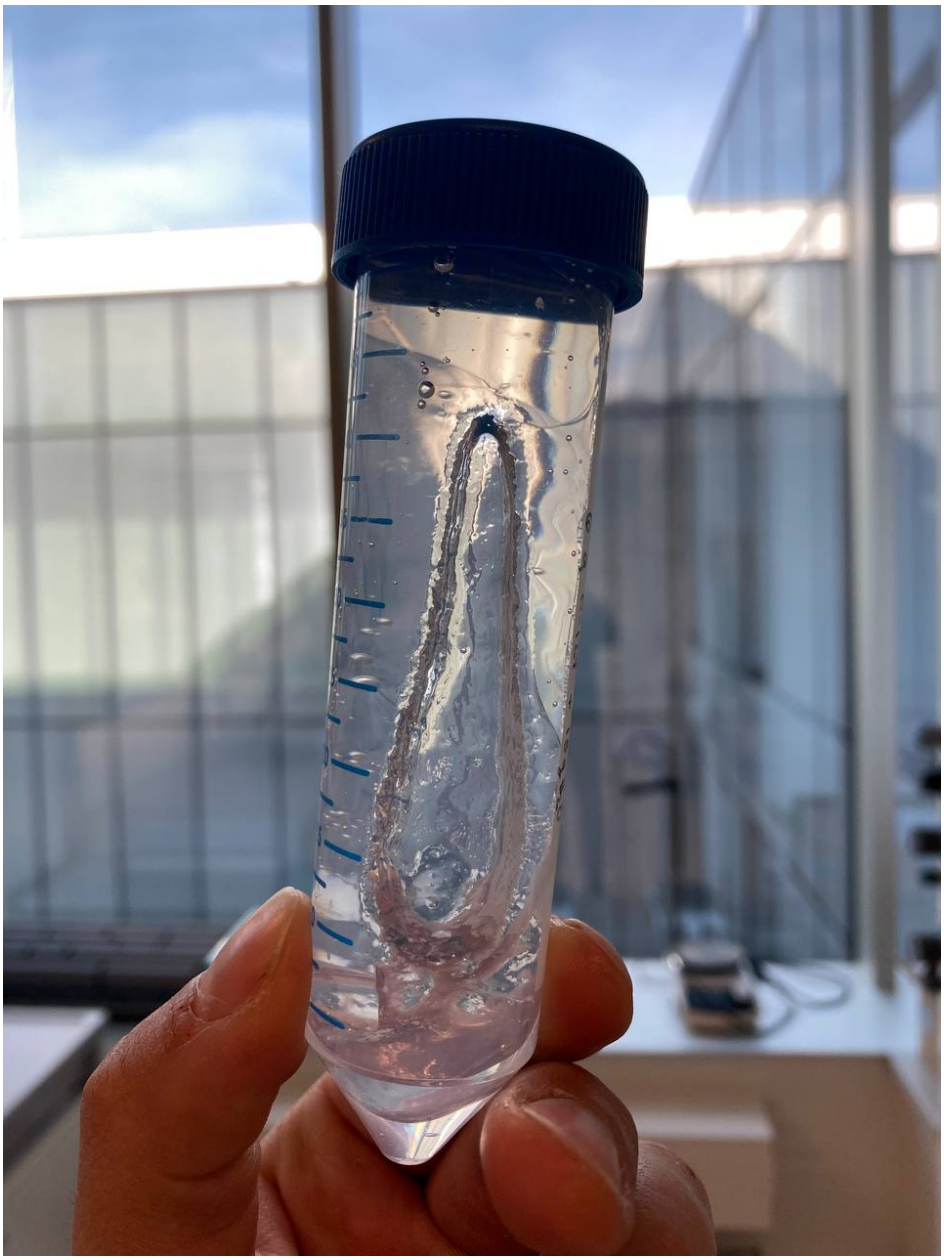

Figure 4.1: First Pluronic paste gelation behaviour sowing the agglomeration of the Pluronic and the formation of gelified parts.

As it can be seen, the gelation behaviour involves the whole structure, forming viscous structures on the surfaces of the bottle. The viscosity was too high for the mixing process. In fact, these structures were attached to the flask walls and only after a cooling into a refrigerator at 4°C the solution became liquid again.

As a second try, a Pluronic solution involving 24g overall has been made. The powder addition have been done step-wisely by dividing the total powder amount in portions. Due to the small quantities involved, six addition steps were chosen. Every powder addition step was followed by a consequent mixing at 3200rpm, as before mentioned. For this solution 18g of deionized water and 6g of Pluronic powder have been used.

Figure 4.2 shows the second Pluronic paste prepared after the cooling down step. Visibly no changes were present in between the first paste and second paste. As it can be seen, the solution is colourless like the solution represented in Figure 4.1.

Figure 4.2: Second Pluronic F-127 paste production.

By not using the cooling down steps in the ice bath, the liquid behaviour cannot be maintained. The Pluronic solution rapidly gelifies following the process explained in the previous chapters. The solution colour passes from translucent to white, as Figure 4.3 shows. In fact the dominant actor is the Pluronic gelation. The gelation affects the mixing process forming agglomerated structures that do not move. These agglomerations are subsequently dissolved by the low temperatures as soon as the solution liquidise.

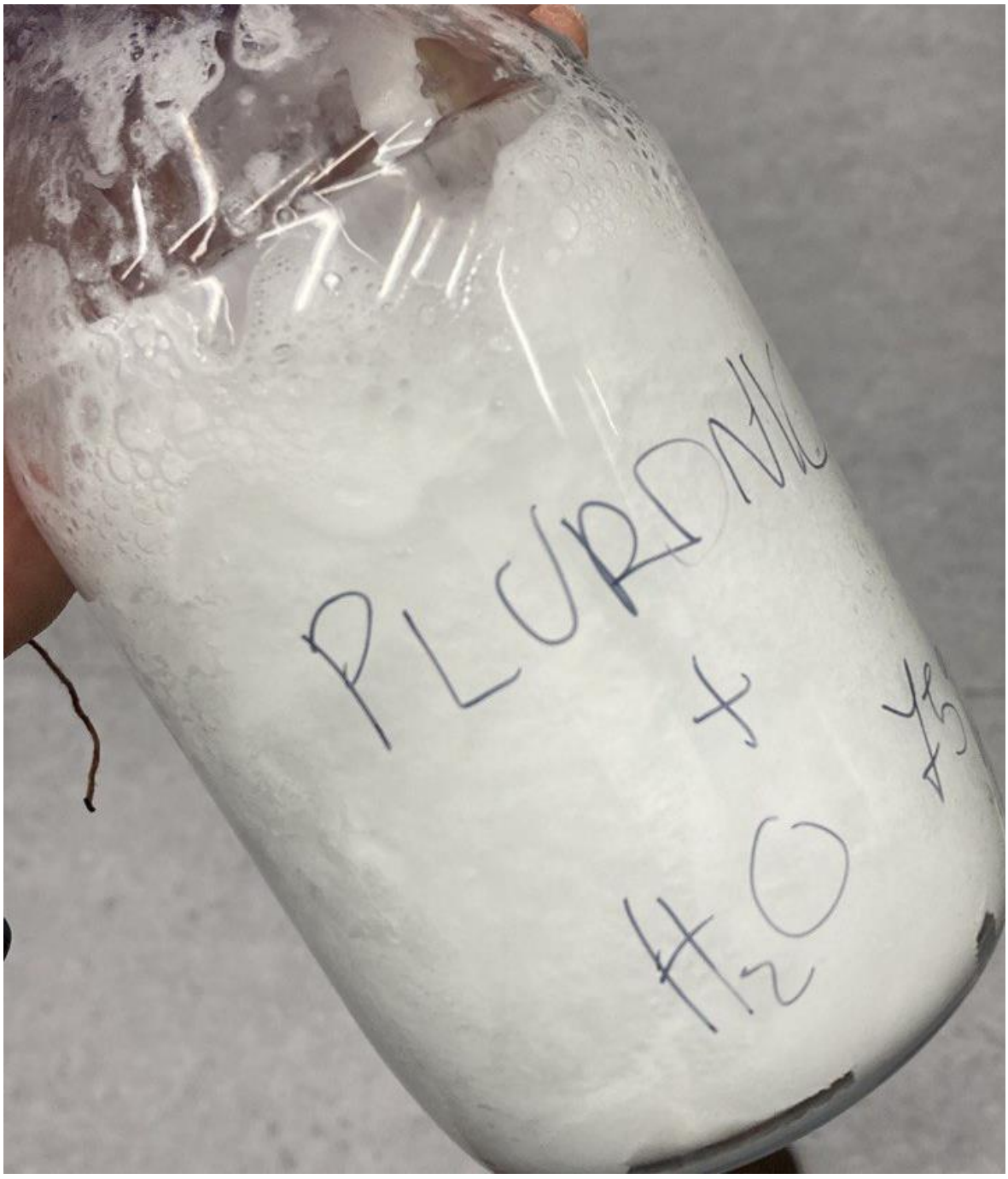

Figure 4.3: Pluronic solution getting white colour due to the wrong mixing with the immersion mixer.

The third try (Figure 4.4) has been done by implementing the ice bath as intermittent step in between each Pluronic addition. This third production try was the most similar to the second one. This process has allowed to keep a liquid structure, making the mixing process easier. This Pluronic paste has been produced with a total mass of 160g, using 25wt.% of Pluronic and the remaining deionized water. The powder addition has been done in ten steps. The weight produced will be used in the following Subsection as a name to indicate the kind of solution under study. The bottle has a higher volume than the samples used previously, as a consequence the immersion mixer wan not perfectly suitable for this dimensions. However, the final result was presenting better characteristics than the previous two solutions.

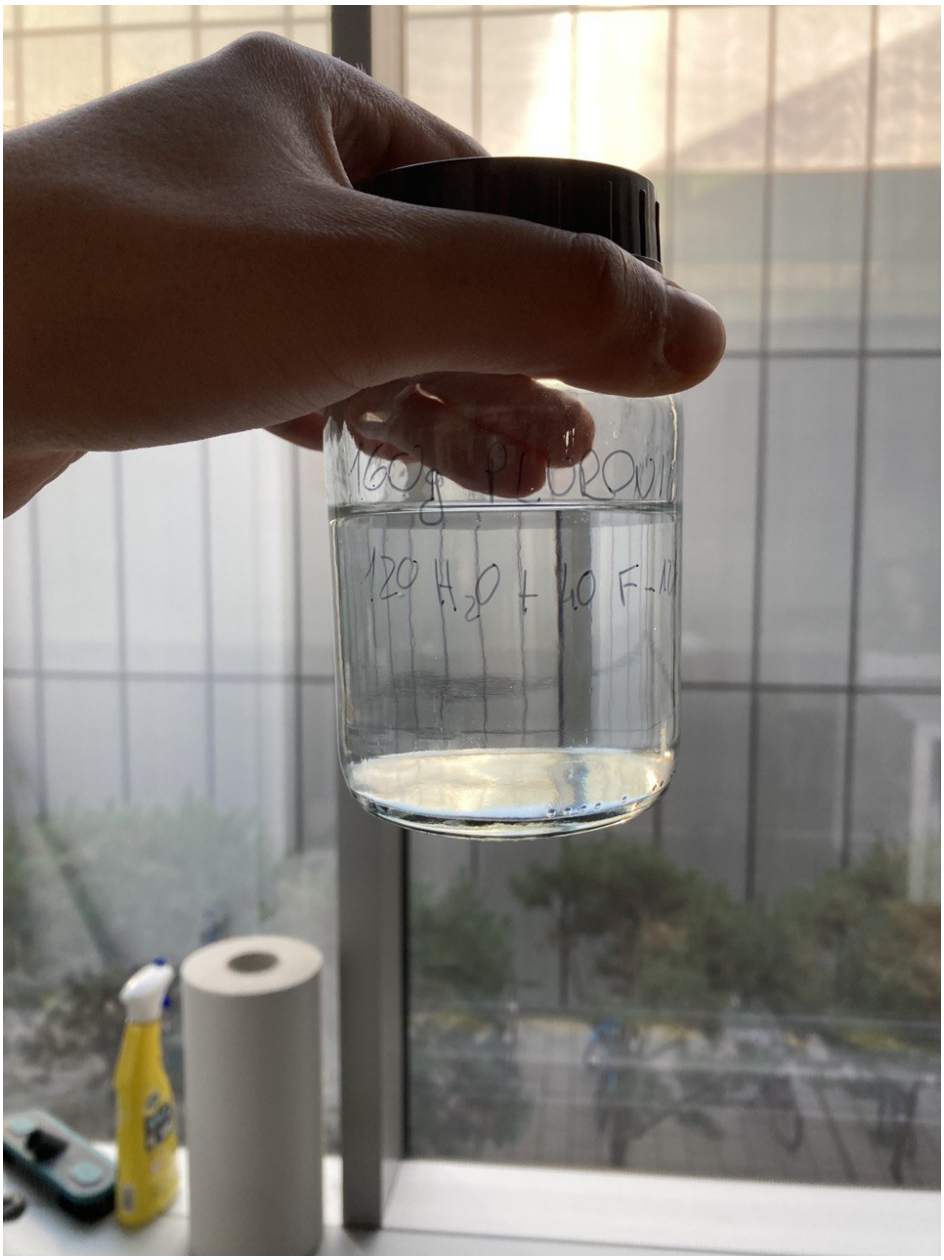

Figure 4.4: Pluronic solution produced in ice-bath in liquid state.

As the previous tries, it got a colorless structure. The visible fluidity could be similar to the water one. However by mixing it consequently, while establishing an equilibrium temperature with the ambient, the solution creates some bubbles that do not disappear as in water but require a cooling down to be liquefied again.

The need of a greater amount of Pluronic paste useful for the ink production and testing has lead to a bigger production of Pluronic. By using the immersion mixer it has been possible to increase the quantities up to 400g of solution. 100g of Pluronic has been added step-wise to the deionized water. Considering the overall amount, ten addition steps of Pluronic powder have been used. The bottle dimension compared to the mixer ones could lead to an inefficient mixing process has it has been obtained. Figure 4.3 shows the same bottle after the mixing process presenting Pluronic agglomerations and white colour. In fact, a lot of accumulations rapidly formed, increasing in dimension as soon as the mixer reached its plateau speed. Due to the big dimensions of the bottle an inefficient process has driven to a final viscous solution production. No ice bath has been used as a consequence of the big dimensions of the recipient. The ice-bath utilization may have prevented this by keeping the viscosity of the solution low.

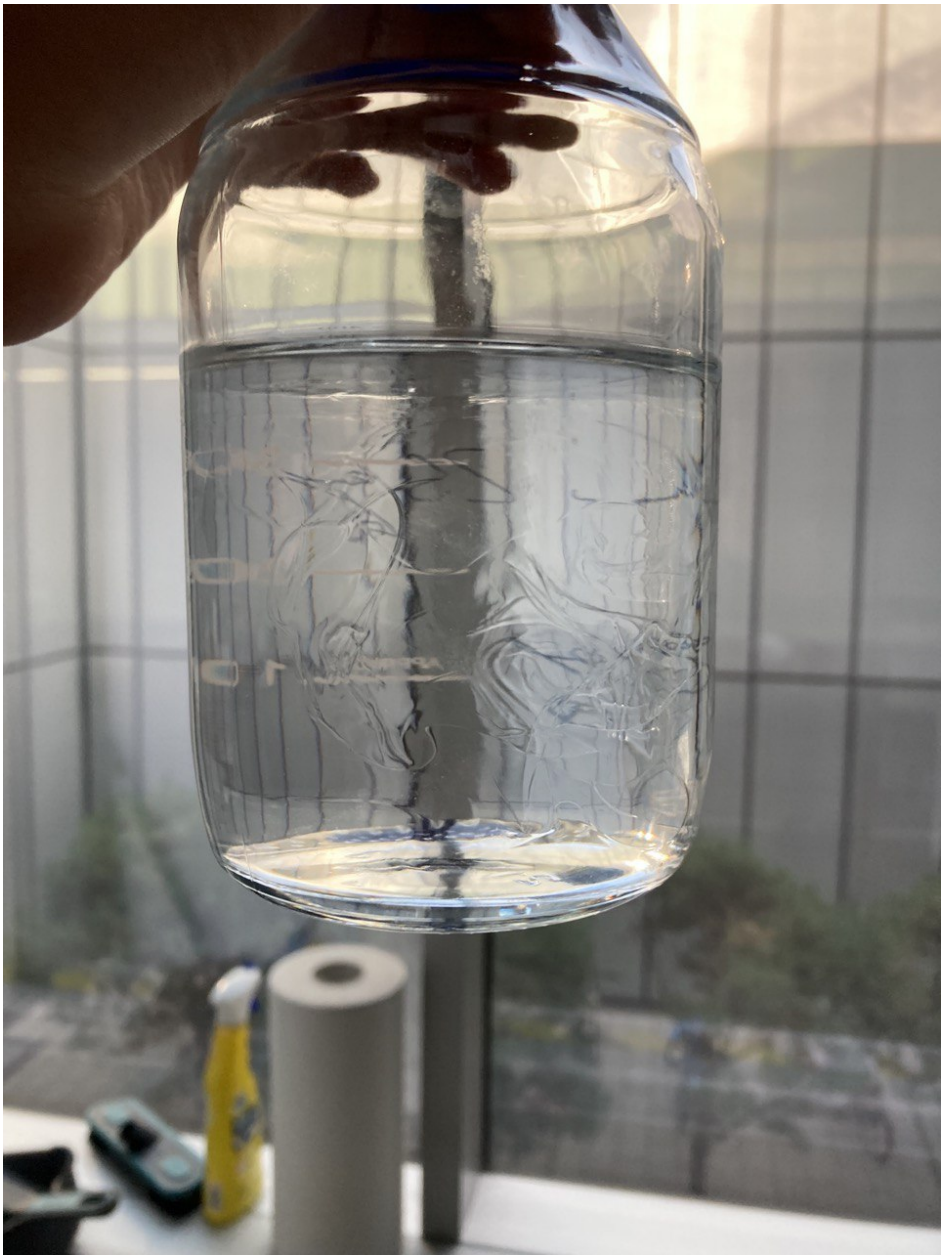

Figure 4.5: Pluronic solution with immersion mixer after been stored at 4°C in the refrigerator. A general inhomogeneity can be observes throughout the whole solution.

The previous figure shows the Pluronic solution after a week stored at 4°C in the refrigerator. As it can be seen the solution is affected by inhomogeneities. The presence of this alterations are due to the non perfect mixing of the powder with the deionized water. In fact, micelle agglomerate forming long chains, behaving like a soap in water [55, 57, 58].

To solve the inhomogeneity issue the solution has been stored again in the refrigerator for a week. At the end of this period, the structure looked like the previous.

The last production procedure was conducted with a magnetic stirrer. This technology has allowed the implementation of an ice bath directly in the production process. A basin full of ice has been put on the stirrer. Inside this ice recipient the beaker has been fixed. By firstly adding the deionized water and consequently the Pluronic powder. Several powder additions have been done, trying to increase the homogeneity during the mixing as much as possible. The mixing process has been performed by

the immersion of a magnet that spins by the action of the magnetic field. The magnet has to be extracted at the end of the process my means of an external magnet.

Figure 4.6: Pluronic solution with magnetic stirrer.

After the mixing, the solution has been moved into the bottle to be then stored in the refrigerator. By decanting some bubbles emerged. Finally the bottle has been stored into the refrigerator at 4°C for 24h. This last cooling step has allowed to the bubbles to disappear, reaching optimal visible conditions similar to the ice bath sample in Figure 4.4, as expressed by Feilden et al. [46].

4.1.1 Rheological analysis

To perform a quality comparison, the rheological properties of the Pluronic solutions produced by the three different production technologies have been studied involving mainly viscosity and temperature dependent behaviour. The Pluronic rheological analysis has been conducted with the Temperature Ramp algorithm, allowing a deep study of the temperature dependent characteristics. For any solution, two analysis have been conducted to be sure the analysis are consistent. The acquisition involved 120 data points per study. All the tests have been repeated two times in order to consider only consistent results and avoid possible inaccuracies. As the results were consistent only one plot significant for each solution is shown.

Considering the Pluronic temperature-dependent behaviour, the minimum temperature has been set to 4°C, representing the temperature at which the Pluronic solution is completely liquid [55]. The algorithm ending temperature has been set to 23°C. The main parameters compared are the viscos-

ity, storage and loss modulus (G' and G"). For all these properties 120 value acquisitions have been performed with an acquisition rate of measurement every increase of 0.1583°C in temperature. The temperature increase steps of 0.1583°C have been maintained for all the further studies involving the Temperature Ramp algorithm.

The atmosphere inside the rheometer has been kept isolated from the outside so to avoid intrusion of contaminating molecules and interaction with excessive air.

Temperature Ramp Algorithm

The Temperature Ramp Algorithm tests have been conducted in both increasing temperature and decreasing temperature in order to verify the hydrogel rheological characteristics after a thermal cycle. Therefore from the analysis of the results obtained it is possible to perform a quality comparison, finding the best Pluronic solution prepared. In the following plots it is possible to see the main outputs related to the Pluronic solution preparation.

The main Pluronic temperature dependent properties studied have been made in comparison with the paper by Lenaerts et al., which is considered to be the main reference for this solution preparation [55]. Moreover, the rheological behaviour of Pluronic solutions can be compared to the already studied by Jalaal et al. [61].

As explained in Chapter 3.1, Pluronic is an hydrogel characterised by a temperature dependent viscosity. The first parameter to be explained is the temperature dependent viscosity behaviour. As reported in Figure 4.7, by increasing the temperature the micelle present in the solution start to agglomerate, causing as a consequence an increase in the overall viscosity. This increasing viscosity attitude is expected to happen around 17°C with a 25wt.% Pluronic content [30, 46]. The starting viscosity value can be addressed around 100mPa*s. Immediately before approaching the transition temperature, the average viscosity value changes, experiencing an increase and differentiation among the three solutions. By getting closer to a thermal equilibrium with the environment, all the samples experience an increase in viscosity. Considering the temperature range between 4°C and 17°C the viscosities are all around 100 mPa*s.

The "y" axis is labelled with "Complex Viscosity" since it expresses the viscosity found by the machine after a calculation of the parameters discovered during the acquisition. In fact, a direct viscosity measurement was possible only by performing other analysis not dealing with temperature present in the rheometer handbook. However, their implementation was not easy to do.

By considering the final plots related to the G' and G" comparison during the temperature ramp algorithm in both temperature increase and temperature decrease, similar conclusions could be made.

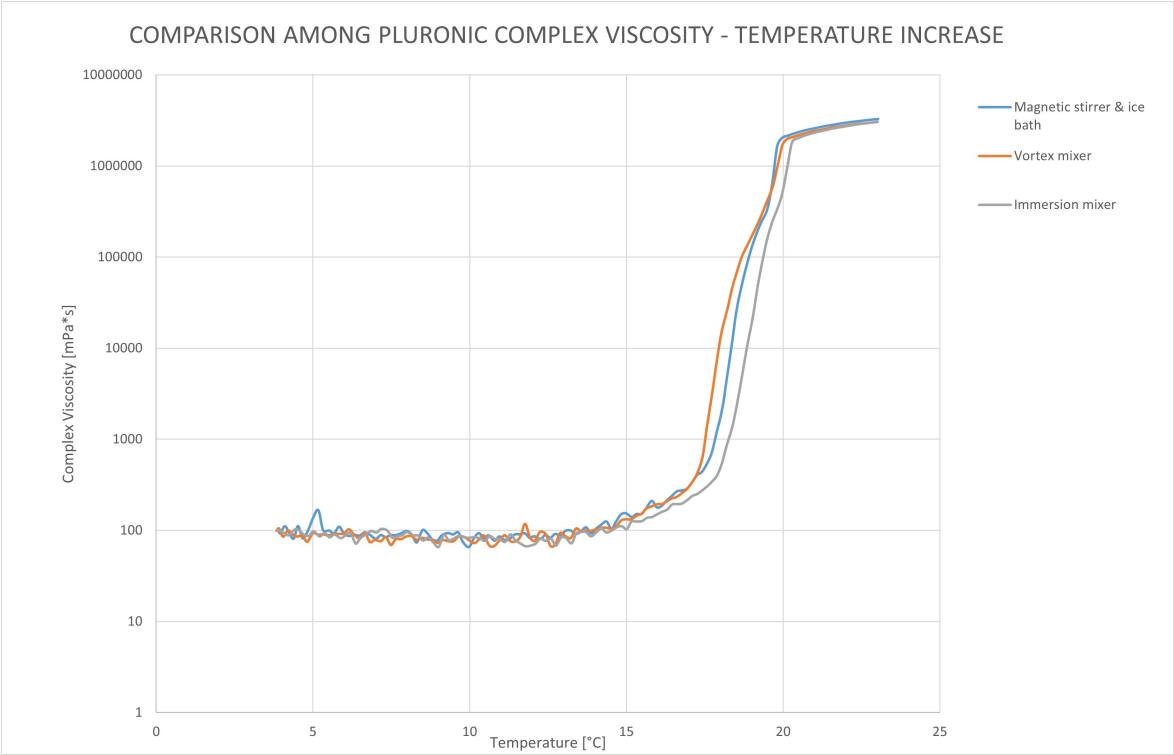

Figure 4.7: Comparison among Pluronic complex viscosities during Temperature Increase algorithm.

From 4°C the viscosities are affected by imperfect measurements around 100mPa*s and some peaks of the different solutions can be distinguished. These trends are noise visible in the first range since their module is up to some tens, while by increasing the viscosity they are no more visible due to the higher order of magnitude considered by the logarithmic scale. By approaching the ramp up, the noise flattens until a homogeneous line is obtained at the highest magnitude levels.

The first ramp up is experienced by the Pluronic solution obtained in the vortex mixer happening from 17°C to 20°C.

By considering the other two solutions, the one obtained in an ice bath was the one characterised by the apparent highest quality since it is more similar to the studies done by Lenaerts et al. but as shown during the transition phase it represents a trade off in between the previously mentioned solution and the one obtained by the immersion mixer [55]. These two have a transition phase between 17.5°C and 20°C. The immersion mixer caused solution agglomeration during the mixing phase and the subsequent imperfection in the liquid solution after the final cooling. The last increasing trend is characterised by a delay of approximately 1°C with respect to the solution obtained in the ice bath.

By completing the transition phase all the solution approach a final ambient value around $3*10^6$mPa*s, uniforming and following a unique trend. As before the final trend is reached firstly by the Pluronic obtained in the ice-bath, and than by the other two solutions.

During the transition phase a slight difference in temperature produces the sooner or later change in state in the solutions. This change is approximately of 0.5°C, difference that goes reducing by increasing the temperature. The first ramp up present in Figure 4.7 is done by the vortex mixer Pluronic solution. The immersion mixer caused agglomerations during the mixing process and the latest ramp up in the Temperature Ramp algorithm, therefore it may be addressed by a lower quality. After the viscosities ramp up, all the values stabilize into a unique plot, being not affected by instabilties.

During the liquid phase, some instabilities are visible due to the logarithmic scale. They can be assumed to be present during the whole measuring phase but they become negligible by increasing the orders of magnitude.

During the temperature decrease algorithm the complex viscosity in all the three solution alternatives are of the same value, showing the final viscosity value of the hydrogel and the effect of the temperature increase that after reaching the final viscosity value does not affect any more changes. During the transition temperature some discrepancies among the solutions are still visible presenting a change in the overall quality. Moreover, the quality affect the start of the transition state, happening before in the 400g bottle. After the transition temperature, approaching the liquid state detected below 17°C some noise in the main trend are visible, moving around a final average value of 100mPa*s.

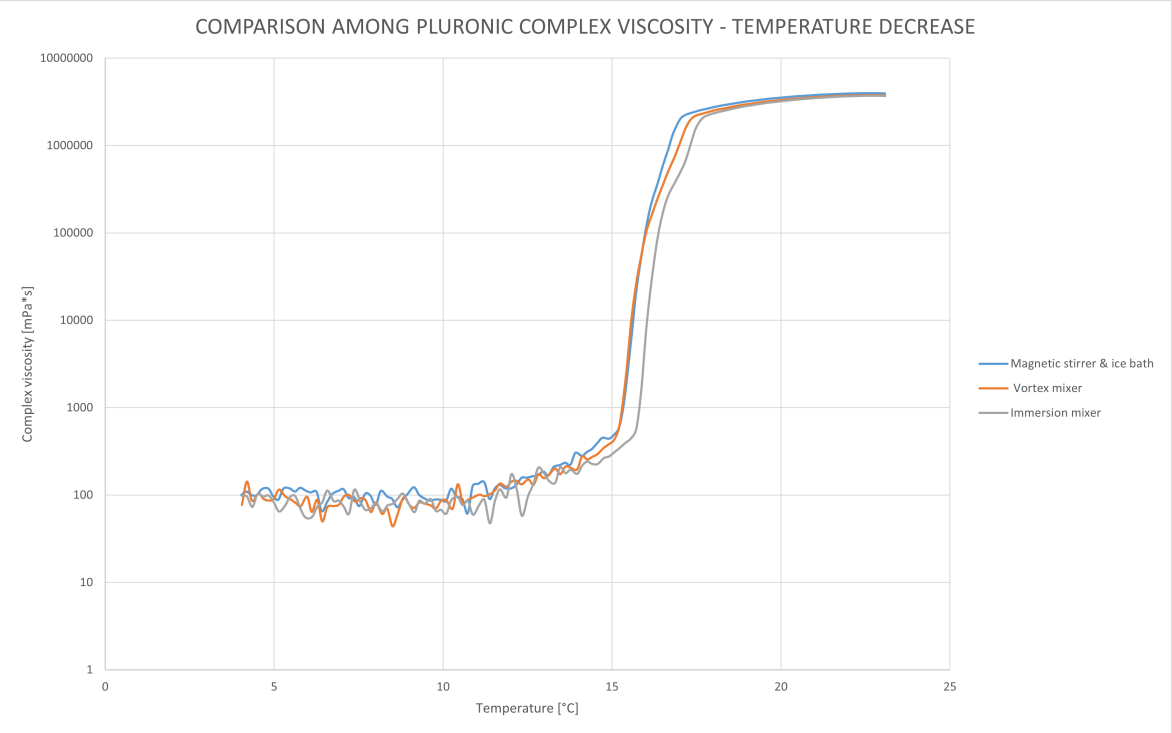

Figure 4.8: Comparison among Pluronic complex viscosities during Temperature Decrease algorithm.

As already mentioned during the Temperature Increase algorithm, the Pluronic solution obtained with the immersion mixer enters into the transition zone with 17°C. During the temperature decrease this solution changes state at 17.5°C, being the first to subdue a viscosity change.

The other two solutions are behaving similarly, being overlapped by the vast majority of the decreasing trend. The transition temperature is detected around 16.5-17°C, happening later than the previous mentioned solution.

By reaching the 400mPa*s all the solution a lower sloped trend going into the liquidus area. Considering the liquid state solutions, the already mentioned noise trend is visible. The not-stable fashion leads to the final liquid viscosity value, the same referred in the temperature increase algorithm as initial value. This represents the completed change in state of the hydrogel solution by lowering the temperature moving towards 4°C.

Similarly by looking at Figure 4.8 the viscosity collapse happen in between 17.5°C and 15°C. Two over three production technologies are almost superimposable. The third one differentiates 0.5°C from the others.

The second fundamental outcome of the temperature ramp algorithm is the comparison among G' and G". As a prior consideration, it can be seen in Figure 4.8 that the overall shape of the functions is similar to the viscosity trend. The transition phase in between liquid and solid state is sloped with a lower angle, differentiating in between storage and loss modulous.

Generally, it can be analysed that in the temperature increase algorithm the G" module is greater than the G' module at low temperatures. By considering the temperature range before the phase transition, Pluronic solutions are liquid. As presented in chapter 3.4, G" exceeds G' when the solution is in liquid state, while G' crosses G" as soon as the transition step has been reached. In the last section of the plots, all the G' and G" tend to assume a constant unique value $18*10^3$ and $5*10^3$ respectively.

As already represented in the viscosity plots, the liquid state solutions are distinguished by a non-stable trend that leads to the more stable transition phase. This behaviour is maintained in both G' and G" moduli. More marked alterations in the general trends are present into the G' plots for all the three solutions due to the logarithmic scale. The G" presents a more stable fashion.

In all the plots, the transition phase happens by reaching a value of G' and G" in a range from 20 to 30 Pa.

By considering G' and G" during the temperature increase, the only concrete differences are during the phase transitions. In fact, a difference of 0.5°C differentiates the various solution alternatives during the ramp up.

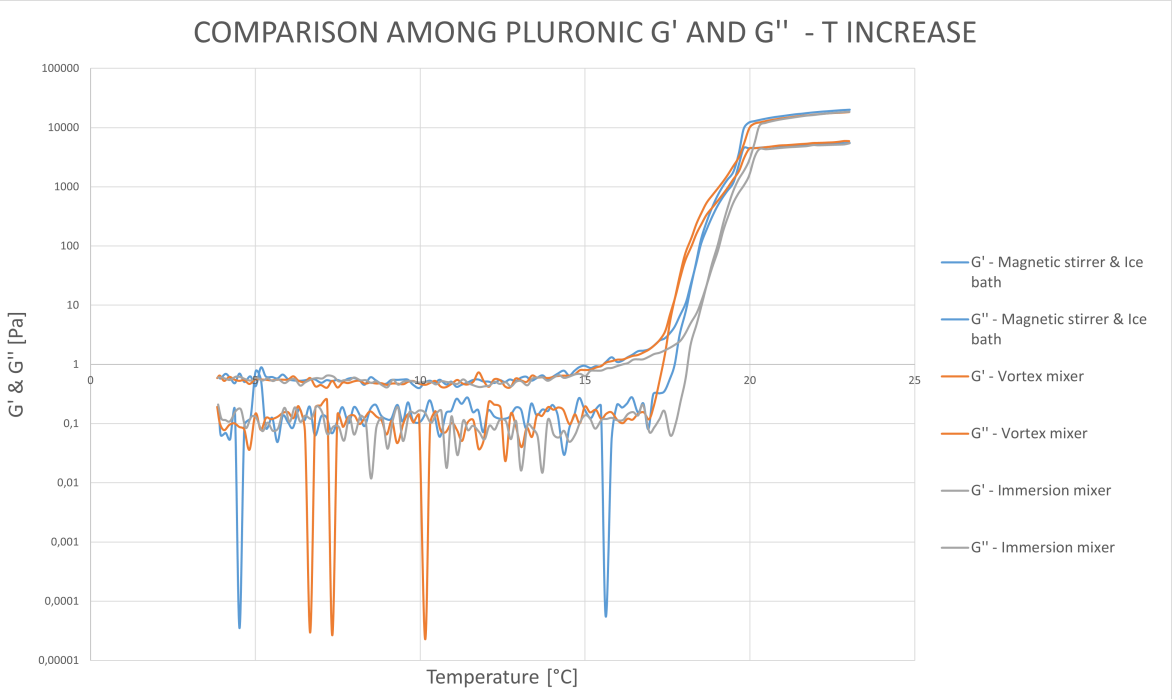

Figure 4.9: Comparison among Pluronic G' and G" moduli during the temperature increase algorithm.

As already explained for the viscosity plots, the solution obtained in the immersion mixer is the last one to undergo the transition phase. This characteristic is present in both the moduli. The effective transition phase happens at 18.5°C when G' becomes greater than G". However, the plot of G' experiences the most stable trend if compared to the same factor of the other two solutions.

The transition phase slightly changes between the ice bath solution and the one using the usual mixer. The temperature that is marked to be the main actor of this phase is 18.21°C for the ice bath and 17.89°C for the normal mixer. However, these two solution alternatives tend to become closer by increasing the temperature, reaching the final state sooner with respect to the already mentioned solution.

The main considerations done for the temperate increase algorithm can be applied to the temperature decrease algorithm since at ambient temperature the G' module is higher than the G" module.

G' reaches values in the order of 20*10^{3}Pa at 23°C while G" are in the order of 5*10^{3}Pa.

In the temperature decrease algorithm, more differences can be detected. Due to some errors during the measuring phase, the G' of two solution alternatives are severely lower in module than the other one. By considering the G", they differentiate for less than 0-5°C in between each one during the transition phase.

A marked difference in between the Temperature Increase algorithm and the temperature decrease algorithm is represented by the huge difference in between G' moduli of the 400g solution (the one produced by the immersion mixer) and the 160g solution (the one produced by the vortex mixer). It can be seen that these values in between 15°C and 4°C reach a module in the order of 10-4Pa. During the temperature increase algorithm all the G' in the liquid phase were in the order of 10-1Pa.

All the phase transitions happen at a temperature close to 15.5°C.

The main G" trend follows a similar approach to the temperature increase algorithm, the noise stabilizes when the solution becomes solid after the transition phase or when the solution is completely liquid by decreasing the temperature.

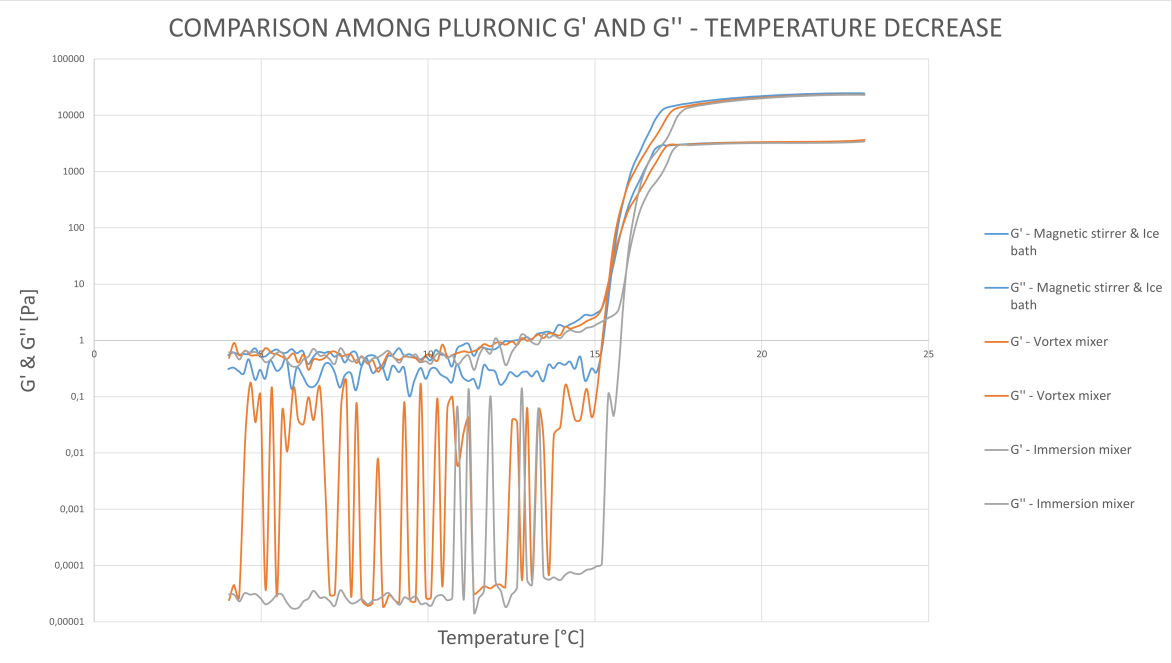

Figure 4.10: Comparison among Pluronic G' and G" moduli during the temperature decrease algorithm.

The 400g solution reaches the minimum G' value after experienced the phase change. Noise in the evaluation is present between 10°C and 15°C. After these instabilities, G' reaches a more stable value of 2*10-4Pa. The huge variation in module could be explained as a more difficult process of homogenization into the hydrogel solution. A possible resolution could be represented by a longer cooling down process at 4°C. As proven with the Pluronic solution produced, after a second and longer stay in the refrigerator the solution was completely homogenized.

The 160g solution is the one characterised by the most significant alteration in value acquisition. After the transition temperature the G' module starts to vary in between 0.1Pa and 10-4Pa. A stable value acquisition has never been obtained.

G' of the ice bath solution during the temperature decrease algorithm tend to be more similar to the one of the temperature increase algorithm. Moreover, the G' value keeps an average in a range in

between 1Pa and 0.1Pa. This difference is greater in value than 0.1-0.001.

4.2 SiC INK OUTCOME

As already written in Chapter 3.2, the SiC paste production follows several steps. The addition of the powder was performed step-wise to allow a proper SiC distribution and avoid agglomerations. However, by increasing the solid load the viscosity changed. By considering the lowest amounts of SiC added, the mixing effect was more successful when the solid load was low and the viscosity in a suitable value.

For the production, SiC 40nm powder by SkySpring has been used. This low dimension particle has been chosen according to the work done by Ferraro et al. since a low diameter of the particle can help in increasing the density and sample compactness [47].

SiC powder has to be added to a Pluronic solution which has been kept at a temperature below or equal to 4°C in order to lower its viscosity. In this way a successful mixing can happen by performing it when the solution is still liquid. If the temperature of the solution approaches the transition temperature (Chapter 3.1) the mixing is impossible to happen due to high viscosities involved.

SiC quantities used are reported in Table 3.1. The proportions of solid load are expressed in vol.% since in the vast majority of the papers it is expressed as a solid loading. However, the volumetric measurement of a powder is difficult. As a consequence, the use of the powder density given by the powder producer SkySpring has been used to calculate the volume through the mass. By considering the SiC density of $3.126 g/m^3$, the correct volumetric quantities have been obtained.

While the Pluronic solution is stored in an ice bath to keep its temperature lower than the transition temperature the powder was added. Normally for the first inks produced into the small bottles an average of six spoons of 2g each have been used. For bigger quantities also the amout of powder has been increased as well as the steps needed for the powder addition.

As last step, the ink has to undergo a final cooling at 4°C so to allow a second liquefaction of the solution thanks to the Pluronic temperature dependent behaviour. In this way, even not mixed solution portions could become part of the final ink without altering the rheological behaviour. The homogenization during the liquefaction avoids the agglomeration formation, solving the incorrect mixing processes. In fact, a solid part inside the complete fluid solution changes the final rheological behaviour (Chapter 3.5). The final cooling down should not exceed 24h so to avoid the solution separation. As seen in some of the experiments, an excessive long cooling causes the separation of solid loading and liquid solution. The solid fraction can be re-dispersed by performing some mixings and a final cooling. As it can be seen into the next picture, the separation is visible into a 20vol.% SiC ink.

Figure 4.11: Solution separation into a 20vol.% SiC ink.

As a general procedure, an additional mixing, performed with the vortex mixer, has been done after the final cooling. This mixing was useful usually in low solid content inks because by increasing the SiC content the final viscosity was high enough to not generate any mixing in the paste structure. By taking advantage of the ink liquefaction a mixing in an ink with the lowest viscosity possible permits to increase the homogeneity. However, when the solid loading exceeded 30vol.% the mixing did not produce any changes since the viscosity was too high and the ink did not move.

By considering a second ink production by a direct addition of the whole solid fraction chosen (20vol.%) to the Pluronic paste, some distinguishing characteristics could be seen at first look after the final production procedure. By looking at the next figure, some bubbles are preset on the solution surface. A complete and prolonged cooling down of the solution did not produce any change.

Figure 4.12: 20vol.% SiC ink with surface bubbles.

The bubbles may affect the final rheological behaviour of the ink For sake of rheological measurements, the state of the paste should be homogeneous to generate proper study data. Air bubbles theoretically present a lower viscosity than the SiC paste. Powder agglomerations cause higher viscosity values. During the measuring phase the rheometer detects all the various data while spinning the upper plate. As a consequence, state variations in the paste must be avoided, using only homogeneous pastes. Moreover, the presence of air bubbles may affect the printing phase. Their popping may generate non existent structures and affect the ink deposition on the printing bed.

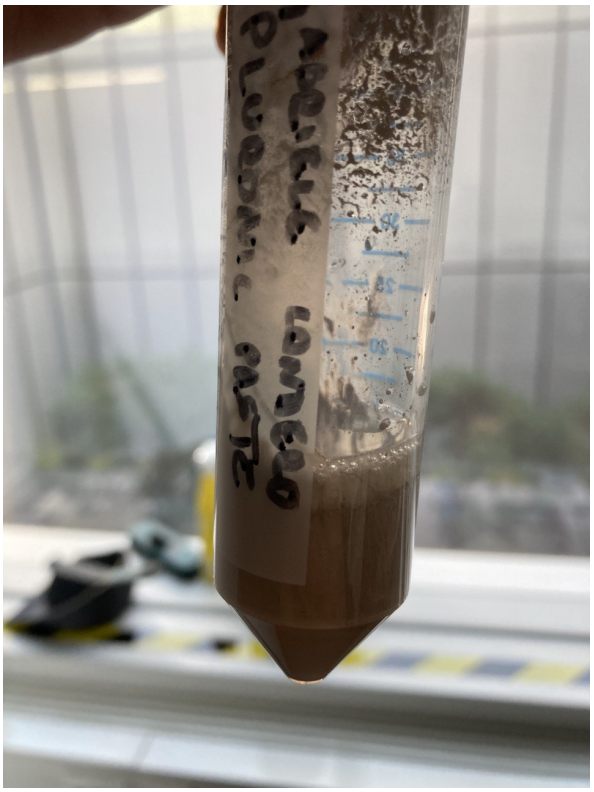

Figure 4.13: Bubble layer on SiC ink.

Considering the step-wise addition of SiC powder to the solution, this characteristic has vanished after the final step. Moreover, as visible in the subsequent picture, some bubbles create on the surface

as consequence of the mixing into the vortex mixer.

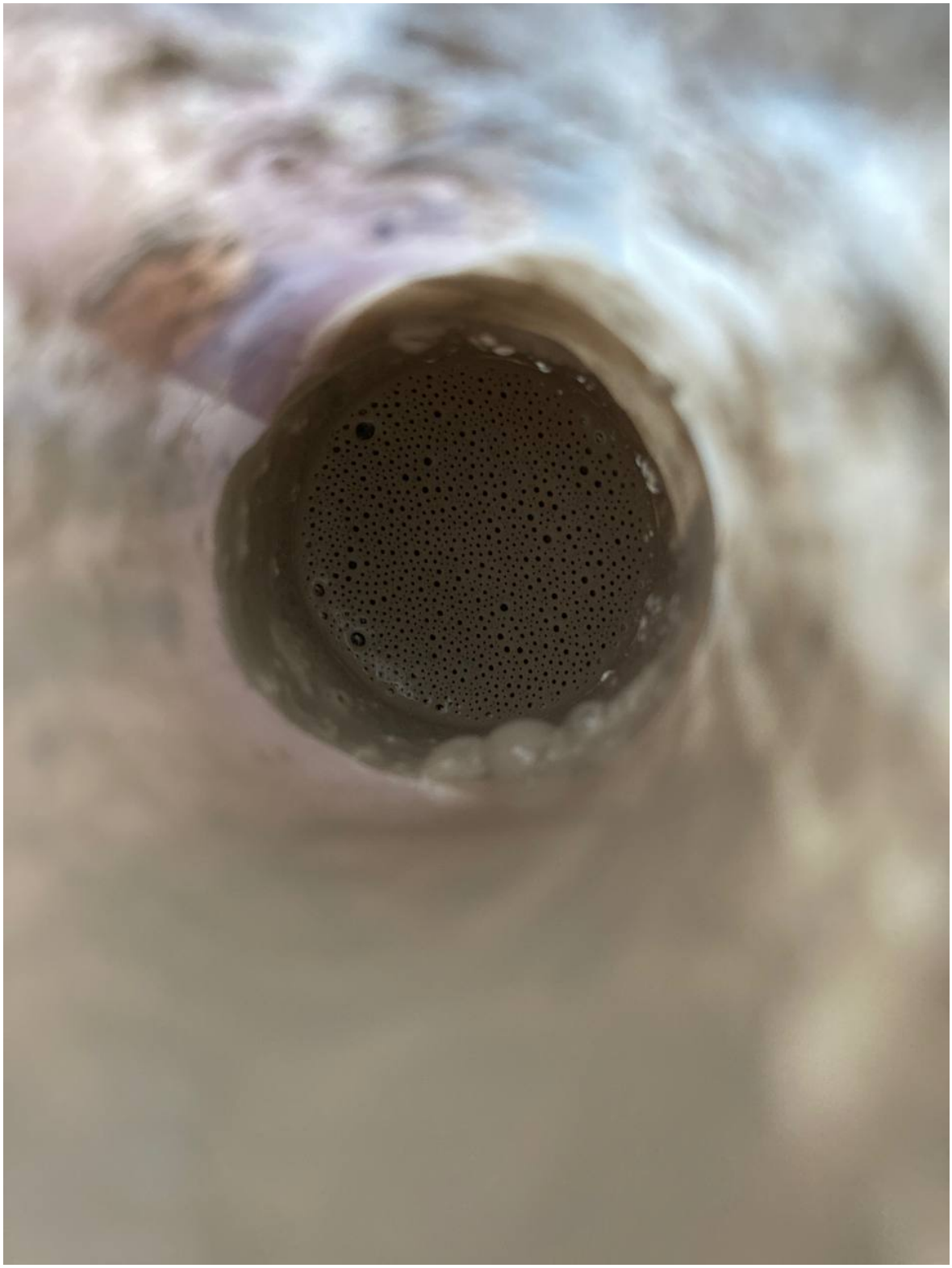

Figure 4.14: Step-wise added SiC ink with bubbles on the surface.

However, after the final cooling these bubbles disappear. By enhancing the solid powder dispersion in the solution, the hydrogel characteristic becomes more important. After the cooling, no bubbles are visible on the ink surface, as it is possible to see in the next picture.

Figure 4.15: SiC ink after the cooling process.

This surface characteristic is maintained even after the ink warming up at ambient temperature. As a result, as the ink temperature approaches an equilibrium with the environment, no changes on the surface can be detected. As a consequence, the next figure shows the previous mentioned SiC ink after several hours in ambient conditions.

Figure 4.16: SiC ink after thermal equilibrium with the environment.

The inks characterised by a solid fraction over 45vol.% of SiC were produced, requiring longer cooling steps to decrease the viscosity and allow a suitable homogenization. The SiC 45vol.% pure ink has not been considered as printable since the rheological studies were not possible to be done

due to impossibility to get to the measuring level of 1mm in between the rheometer plates. By using the TMAH addition as reported in Chapter 4.3, 45vol.% of solid fraction becomes printable due to a decrease in viscosity as a consequence of the stabilizer effect. Generally the temperature dependent behaviour of the solution viscosity has been an aid in performing such measurements, by liquifying the solution shorter distances in between the plates have been reached, keeping as a standard 1mm in order to be consistent in the measurements.

The inks with a solid loading of 36vol.% of SiC and 45vol.% of SiC have been chosen to be the final printable inks due to the properties studied during the rheological analysis. The study will be deeply explained in the next section.

Considering the best production methodologies, implying the step addition of powder to a cooled Pluronic solution in an ice bath and consequent final cooling and mixing, the final inks have been produced inside a speed mixer so to enhance the final quantities. By using the speed mixer, the spinning speed is affected by the amount of paste considered. Therefore a constant use of a speed was not possible. As maximum spinning speed 2000rpm have been used at initial mixing, leading to a final spinning speed of 800rpm. As a consequence the mixing was performed in a more precise way and a visible better homogeneity was achieved.

4.2.1 Rheological analysis

A rheological analysis of the main inks containing up to 40vol.% of SiC has been performed to understand the main properties related to printability. All the four algorithms presented in Chapter 3.5 have been used, leading to a deep understanding of the main characteristics related to a printable ink. In this section the main inks are characterised with a solid loading ranging from 25vol.% to 40vol.% of SiC. The remaining inks from SiC 10vol.% to SiC 20vol.% (Table 3.1) have not been considered since the volumetric loading was too low (<25vol.%), which could have lead to crack formation according to Feilden et al. [46]. The rheological studies of inks with a greater amount of powder have not been possible due to high stress on the rheometer. In order to embed the paste between the plates, reversible temperature behaviour of the hydrogel has been used, avoiding the compression of the paste and generation of stresses. By doing so, the solution viscosity was low enough to fill the 1mm gap in between the plates and the whole plate area. In this way all the pure SiC inks up to a solid content of 40vol.% were rheologically tested. By exceeding 40vol.% of solid content the stress generated caused the impossibility for the plates to stay at 1mm. The addition of a stabilizer to decrease the generated stress and improve the material distribution was necessary. Moreover, by increasing the solid content and using the TMAH, the rheological analysis of highly loaded ceramic inks were possible. In the next section, an analysis of inks containing 45vol.% of solid load has been done after the addition of TMAH.

The atmosphere inside the rheometer has been kept isolated from the outside so to avoid intrusion of alien molecules and interaction with excessive air.

Temperature Ramp Algorithm

By considering the temperature ramp algorithm, only the temperature increase behaviour is significant for sake for study since the ink is formulated to be printable at ambient temperature after the final cooling down step. During the Pluronic analysis the temperature increase and temperature decrease have been simulated in order to understand the quality variation during the production procedure. In fact for printing the ink is stored in ambient conditions after being left at 4°C for 24h. As a consequence, the temperature decrease behaviour could simulate the behavior once the ink is left into the refrigerator before the final mixing.

During the temperature increase plot the viscosity was analysed first. Viscosity, as already explained during the Rheological introduction chapter is fundamental for an ink to be printed since it has to allow the ink to flow and to not spread all over the surface over which it is extruded.

In both the cases, several attempts for ink has been done to perform a suitable analysis. Moreover, 120 data points have been collected per analysis.

The ink viscosity trend appears to be comparable to the one of the pure Pluronic solution, following an "S" increasing shape. Moreover, stable viscosity values are present when the transition phase has been overcome. By reaching the ambient temperature the viscosity plot becomes flat. The same consideration can be done while analysing the temperature between 4°C and 15°C, during which the solution is in liquid state and the viscosity is constant.

It can be seen that by increasing the solid load the viscosity of the inks increases. By adding a solid powder the solution becomes less and less fluid.

As already reported in the previous chapter, the "y" axis is labelled by "Complex Viscosity" due to the not direct viscosity measurement but its mathematical calculation through the parameters discovered during the acquisition.

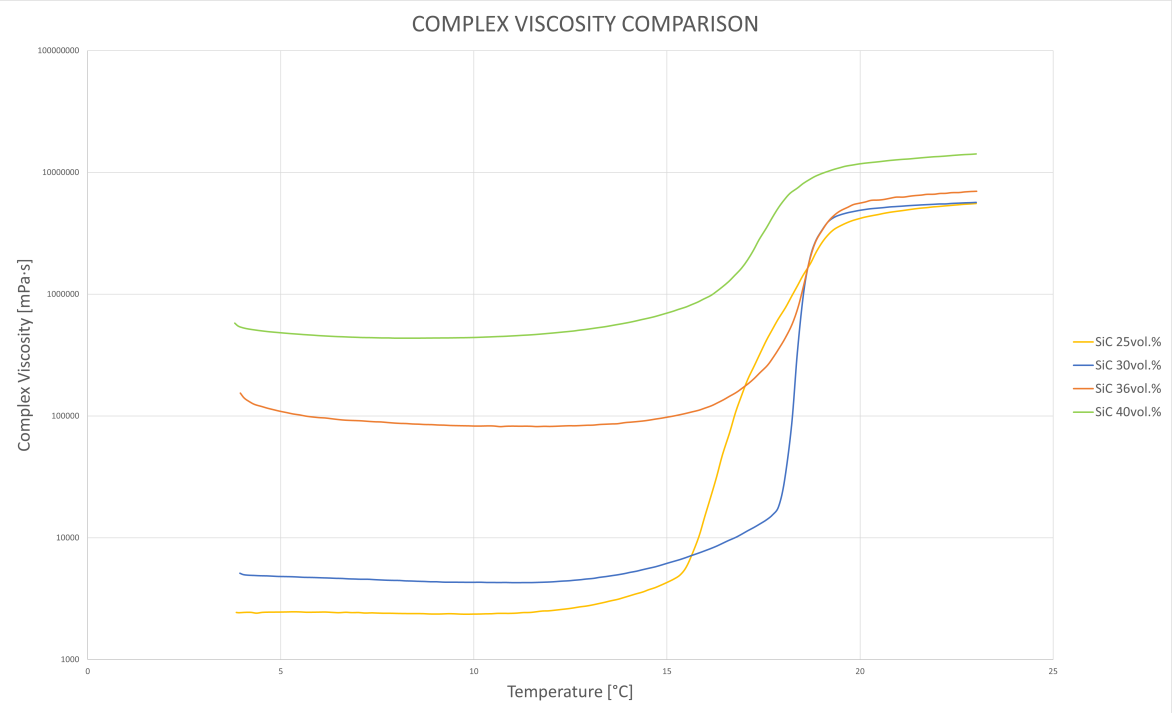

Figure 4.17: SiC ink viscosity comparison.

The ink SiC 25vol.% is characterised by the lowest initial viscosity of 2429mPa*s. By considering a lower volumetric load the effect of the Pluronic solution is more visible. By approaching the transition temperature a lower slope was shown, allowing the transition to the solid state. After the 19°C the solution is completely gelified and it is characterised by a stable viscosity value of $6.5*10^6$mPa*s.

By increasing the solid content, the curves elevate towards a greater starting viscosity. In SiC 30vol.% the initial and stable viscosity value is 4935mPa*s. the change in slope happens at 12.C°. By reaching 17.8°c an abrupt change is slope causes the final transition into the solid state. The same final viscosity of SiC 25vol.% is reached.

The SiC 36vol.% ink represents the recreation of the ink proposed by del Manzo et al. [30]. The viscosity in liquid phase shows an increase, reaching a value of $8.5*10^4$mPa*s. This value represents an approximation since as tested several times, a volumetric loading of 36vol.% of SiC 2) is characterised by a viscosity which undergoes a decrease in value by increasing the temperature, presenting a flat parabolic behaviour. At 17°C the phase change is visible. The final viscosity value is in accordance with the previous two, being of $7*10^6$mPa*s.

A solid loading of 40% represents the highest pure solid content into the Pluronic solution. The

effect of the distribution of the solid particles into the liquid Pluronic solution causes the final liquid state viscosity to be around $5*19^5$mPa*s. The viscosity now keeps a stable trend until the phase change is reached. The viscosity in solid state keeps a gap of half order of magnitude from the other inks, being $1.4*10^7$mPa*s.

Considering the general rule presented by del Manzo et al. an ink is printable when G'>G" at the temperature of operation, meaning that the solid load is greater than the liquid one [30]. This behaviour allows the shear stress to decrease the viscosity by spinning the ink while the solid like behaviour allow the stability of the ink once it is deposited on the surface (Chapter 3.5). By using this theory, the ration in between G" and G' allows to understand if an ink is possible to be printed. G"/G' can be generally called as printability index.

To highlight the theoretical printability of an ink imposed by the del Manzo et al.'s consideration, a red line has been drown in the plot [30]. G"/G' values that go below this limit are theoretically printable.

Generally, only two inks behave similarly showing a descending behaviour during the transition phase. As a consequence, SiC 25vol.% and SiC 30vol.% are the ones characterised by the lowest solid content. SiC 36vol.% and SiC 40vol.% are characterised by a similar initial trend that leads to a consequent divergence happening after the 18°C, when the solution behaves as a solid.

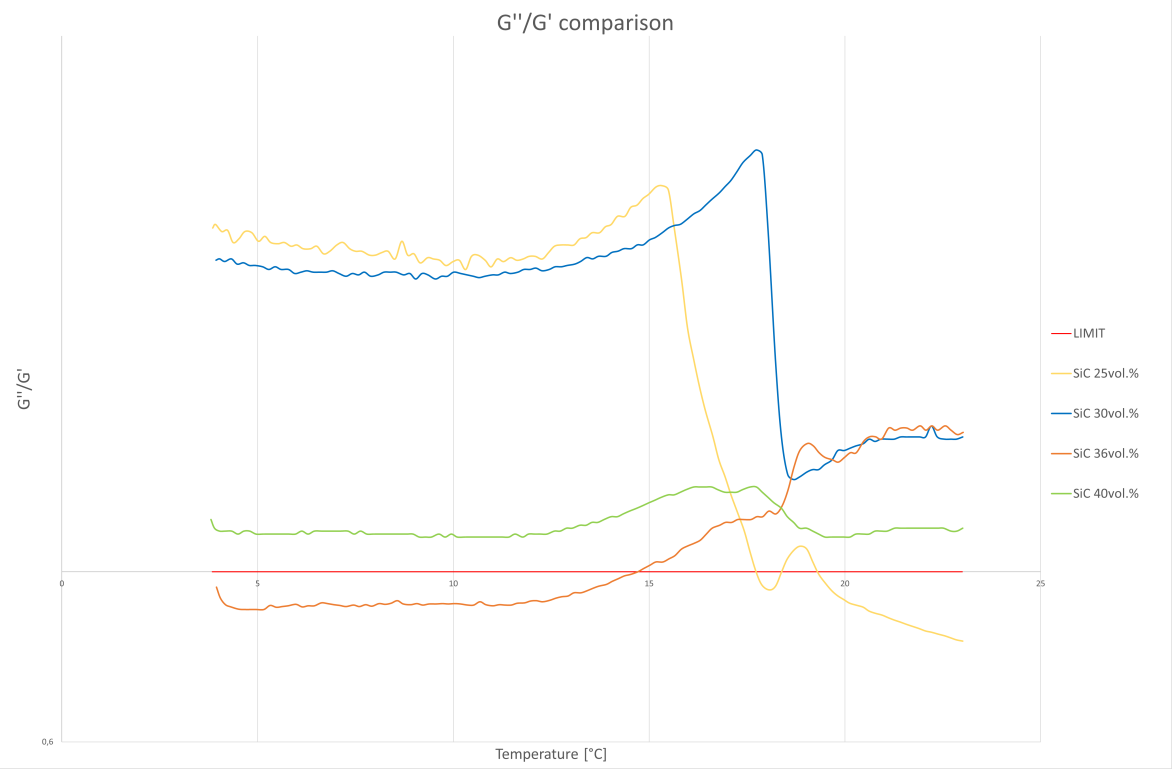

Figure 4.18: G"/G' comparison.

The initial stable value of SiC 25vol.% is kept until the beginning of the transition phase. The transition phase causes the decrease of the plot, leading to a final modulous lower than 1. Theoretically, being characterised by a ratio G"/G'<1, the ink could represent a printable alternative.

A similar trend is kept by SiC 30vol.%. The main trend follows a same general path, lasting until the transition temperature is approached. Experiencing a phase change, the printability index shows an abrupt decrease, reaching a newly increasing trend from 1.37 to 1.58.

Differently than the other two inks, SiC 36vol.% trend starts at 0.893 indicating that the ink

could be printable at low temperatures. By increasing the temperature, the ratio presents an increasing growing trend. At 15°C G"/G'=1 while the final value approaches the same final value of SiC 30vol.%. As a general consideration, SiC 36vol.% could be theoretically used into a printer if kept in between 4°C and 15°C.

A value greater than 1 is measured during the whole temperature evolution by SiC 40vol.%. A small increase in modulus happens during the transition phase, decreasing again as soon as the final viscosity is achieved.

The same printabilty index considerations done on Figure 4.18 could be done by analysing the subsequent plot in which G' and G" are compared by analyzing their real value. In advance, it can be seen that G' and G" are affected by the presence of the SiC particle dispersion as well as viscosity. A general increasing trend is present in all the ink alternatives as the transition temperature is reached.

As it is possible to see, the G' and G" plots are grouped depending on the solid content. Theoretically, the printable inks should present a crossing in between the two parameters. This has only been detected in SiC 25vol.%.

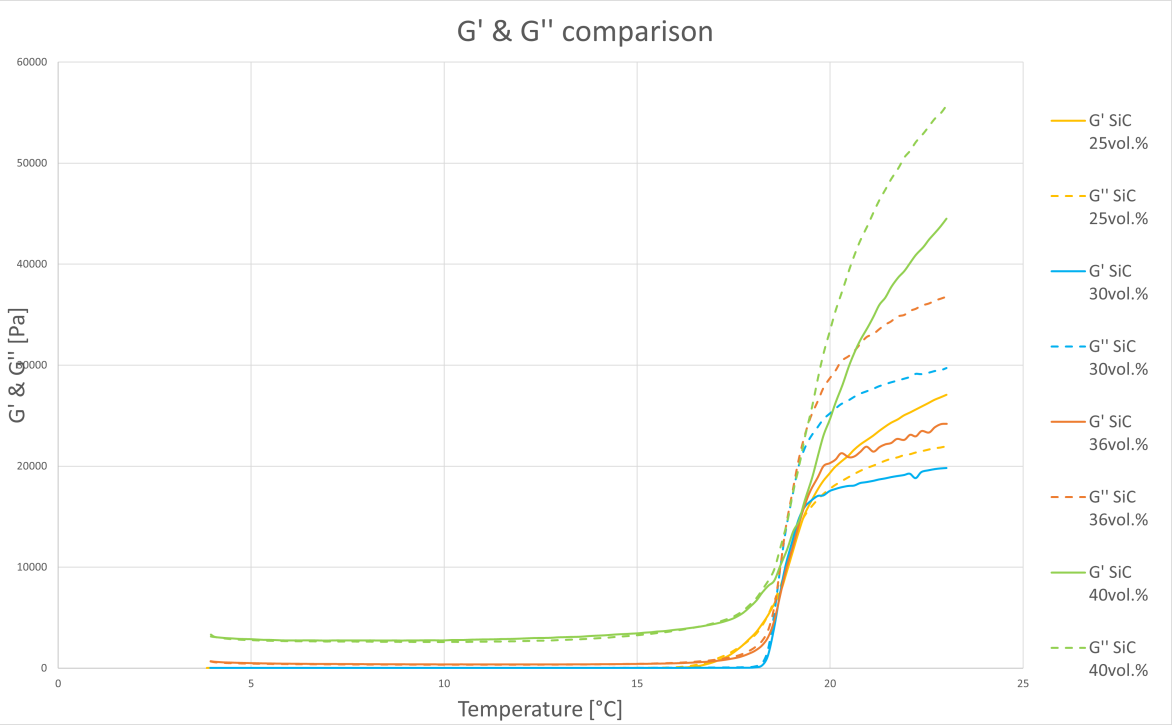

Figure 4.19: G' and G" comparison.

Shear Rate Algorithm

As already explained in Chapter 3.5.1 the Shear Rate algorithm permits to understand the viscosity behaviour of the inks when a shear stress is applied. In detail, the shear rate affects the micro-structure by applying a constant increasing stress, producing the spinning of the whole structure considered. The application of a shear stress causes the material to completely change structure affecting the viscosity, but after the load release, due to the hydrogel visco-elastic characteristic, the structure deformation is completely recovered.

By considering the effect of a shear stress on a visco-elastic material, the deformation caused as a consequence of a load would change the viscosity. Moreover, by tuning the viscosity an ink characterised a printability index higher than the limiting value in ambient condition would become possible to be printed. In this consideration, the application of a certain shear stress is fundamental since all the inks have a different yield shear stress. When the yield stress is reached G'=G", the hydrogel

transition from solid state to liquid state happens, allowing the ink to flow.

The data acquisition has been performed by analysing 100 data values per ink tested. Each test has been performed different times in order to allow a comparison among consistent results of the ink behaviour. Un-expected trends have been demonstrated or discarded by performing several attempts on the same solution.

By considering the first output plot, the relationship between shear rate and viscosity can be seen. A decreasing trend is the general observation that detects the microstructure change due to a shear stress. Moreover, all the inks present a particular trend that is characteristic of that solid loading.

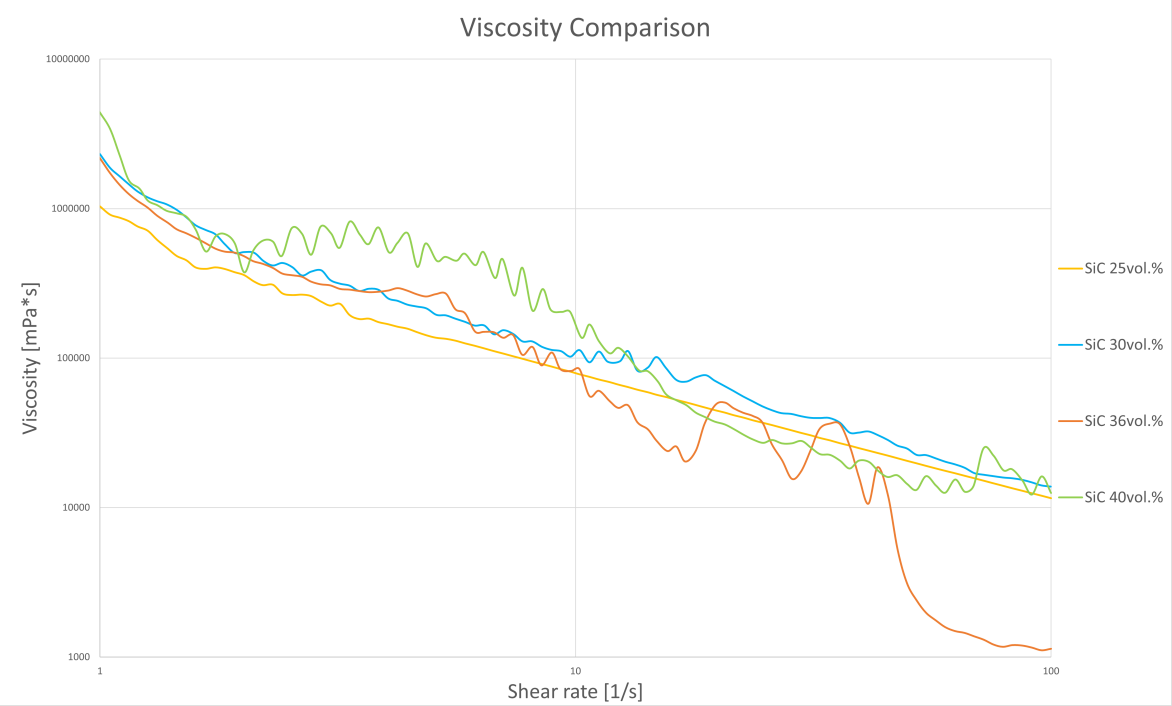

Figure 4.20: Viscosity comparison.

SiC 25vol.% is characterised by the lowest solid content and it is the one that shows the most linear trend during the transition from 1/s to 100/s of shear rate. Some small variations in the trend are present before reaching a shear rate value of 4/s, highlighting the presence of particles that interfere with the action of a shear load. After this threshold value, the main trend assumes a linear form in a double logarithmic scale. This linear descending style may imply the complete reassembly of the microstructure, leading to a new final microscopic assembly with final viscosity $1*10^4$mPa*s.

By considering 5vol.% of SiC more in solution, the main plot presents some deviations from the linear style. Moreover, SiC 30vol.% starts from a viscosity level greater than the one of SiC 25vol.% and by increasing the shear rate the slope changes. A more flat slope brings a differentiation from the previous plot. Generally, an unstable path is drawn by the constant increase of shear rate. Small instabilities characterise the entire trend implying the action of particulates that interfere with the main SiC matrix. A linear trend is never reached. Before 10/s of shear rate, the trend instabilities are stronger, implying a greater effect on the particles to obstruct the change in microstructure. As for SiC 25vol.%, 10/s represents a transition from a more disordered path to a more ordered one. By crossing this limit value the instabilities mitigate, leading to a final viscosity value close to the SiC 25vol.% one. The final viscosity value is in the order of 10^4mPa*s.

An initial similar trend to SiC 30vol.% is held by SiC 36vol.%. Until a shear rate of 2 1/s is reached the behaviour is completely comparable. By increasing the shear stress the ink behaves differently showing a viscosity trend affected by numerous alterations in slope. At 7.5 1/s of shear rate a com-

pletely different slope than the already two mentioned plots is visible. The descending trend leads to the lowest viscosities found. A small ramp up can be detected at 12 1/s where non-uniformities lead to an increase in viscosity [55]. By approaching the final shear rate values the viscosity plot collapses to 10^3mPa*s. The fall has experienced a decrease in viscosity by an order of magnitude if compared to the SiC 25vol.% and SiC 30vol.%. The test have been repeated three times showing always a similar trend.

SiC 40vol.% starts at a greater viscosity value than the previously mentioned inks. Some more marked unstable trends are visible by reaching 10 1/s of shear rate, leading to an apparent increase and a consequent decrease in viscosity. The main decreasing shear-thinning behaviour is generally respected even by presenting an initial increase in viscosity. The concavity presented up to half of the measurement is not respected after the 10 1/s shear rate, producing a second derivative positive and the same final viscosity value of SiC 25vol.% and SiC 30vol.%. The second descending part that crosses 10 1/s represents the shear stress that has deformed the structure, impeding the particles to keep their effect increasing the viscosity. Some more marked deviations are present into the final plot parts. A stable path is never reached.

As a second outcome of the Shear Rate algorithm, the shear stress on the ink can be analysed. The shear stress is a consequence of the rheometer upper plate spinning over the tested material. The cohesion of the solid particles leads to a greater shear stress, while a more dispersed structure leads to a lower shear stress.

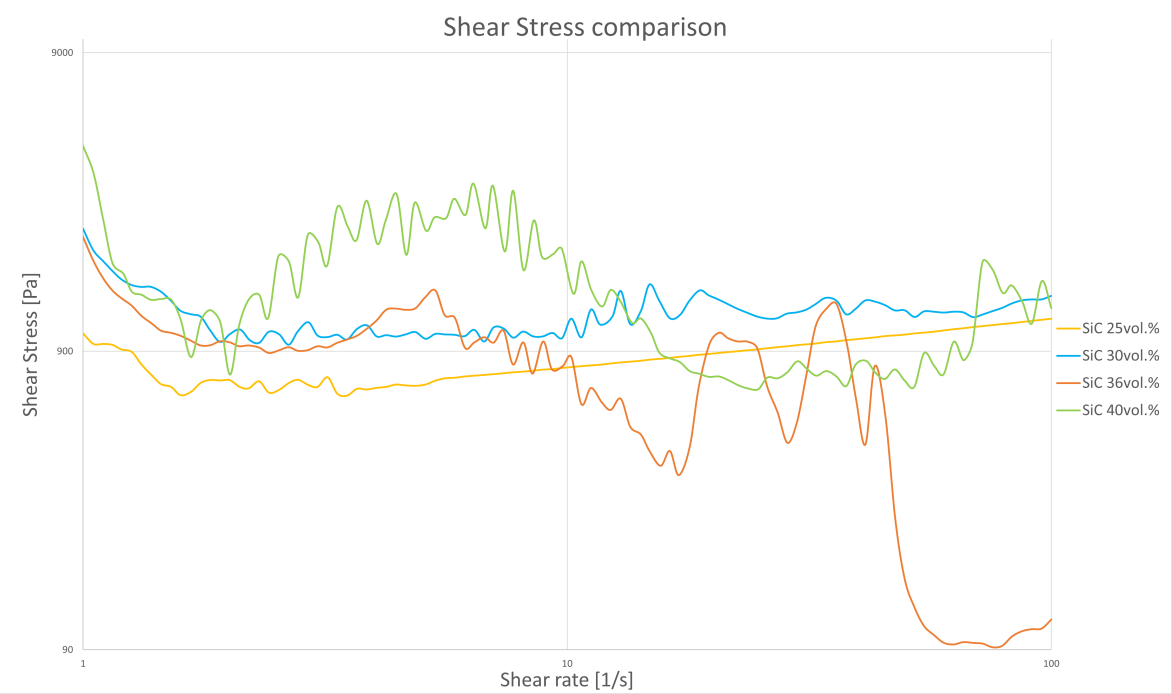

Figure 4.21: Shear Stress comparison.

By starting the shear rate analysis the SiC 25vol.% shear stress starting value counts for 900Pa. A first instability trend brings than a following decrease in shear stress measured. This first behaviour can be compared to the already mentioned viscosity trend until the shear rate value of 4 1/s. As the viscosity decreases, the shear stress increases by following a linear trend.

SiC 30vol.% shear stress behaviour starts at 2000Pa. A first decreasing path leads to a more stable trend. The first section can be analysed as the action of the decreasing solid behaviour of the microstructure when a shear stress is applied. By increasing the shear rate, no other decreasing trends can be detected. An unstable trend is kept until the end of the measurement. The subsequent and almost flat shear stress plot can be summarised in a range in between 1000Pa and 1500Pa. By comparing with the viscosity trend, the constant decreasing path reported in Figure 4.20 is followed by the flat shear stress trend.

A more similar trend to the viscosity one is held by SiC 36vol.%. An initial descending path is similar to the one shown by SiC 30vol.%. By increasing the shear rate a small increase in shear stress is measured. By crossing the 10 1/s a similarity with the viscosity plot is represented. The shear stress experiences a small decrease comparable to the one previously mentioned. The final part of the shear stress study can be superimposed to the viscosity one. Some more similarities can be detected in the final three peaks. Moreover, the final shear stress is the lowest found, counting for 110Pa.

SiC 40vol.% is characterised by three main changes in slope, being similar to the viscosity study. By considering the concavity of the plot, there is a change in slope causing the change from concave to convex. This trend approach is repeated until the end of the measurement following a quasi sinusoidal plot.

Shear Stress Algorithm

The general law for a printable ink of G'>G" in the Temperature Ramp algorithm, respected by del Manzo et al. and Feilden et al., can be related to the results of the Shear Stress Algorithm. In fact the yield stress represented by the crossing in between G' and G" implies the changes i behaviour from solid to liquid, allowing the flowing through a nozzle. An ink with G'>G" represents a solid behaviour as dominant. By reaching the yield stress the state change happens and the ink can be extruded.

A collection of 50 acquisitions per sample have been performed [30, 46]. The shear stress have been chosen to vary from 9Pa to 10000Pa in order to be comparable to the results presented by [30]. The Shear Stress algorithm measures as main results G' and G" by varying the shear stress. The evaluation of these two modulus can lead to the understanding of the ink printability. Moreover, considering as already mentioned in Chapter 3.5, the G">G' is useful while the ink is extruded through the nozzle, so to take advantage of the flowing behaviour of a fluid. Once deposited the ink on the surface, the load acting on the ink shall stop. Therefore G' and G" are only dependent on the temperature, being now dependent on the general rule of del Manzo et al. [30] stating that it behaves as a solid while being deposited and showing a G'>G".

By doing a general consideration, it can be seen that the G' moduli are greater than the G" moduli at the study beginning, when the shear stress is in its smaller values. Moreover, by increasing the shear stress a general flat trend is experienced by all the parameters, representing the elasticity field that can be used while keeping the ink inside the syringe. As soon as the yield stress is reached, the G" overcomes G' meaning that the liquid fraction is dominating the ink behaviour despite the solid fraction.

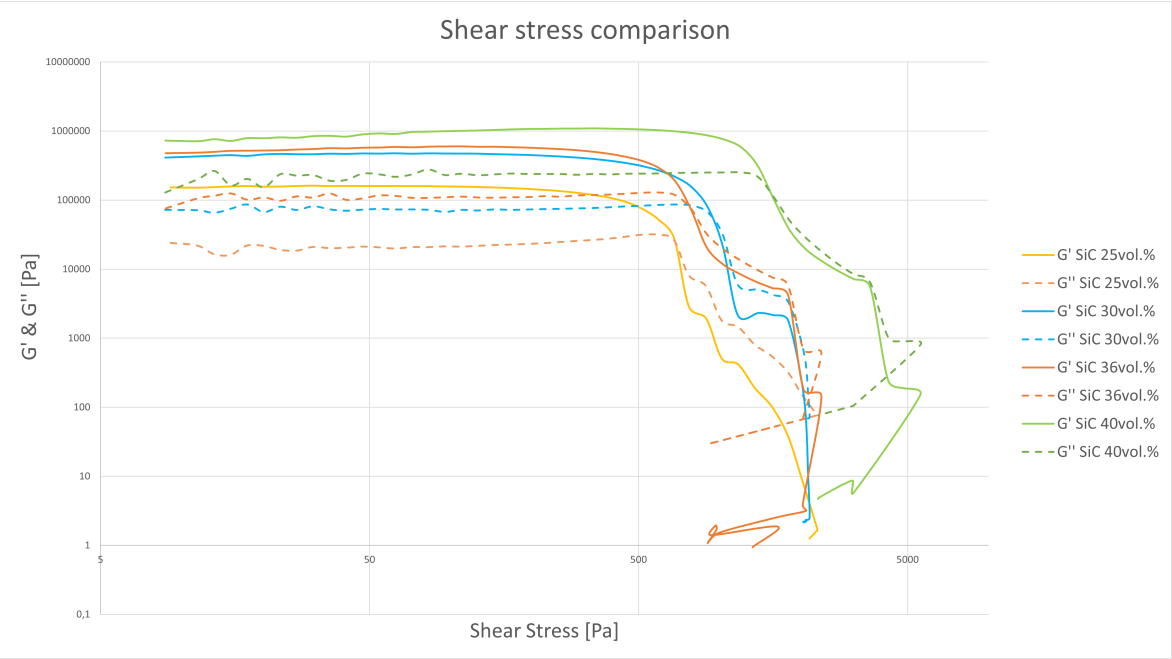

Figure 4.22: Shear Stress comparison.

SiC 25vol.% behaves as a solid like structure until 680Pa shear stress is applied. This value represents the yield stress necessary for the G" to overcome G'. After reaching the yield stress, a collapse in the two parameter value is detected, meaning a complete change in the ink behaviour.

SiC 30vol.% follows the same trend of SiC 25vol.%, differentiating by a value of 500Pa in both the moduli. The yield stress is reached at 905Pa when G' and G" reach a value of $65*10^3$Pa.

SiC 36vol.% yield stress is detected at 780Pa, being lower in modulus than SiC 30vol.% but still greater than SiC 25vol.%. However, G' and G" value of $78*10^3$Pa is greater than the previous two demonstrating a greater solid load. By increasing the SiC volumetric fraction a greater shear stress is needed to generate a change in the G' and G" moduli.

SiC 40vol.% represents the SiC ink characterised by the highest values of G' and G". By having 40vol.% of SiC, the yield stress is greater than the already mentioned inks. A shear stress of 1500Pa represents the minimum value to allow the flow of the ink.

Frequency Sweep Algorithm

Considering the last tested algorithm, the application of the Frequency Sweep algorithm can be crucial for the spinning of the screw in the 3D printer. As already expressed in the results explanation of the Shear Rate Algorithm, by tuning the spinning of the screw the viscosity can be manipulated. The test has been performed by collecting 100 data per ink.

By considering the conditions of applications of Frequency Sweep algorithm, there is the absence of normal force. Moreover, the shear stress detected is limited by the 1% deformation allowed by the algorithm.

Differently than the Shear Rate algorithm, the viscosity detected shows an overall increasing trend in all the inks.

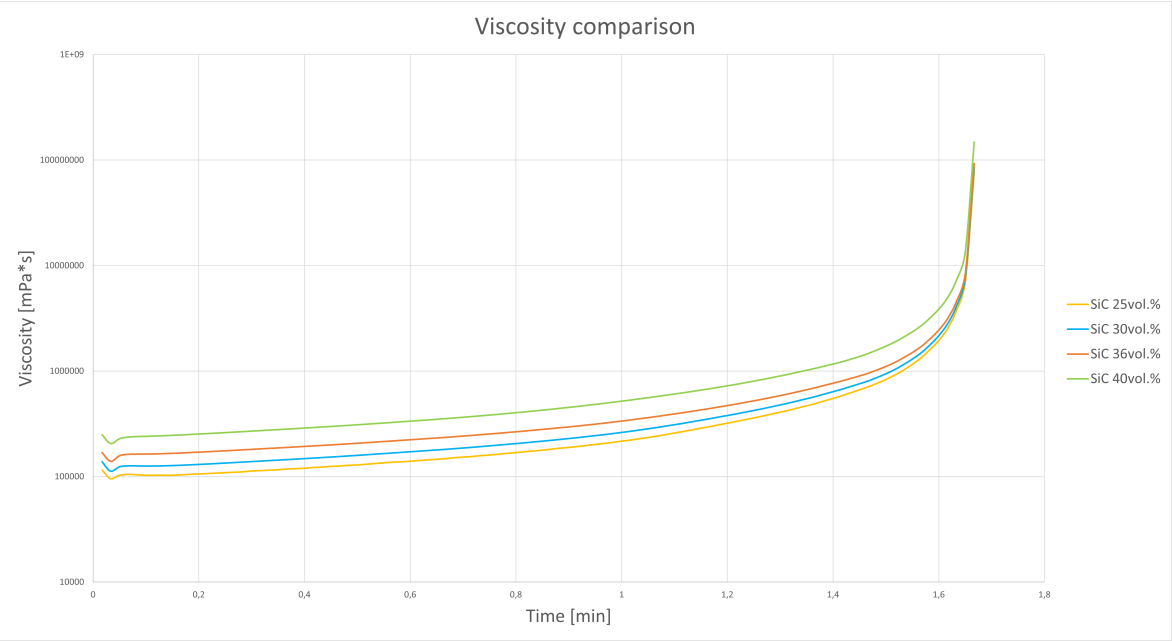

Figure 4.23: Viscosity comparison affected by a change in plate spinning frequency. It has used a time scale instead of the frequency evolution due to the not achievable frequency change scale.

Depending on the initial viscosity values of the plots start with an increasing trend at a constant slope. However, by approaching the maximum frequency imposed of 100Hz (reached at the end of the study) the viscosity undergoes a consistent increase, tending towards magnitude levels around 10^8mPa*s.

Every ink's plot vary from the others comparable to the difference in between inks initial viscosities. This difference is kept until the change in slope happens, around 10^6mPa*s. During the final ramp up the plots superimpose tending towards magnitude levels of 10^9mPa*s.

The greatest difference in plot is visible with SiC 40vol.%, being characterised by the greater SiC amount. By decreasing the SiC amount, the plots tend to become closer approaching a similar trend in the same viscosity levels.

4.3 INK STABILIZATION

By increasing the solid fraction in the inks over 40vol.% a low viscosity at low temperatures is not achievable. By performing the rheological analysis consistent, the rheometer plates must be kept at 1mm. Due to the temperature dependent viscosity behaviour the paste can be spreaded reducing the stresses involved. The inks exceeding the threshold value of 40vol.% SiC did not show a visible temperature reversible viscosity behaviour to produce consistent measurements. In addition, at ambient temperature the viscosity condition worsen and the solutions became impossible to be mixed while performing the last powder additions. With the cooling steps a not enough low viscosity characterised the samples, making the mixing impossible. After the final cooling in the refrigerator for 24h, the solutions were still impossible to be mixed.

This difficulty in preparation limits the maximum amount of solid powder to be added to the ink. A too low viscosity makes the mixing process of the solution impossible, creating non-uniformities and powder accumulations.

In order to permit a greater solid load and still maintain the main printabilty characteristics, TMAH has been used as binder. The stabilizer utilization comes from the literature and it has been applied in order to obtain viscosity values sufficient to produce a flowable paste.

The TMAH addition has been reserved to the highest theoretically solid loaded inks as expressed by Feilden et al. [46]. As a consequence, the ink in which TMAH has been added is the one with 45vol.% of SiC. By considering the work done by Feilden et al. 45vol.% represents the maximum allowable value over which the viscosity is high enough to block the printing [46]. As a consequence, this ink was chosen as targeted by the highest solid volumetric content and not sufficient viscosity to be printed or measured into the rheometer. By considering the temperature decrease to let the hydrogel temperature dependent characteristic to act, the 45vol.% SiC caused excessive stresses on the rheometer plates, making impossible the reaching of 1mm gap in between the plates.

The TMAH addition permits to liquefy the solution depending on the amounts and it does not need any particular procedure nor subsequent cooling. As it will be explained in the rheological part (Chapter 3.5), there is no temperature effect on the structure of the structure. After the TMAH addition a final solution mixing allows the stabilizer distribution in the paste, homogenizing the final result.

As reported in Table 3.2 the additions have been performed by increasing the TMAH addition by half order of magnitude in between each step. By doing experiments, the smallest effect on the ink fluidity was obtained with 500μl of TMAH in the final solution, implying a precise utilization of 6,87vol.% This value represents an approximation of the Li et al. paper [44] targeted around 6vol.%. However, the viscosity obtained was not sufficient to be studied into the rheometer.

The subsequent TMAH ceramic inks have been performed by considering greater basic loads. The 45vol.% of SiC solid load in the ink has been maintained. Considering additions below 6.875vol.% no results were obtained.

The rheological analysis were conducted on all the various paste produced, containing TMAH content from 6.87vol.% to 13.75vol.%. However, satisfying rheological values were closer to the 13.75vol.% concentration. As a consequence, the next 9.64vol.%, 11vol.% and 12.37vol.% have been undergone rheological analysis.

No figures showing the TMAH solutions have been reported since no visible characteristic were present on the surface. The mixing speeds involved in the vortex mixer were of 3200rpm in the case of the smallest and firsts studying flasks, while for the final printing inks 800rpm was the highest usable speed.

4.3.1 Rheological analysis

By increasing the solid content, as already expressed previously the main plots shift by greater viscosity levels and higher storage and loss modulus. For the rheological analysis all the algorithms explained in Chapter 3.5 have been used, using the same acquisition rate of the SiC inks and the same amount of data. In addition the tests have been repeated several times for sake of correct measurement.

The inks considered during the rheologial analysis are characterised by a SiC volumetric fraction of 45vol.% The TMAH addition have been done depending on the syringes present into the lab. The labelled names present in Table 3.2 are depending on the quantity of TMAH added to the paste. Letter "a" stands for the an amount of 5μl, "b" 10μl, "c" 50μl, "d" 100μl, "e" 500μl, "f" 1000μl. By coupling the different syringes used, quantities of 700μl, 800μl and 900μl have been considered, giving them the names of "edd", "ccedd", "deddd" respectively. The used volumetric amount of TMAH added has already been shown in Table 3.2. By considering the stabilizer utilization the mixing has been improved so during the production procedure the accuracy was greater than the previous inks with high powder amount. Moreover, the lower viscosity allowed to study the inks with a high volumetric amount into the rheometer without implying any excessive stresses. A volumeteric content of TMAH lower than 6.875vol.% were produced. However, the stabilizer effect was not obtained, resulting in too high viscosities in the paste. On these low TMAH amount inks the rheological analysis were not possible to be conducted.

In order to allow the rheological measurement of the inks with the lowest TMAH content possible the use of temperature decrease technique was fundamental to allow the viscosity decrease behaviour

of the hydrogel. The temperature behaviour of the pastes will be shown in the next section.

The atmosphere inside the rheometer has been kept isolated from the outside so to avoid intrusion of alien molecules and interaction with excessive air.

For the inks containing TMAH the rheological analysis have been repeated after some days in order to analyse the aging effect. The aging effect is expected due to the similarity with the study done by Feilden et al. introducing Dolapix as stabilizer for the Al_2O3 inks.

Temperature Ramp Algorithm

As already mentioned for SiC, by considering the temperature ramp algorithm only the temperature increase behaviour is significant. The inks have been left into the refrigerator for 24h in order to increase the paste homogeneity. After cooling, the ink is stored in ambient temperature in order to allow the complete phase change to happen and simulate the effective using state. As a consequence only the temperature ramp simulation allows to have a good understanding of the behaviour of the microstructure while experiencing a heating phase. By considering the various papers that study the temperature dependent behaviour of the Pluronic, the cooling step is useful to avoid impurities in the solution.

A collection of 120 data points allows to have a look to the viscosity behaviour when temperature increases. The collections were all been performed by keeping the same rheometer settings used for the pure SiC inks, both in temperature and in number of data collected.

The viscosity represents the first outcome of the Temperature Ramp algorithm to be analysed. The yield strength allows the ink to flow while keeping a sufficient structure stability when it is deposited on the bed. Moreover, a proper viscosity could allow to prevent ink spreading on the deposition surface by keeping a proper drawn structure.

Firstly, depending on the TMAH amount the curves are considerably different. By increasing the stabilizer concentration, the starting viscosity value moves towards higher levels. The Typical "S" shape of the viscosity plot during the temperature ramp is affected by a change in slope by increasing the temperature. A completely different behaviour is present by considering a different paste if compared to the pure SiC ink. The Pluronic hydrogel effect can be seen in the ink with 6.87vol.% in which the temperature affects the viscosity approaching the highest levels by heating up the solution.

In addition, a different order of magnitude is measured in all the samples containing TMAH. The viscosities range from 10^6mPa*s to 10^7mPa*s. Final values however are in the same range of variability of the other inks containing only SiC and Pluronic.

By looking at the higher amounts of TMAH inks, the slope that causes the change in viscosity becomes more flat increasing the initial viscosity. However, in some pastes the final viscosity is lower or in the same level of the initial viscosity. By considering the highest TMAH contents, the viscosity behaviour changes assuming a "hill like" shape.

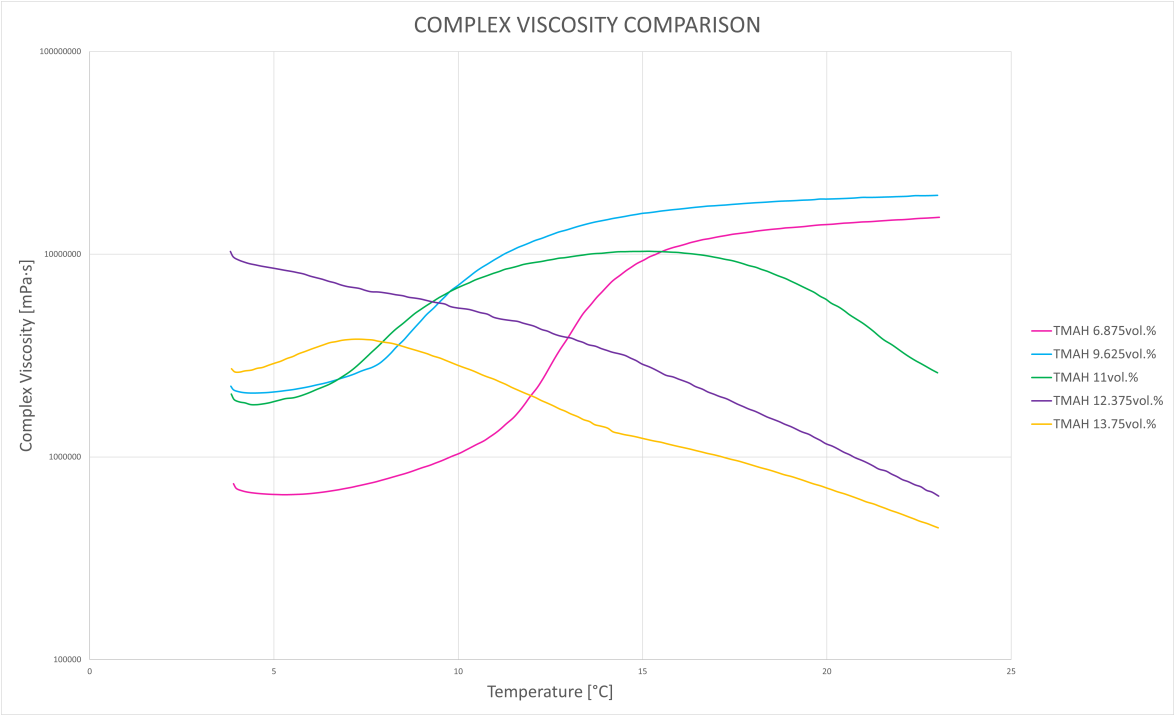

Figure 4.24: Viscosity comparison of the SiC inks containing TMAH.

By considering SiC 4e) the amount of TMAH added is 6.875vol.%. The shape is similar to the inks containing a lower SiC content by keeping the higher viscosity values. The starting viscosity value is around 6.6mPa*s and a plateau is maintained until the phase change happens. the slope of increasing viscosity is lower than the previous pure inks. However, by considering the previous change regarding the transition temperature, the plot strongly changes. The phase change is detected as starting before 10°C while at 15°C the solid structure is already dominant. After 15°C the viscosity keeps a stable viscosity value around $1.4*10^7$mPa*s.

SiC 45vol.% that considers an amount of 9.625vol.% of TMAH more than the previous ink. The shape still shows an "S" plot starting at a slightly higher viscosity than SiC 4e), around $2.07*10^6$mPa*s. The transition phase happens around 6.5°C following then a greater slope up to the higher viscosity. When a temperature of 15°C is reached, the solution is completely in the last state stage. From 15°C on the viscosity keeps a constant value without being subjected to any change .

A different plot is present in TMAH 11vol.%. The phase change happens at 5°C by having a ramp up similar to the SiC 4e). Between 10 and 17°C an inversion in slope is visible. The viscosity increases up to its highest value of 10^7mPa*s decreasing with the same slope of the increasing trend. This behaviour is the first detected in an ink, representing the first behaviour different from the Pluronic solutions. In fact, the effect of Pluronic while increasing the temperature is no more visible. Instead of having a constant and slightly increasing viscosity trend, with a higher TMAH amount the solid state at ambient temperature is substituted with a liquid one.

With a 12.375vol.% addition of TMAH the plot becomes completely different. The plot shows a descending trend for the whole study duration. The initial viscosity represents the highest initial viscosity value for all the solutions considered. $6.4*10^5$Pa*sis the final viscosity value detected for the ink at 23°C. The final viscosity level is comparable to the next that will be explained and still lower than the TMAH 11vol.% already explained. A hill like plot should be a better approximation of this plot, representing a trade off in between TMAH 11vol.% and TMAH 12.375vol.%.

13.75vol.% represents the ink with the highest TMAH content. The high concentration should theoretically decrease the viscosity, working at molecular level avoiding the solid agglomerations. Considering the previous plots it is clear that the viscosity plot should represent an attenuated hill, completing the trend at a lower viscosity levels than the other inks explained. The trend starts at $2.63*10^6$mPa*s,

greater than the vast majority of the other inks studied. An increasing trend starts from the algorithm starts, proceeding up to 7°C reaching the maximum viscosity level of $3.81*10^6$mPa*s. A consequent descending part follows, proceeding towards the end of the study, until a viscosity level of $4.47*10^5$mPa*s. The descending path has a inclination similar to the descending path of 12.37vol.% of TMAH. The last path is a descending one after being flattened in a plateau.

In the next two plots the aging effect is shown. The addition of TMAH causes a molecular behaviour change, being dependent on the conditions in which the flasks containing the ink are conserved and the time window in which the measurements are performed [44]. By considering the samples containing TMAH 9.625vol.% and TMAH 13.75vol.% the measurements have been done for the second time after a week. Generally it is expected that due to the reactions involving TMAH leading to an increasing oxidation state (Chapter 3.4) the solid content increases, increasing as a consequence the viscosity. By considering the temperature increase, the same path has to be followed, since the final state is a complete solid structure at 23°C.

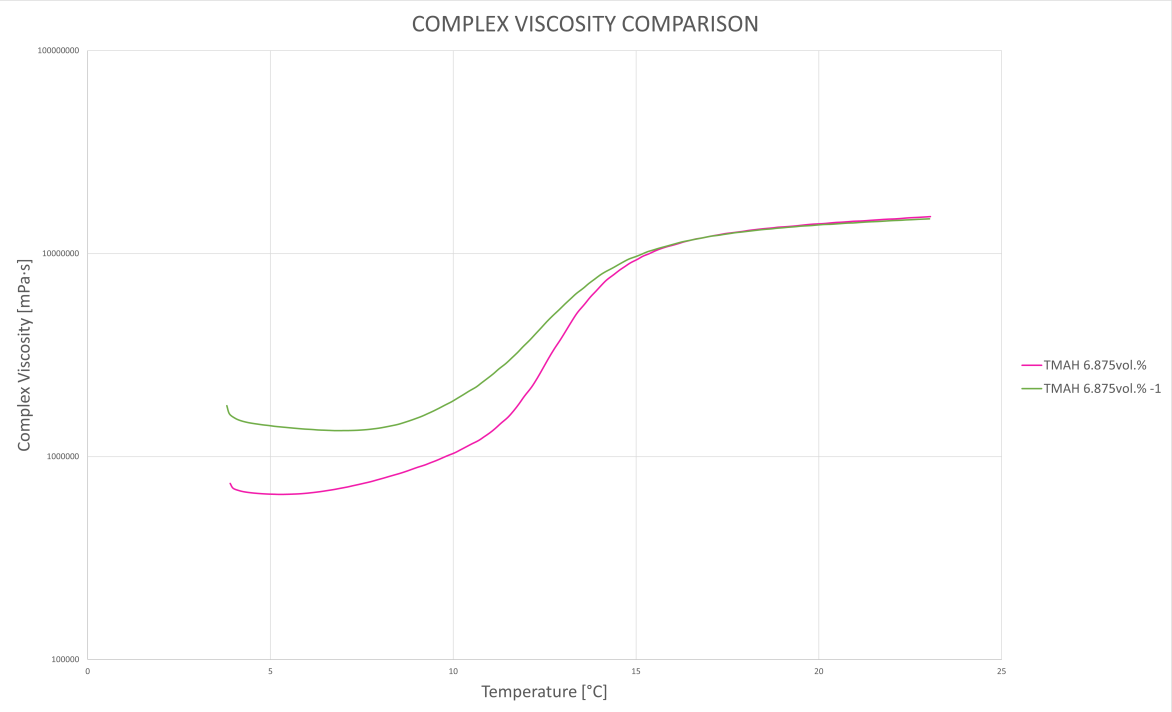

Figure 4.25: Aging effect on TMAH 6.87vol.%.

The viscosity starting point in both the measurements of TMAH 6.87vol.% is around 10^6mPa*s, more precisely the first measurements $6.8*10^5$mPa*s while the second one $1.62*10^6$mPa*s. The trends follow a first stable path until an increasing path starts before 10°C. For TMAH 6.87vol.% which is the first ink containing TMAH to be analysed, the increasing trends starts immediately after the begin of the measurement, ramping up with a low slope. The slope increases after crossing 10°C. Once 15°C is reached, a viscosity plateau implies a variation in module by only a negligible amount by approaching the ambient temperature.

The measurement done after a week, TMAH 6,87vol%-1, starts from a higher viscosity value. This characteristic can be due to a longer storing at ambient temperature inside a flask and the longer contact with the laboratory atmosphere due to the subsequent measurements done for rheological analysis. Moreover the increasing trend is not reached immediately after the start but when 10°C are reached. The difference in between the plots shortens by increasing the temperature. When the sample reach the ambient temperature no more differences in the measurements can be detected. Both diverge to a plateau greater than $1*10^7$mPa*s.

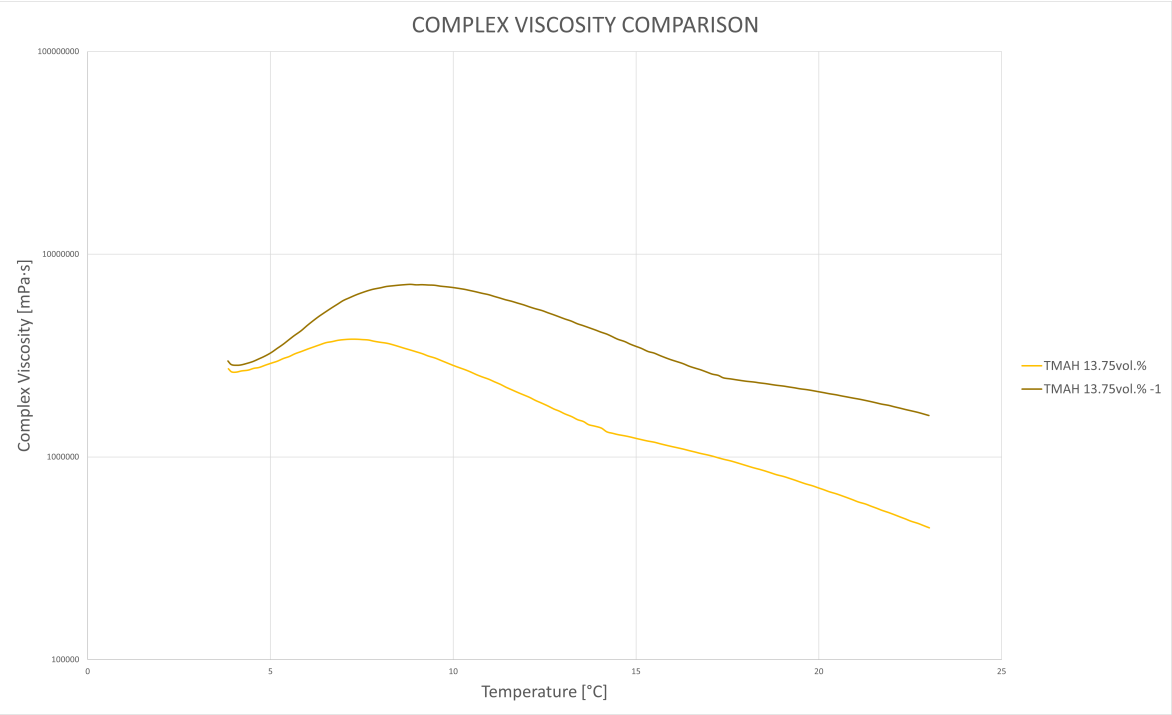

Figure 4.26: Aging effect on TMAH 13.75vol.%.

By considering a higher amount of TMAH added to the solution, the plots should be characterised by a different shape. Considering TMAH 13.75vol.% the shape is the one already mentioned dating the Temperature Ramp overview. The plot represents a descending trend from 7°C to the end of the study. The highest viscosity value is $3.81*10^6$mPa*s.

In the plot obtained one week after the previous measurement, TMAH 13.75vol.%-1 is represented. The initial viscosity value measured at 4°C is approximately the same. By increasing the temperature, the peak is reached always at 7°C but the value of viscosity now is up to $7.11*10^6$mPa*s. The plot starts than to decrease, following a similar trend to the previously mentioned one. The difference in between the studies is constant until 23°C in which the final viscosity can be measured as $1.6*10^6$mPa*s.

The difference in time did not cause a similar behaviour to the TMAH 6.875vol.% situation. The starting point is approximately the same while after being subjected to the phase change temperature the viscosities do not assume a unique plot but they vary assuming different viscosity values.

As presented for the other two case studies, also for the TMAH addition the G" and G' study has been done. Moreover in this situation the understanding of the printability index value trend is even more crucial since the amount of SiC has increased and the addition of TMAH has been done, therefore the general printability rule can be mantained. By considering the same printability parameter $G''/G' < 1$, by adding TMAH the solution should become more printable as more TMAH has been added to the solution. This theoretical result is the consequence of the increasing fluidity and decreasing viscosity caused by the addition of the binder. By considering the smallest amount of TMAH added to the SiC ink, the printability should be enhanced proportionally due to a decrease in viscosity. In the next figure it is expressed the general behaviour of the solutions. The red limit has been maintained in order to have a clearer look at the limiting factor.

As a general overview, by increasing the TMAH amount the ratio G"/G' changes, reaching values smaller than one during the whole experiment. By doing the rheological analysis it can be seen that as the binder concentration increases, the ratio G"/G' tends to be always lower than the limit values.

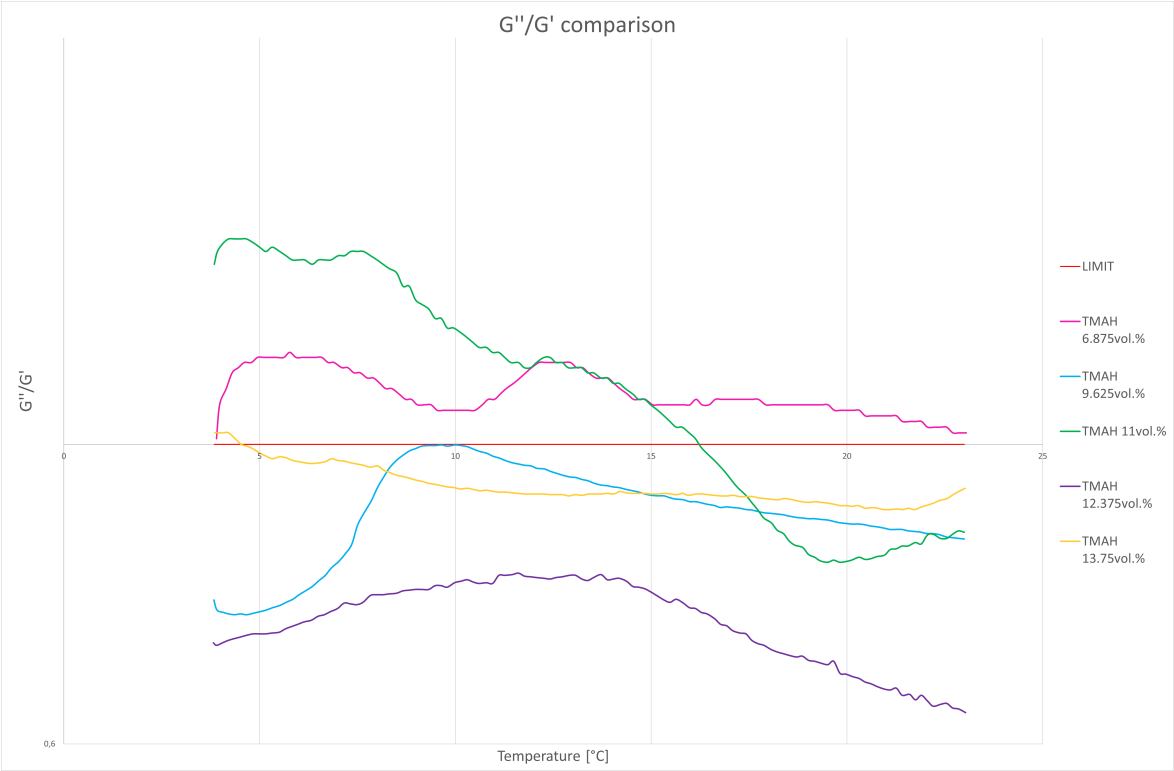

Figure 4.27: Printability index comparison.

The first ink to be analysed is TMAH 6.875vol.% In this case, the volumetric content of SiC which is 45vol.% has the main responsibility since as it can be seen the parameter is always lower than one. Generally, an unstable behaviour is kept. A first ramp up and a second stabilization happens in between 5°C and 10°C. By increasing the temperature a second increase can be detected at 12°C after which a final plateau is kept until the end. During the whole trend the ratio values are in between 1.01 and 1.16.

Considering TMAH 9.62vol.% the trend changes, by starting from a smaller value: 0.767. As the temperature increases the plot rises up to 1 at 10°C. A consequent decreasing trend at an almost constant slope is maintained until the end of the algorithm, reaching a value of 0.861 at ambient temperature.

TMAH 11vol.% starts from the higher ratio value of 1.42. However this plot is affected by a high variability showing a change in slope after a first instability. Around 16°C the limit line is intercepted, characterising the ink as printable at ambient temperature. Afterwards, by approaching 20°C a new increasing part starts, showing a smooth inclination that leads again to values around one. However, by considering the application of this ink at ambient temperature no further studies have been performed. In this way the results are reliable and comparable with the others.

The TMAH 12.37vol% is targeted by the lowest ratio values. The trend is composed by a first ascending path that starts at 4°C and ends at 12.5°C. The second part is characterised by a decreasing trend, that leads to the final ambient value of 0.633 at 23°C. The highest ratio values are measured as 0.797. The initial one is the lowest initial G”/G’ value, around 0.7.

TMAH 13.75vol.% has the highest amount of stabilizer. This characteristic should also be cause of the highest liquidity and so greater G” value. Considering the ratio, the value starts at 1.02 but it is kept always lower than 1 by increasing the temperature. The variability in trend are not excessively marked. However, after 20°C the value starts slightly to increase as done by TMAH 11vol.% but with a smaller slope.

However, it must be said that by doing studies in different days after a week of storing in ambient

conditions without the intrusion of air nor external particles, the aging effect is visible. This time the value has been presented only in the ink TMAH 13.75vol.% since it is the only one in which the aging effect has been detected and is clearly visible.

It can be seen that by storing the ink for some days after having opened the sample and let the atmosphere interact more with the paste, the plot is completely changed. In fact a parabolic shape is represented, showing a decrease in module and the subsequent increase upon reaching ambient temperature.

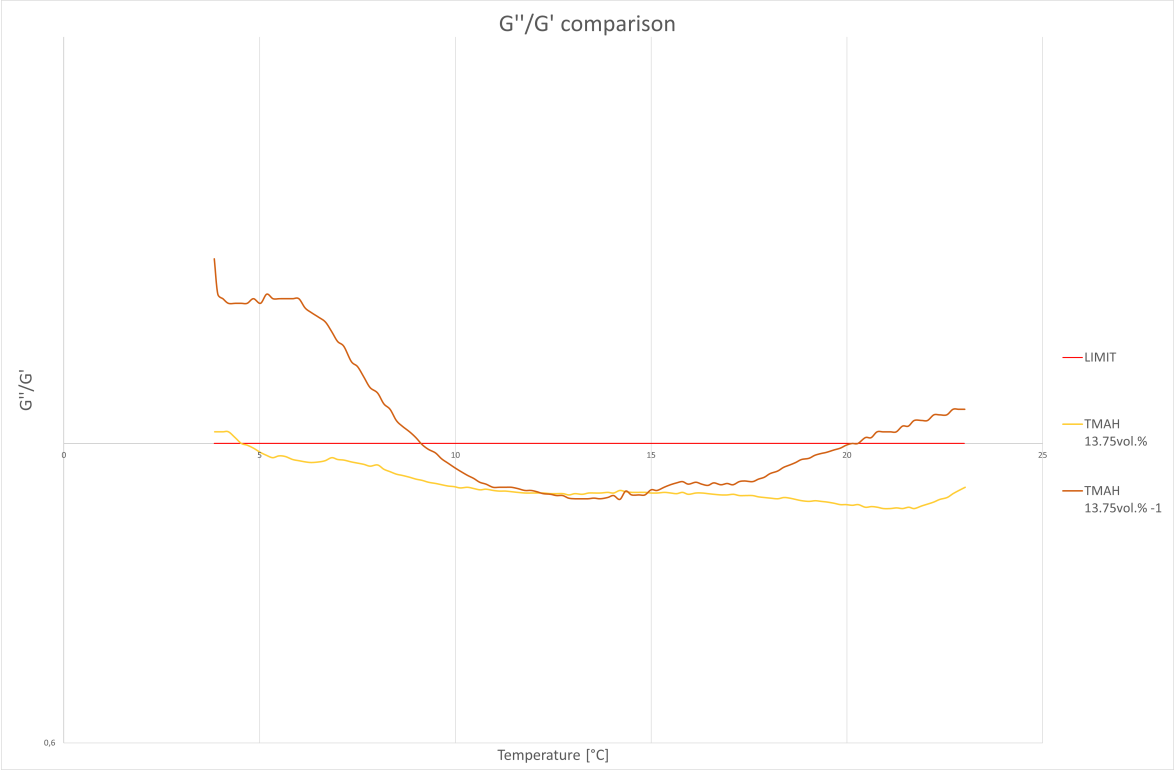

Figure 4.28: Aging effect on TMAH 13.75vol.% in G”/G’ plot.

It can be seen that by considering the same ink after a week (TMAH 13.75vol.%-1), the G”/G’ parameter follows a different trend. The initial value is 3.84, so three times the initial value of the ink as soon as it was taken out of the flask. By increasing the temperature the path descends, becoming <1 before 10°C. A second stable trend is kept with a value of 0.91 from 10°C to 15°C. This short stability is completely similar to the original ink path, crossing moreover the same values. As soon as 15°C are crossed, the ratio increases again, reaching values greater than 1.

Similar considerations can be done by analysing the singles G’ and G” trends. Since they represent the factors that determine the ratio values, a more clear overlook of the effects that might effect the behaviour may be detected. The solution behaves more like a liquid being characterised by a constantly decreasing viscosity values. G’ and G” must be subsequently affected both in module and in plot characteristic by changing the temperature. The transition temperature, as already seen, does not imply any concrete change in the thermal behaviour.

G’ and G” plots are associated by type of ink being characterised by similar values. By considering the viscosity plots and the G”/G’ plot a first assumption of the trends can be done. Considering the lowest amount of TMAH the plots should not be much different than the pure SiC inks. By increasing the TMAH concentration a different behaviour is expected, changing also the slope after a certain temperature. In addition, the temperature at which a change in behaviour happens is expected to vary by using a different stabilizer amount.

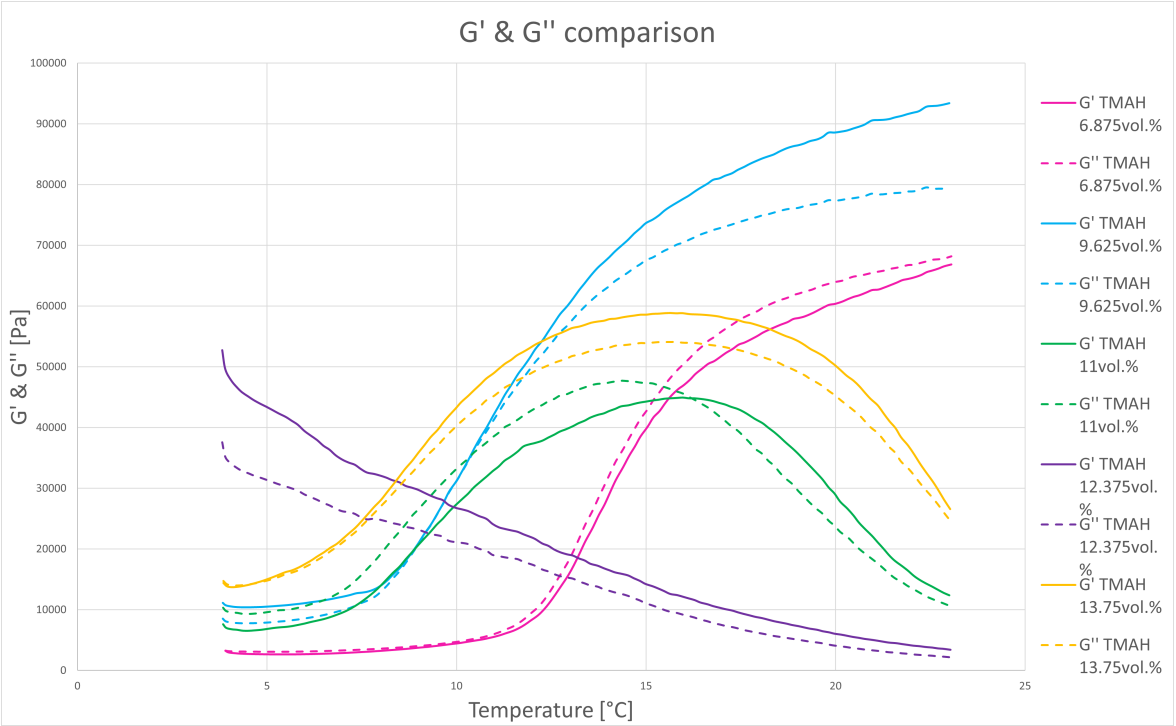

Figure 4.29: G' and G" comparison.

TMAH 6.87vol.% and TMAH 9.625vol.% represent the only two plots that approximate the pure SiC ink behaviour. By increasing the TMAH content, the typical "S"-shaped trend is lost.

As mentioned in the previous picture explanation, TMAH 6.87vol.% is characterised by a G"/G' always greater than one. By considering the ratio definition, it means that the G" value is never crossed by G' implying a liquid like behaviour.

A similar plot is shown shown for TMAH 9.625vol.% that follows the same slope of TMAH 6.875vol.%. However, G' becomes greater than G" before reaching 10°C. This values is visible in the previous plot, representing the temperature dependent area of printability.

By considering TMAH 11vol.%, a change in slope implies the difference from the previous two inks. Two consequent changes in concavity bring the plot from a first increasing path to a decreasing path. G' is greater than G" from 5°C on. The difference in modules in between G' and G" can be analysed in comparison to the slope of the G"/G' curve of TMAH 11vol.%. The difference is kept mainly constant during the whole evolution. By going towards the end of the algorithm the difference reduces, down to the minimum value detected at 23°C.

The G' and G" modules of TMAH 12.37vol.% the plots are different to the others mentioned. It represents a descending path for both the moduli, tending towards a plateau at ambient temperature.

The last group of curves are of TMAH 13.75vol.%. The behaviour is comparable to the TMAH 11vol.% representing a change in concavity that leads to a first increasing trend and a second decreasing one.

Shear Rate Algorithm

The correlation in between shear stress and viscosity has already been explained during the Rheological analysis in the previous chapter and in Chapter 3.5.1. By applying a shear deformation the viscosity undergoes a decrease. This effect is particularly useful while passing through the nozzle since a conical nozzle causes the increasing shear stress by flowing towards down. The microstructure is affected by the variation in shear stress, decreasing the viscosity and allowing a better flow. Due to

the viscoelastic behaviour, once the load is removed, the initial structure is recovered. However, by considering the TMAH addition the microstructure is being changed.

G' and G" are the primer parameters affected by the change in shear stress. They are crucial to determine the printability characteristic of the inks. By considering a printable ink characterised by G"/G'<1, by being G'>G" the structure is characterised by a solid like behaviour. A solid like behaviour would imply a non flowable ink. By flowing trough the nozzle G" becomes greater than G', assuming a liquid like behaviour. Once the ink is deposited, by removing the load the dominant state is the solid one. By reaching a sufficient shear stress therefore the viscosity allows a state transition allowing the ink to pass trough the nozzle. By considering the phase transition, the yield stress implies the change in state, determining the printability behaviour. It is therefore crucial to understand the minimum shear stress value to allow the ink to be printable (Chapter 3.5).

A key factor is the correlation with the pure ink behaviour. In fact by considering a greater volumetric SiC fraction and the TMAH addition the viscosity change could present a different path if compared to the pure silicon ink.

All the tests have been repeated in order to obtain comparable results. The data acquisition considers 100 values per test.

In the first plot the main decreasing trend of the viscosity with respect to an increasing shear rate can be observed. The same range of variability of the plot of the pure SiC ink is maintained. However, the inks present a greater linearity even if presenting marked variability at half way.

As a prior observation, by adding TMAH the curves move down towards lower viscosity values. Moreover, instabilities during the whole shear rate range of variation are present in different magnitude. Around range in between 1.67 and 19.67 the use and down can be observed. In its extremes a more stable path is present.

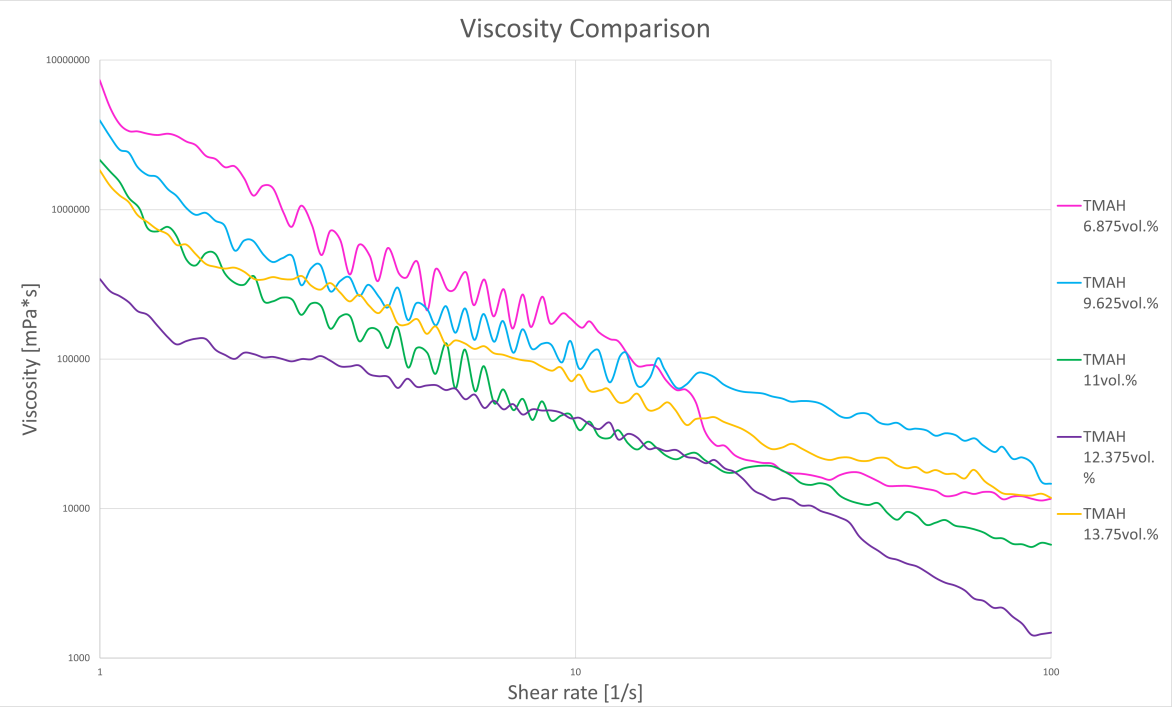

Figure 4.30: Shear Rate viscosity result.

TMAH 6.785vol.% is the plot that starts from the highest initial viscosity. By increasing the shear rate, a series of fast instabilities are present up to 10 1/s, after which a more even flat path leads to the final linear viscosity value. $1.18*10^4$mPa*s represents the final viscosity value. At 17.1 1/s a small

decrease happens, causing a moving down of the remaining part of the plot.

TMAH 9.625vol.% follows a similar trend of TMAH 6.875vol.% but it is characterised by a longer instability. From 20.5 to the end the plot is not affected by a huge variability by a flat trend leads to 1.47mPa*s of viscosity. In articular, the trend presents grater viscosity values from a shear rate level of 18.7 1/s.

A similar trend is shown by TMAH 11vol.%. A comparable variability range to the TMAH 9.625vol.% is present but starting at 1.24. Some smaller instabilities are than present until the algorithm end.

A more flat trend is present for the entire duration of the TMAH 12.375vol.%, presenting a smoother trend. The final viscosity level is $1.43*10^3$mPa*s.

Considering the highest TMAH amount, the TMAH 13.75vol.% is the one that should behave as characterised by the lowest viscosity values due to the stabilizer effect. However it presents a similar trend to an average of the already mentioned. The majority of the trend is represented in between TMAH 6.875vol.% and TMAH 11vol.%. The intermediate trend presents instabilities comparable to the ones present in TMAH 12.375vol.%. The final viscosity value is the same of TMAH 6.875vol.%.

Since TMAH has been added in different quantities, some tests have been repeated after some time to investigate the aging effect. As already represented in the temperature ramp algorithm, the effect on viscosity and G"/G' is visible. The same explanation can be done during the shear rate algorithm.

Considering the viscosity trend, the aging effect causes a sensible change in the plots depending on the quantities of TMAH that has been added.

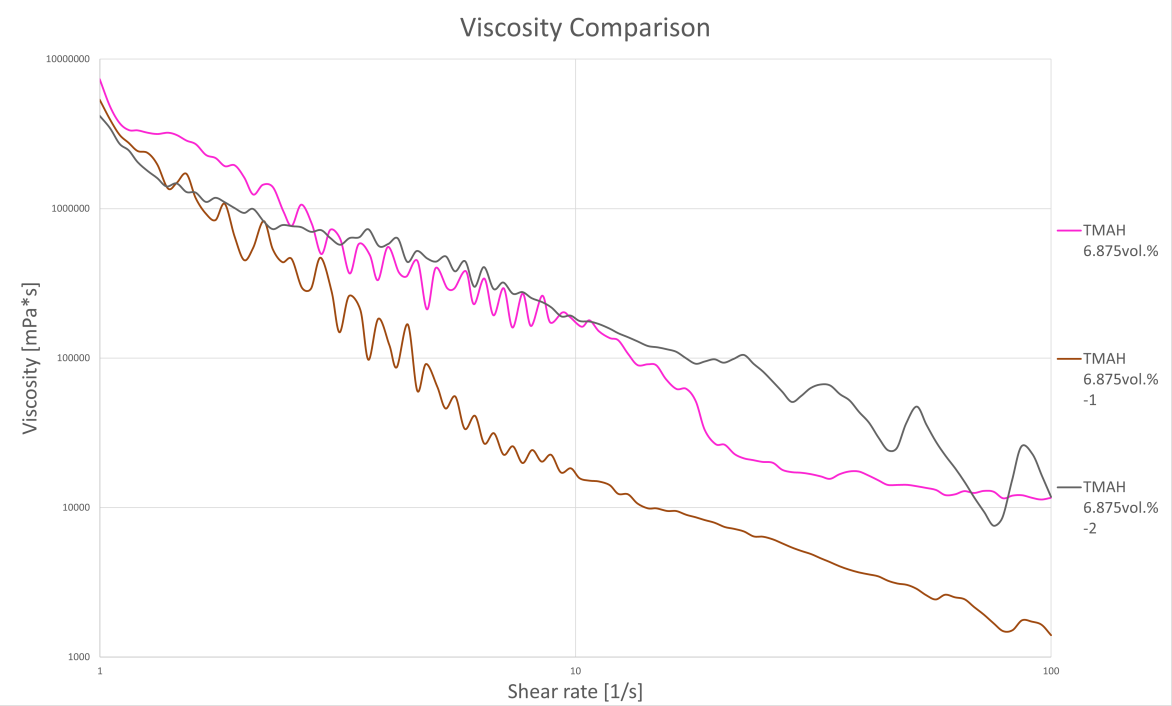

Figure 4.31: Aging effect on TMAH 6.875vol.%.

By considering the TMAH 6.875vol.%, the second plots has been measured one week after the previous one. The main trend shows a lowering in the whole path being characterised by a lower change in viscosity module without experiencing a decrease as in the previous one, The main difference is the lower values detected by increasing the shear rate. The path follows a more flat trend without excessive amplitude instabilities.

The third plot represents the same sample after nine days from the original measurement. It can be seen that the trends is completely different and the values measured are similar for the first part up to 10 1/s of shear rate to the TMAH 6.875vol.%. However, after this shear rate value the plot assumes higher values, ending in the same final value of TMAH 6.875vol.% but presenting visible instabilities with a significant magnitude.

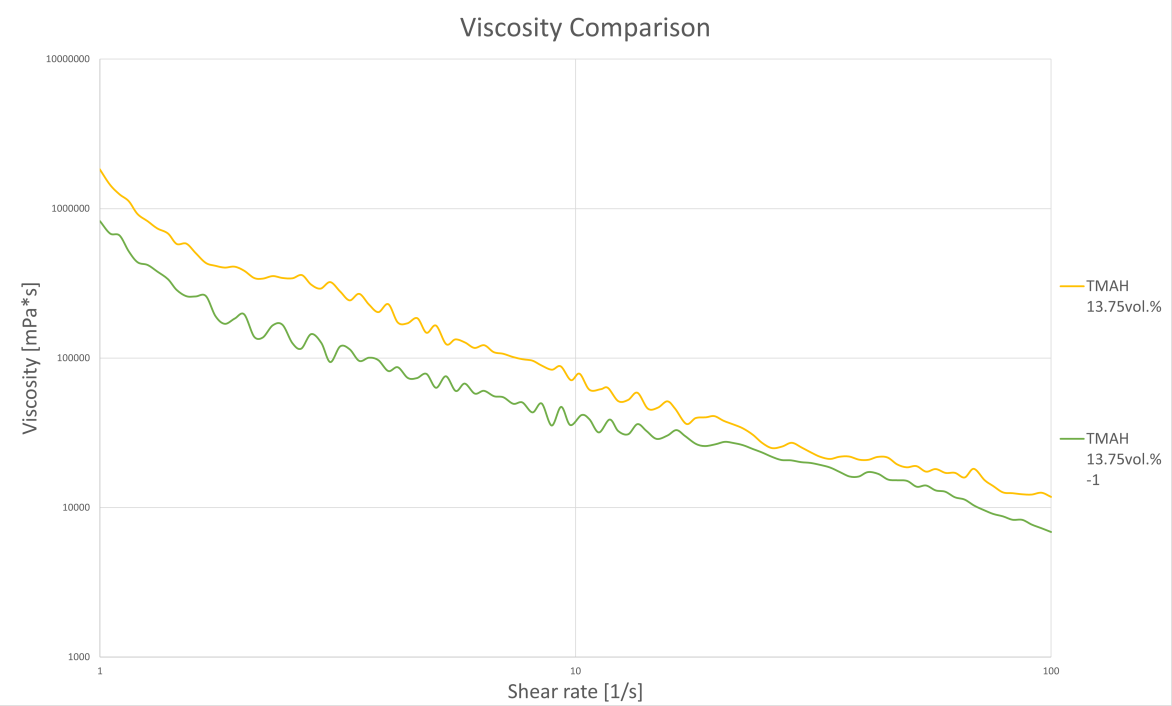

Figure 4.32: Aging effect on TMAH 13.75vol.%.

The TMAH 13.75vol.% measurement has been repeated after a week of storing at ambient temperature to investigate the aging effect. As it can be seen, the main trend is respected, as if the only effect is a small transition towards lower modules. The second Shear Rate algorithm solution plot shows the shear stress evolution on the tested ink as a consequence of the upper plate spinning.

Generally it can be seen that by increasing the stabilizer addition the shear stress detected decreases. The plots are characterised by a similar trend following a first decrease and a second stabilization. Some instabilities from 1 1/s to 100 1/s of shear rate are measured.

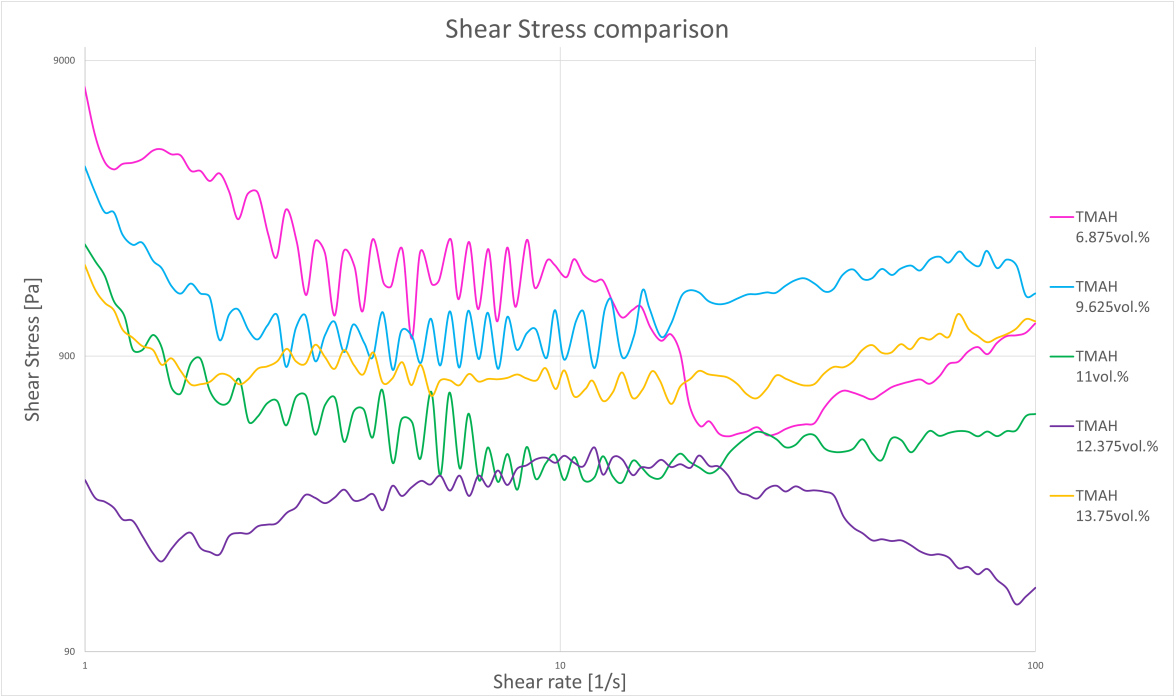

Figure 4.33: Shear stress output of the Shear Rate algorithm.

The highest shear stress values detected are found in TMAH 6.875vol.%. Similarly to what happened during the viscosity behaviour, at 1.92 1/s the first instability is detected. As happened in the viscosity study, at 17.1 1/s a decrease in trend happens. The instabilities are than smaller in amplitude. A consequent increasing trend follows from 22.6 1/s until the end. The last shear stress value is measured as 1180.3Pa.

TMAH 9.625vol.% shear stress behaviour starts at 3949Pa. A first decreasing path leads to a more flat average trend, instabilities are present in different intensities during all the evolution. A more stable path than the TMAH 6.875vol.% is present at 17.1, part in which TMAH 6.875vol.% decreases while TMAH 9.625vol.% slightly increases up to the final value of 1467Pa.

A lower starting value is shown by TMAH 11vol.% by assuming 2150Pa of shear stress. Instabilities have been measured throughout the entire evolution path. A first decreasing path lasts until 12.9 1/s, after which the path stabilized continuing in instabilities. The final shear stress value was measured at 537.4Pa.

TMAH 12.375vol.% is characterised as already mentioned several times by the lower values in module of an order of magnitude. By considering the shear stress trend it can be seen that a smoother trend is present, By reaching 10 1/s the maximum shear stress value is measured, around 442Pa. Instabilities are present with lower amplitude than the other ink alternatives during the duration of the algorithm. The final shear stress is detected as lower than 150Pa, being lower than the pure SiC inks.

TMAH 13.75vol.% as in the viscosity representation, the plots represent a trade off in between the previously mentioned inks. It represents the most stable trend even if being characterised by a huge instability but low amplitude. The final shear stress value is 1180.3Pa. The initial decreasing rate up to 1.75 1/s follows the same slope of the previous inks.

More visible alterations due to aging effect can be seen in the shear stress plot in which the difference in module of the TMAH 6.875vol.% are more visible.

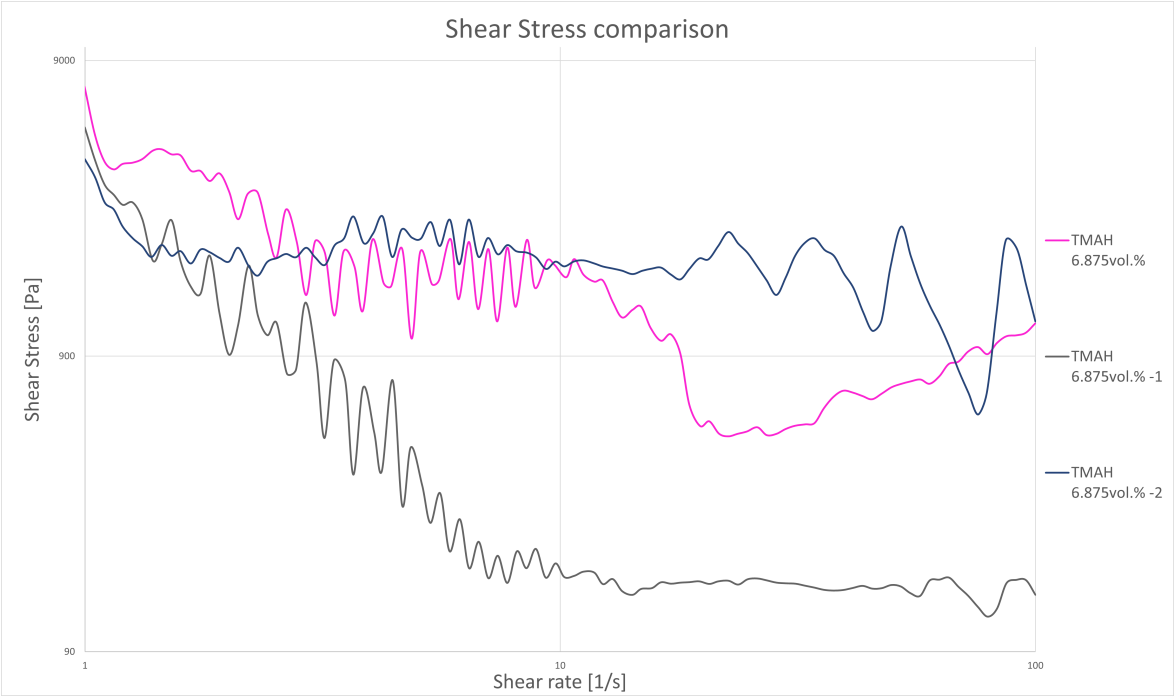

Figure 4.34: Aging effect on TMAH 6.875vol.%.

Similar changes as in the viscosity trend can be seen in the Shear Stress plot. From the starting similar value of shear stress, the plots are firstly lowered towards lower viscosity values. However, by performing again a measurement after a certain time, the plot of TMAH 6.875vol.%-2 assumes greater shear stress values than TMAH 6.875vol.%-1, going back to the initial levels presenting a more stable trend but final greater instabilities in module.

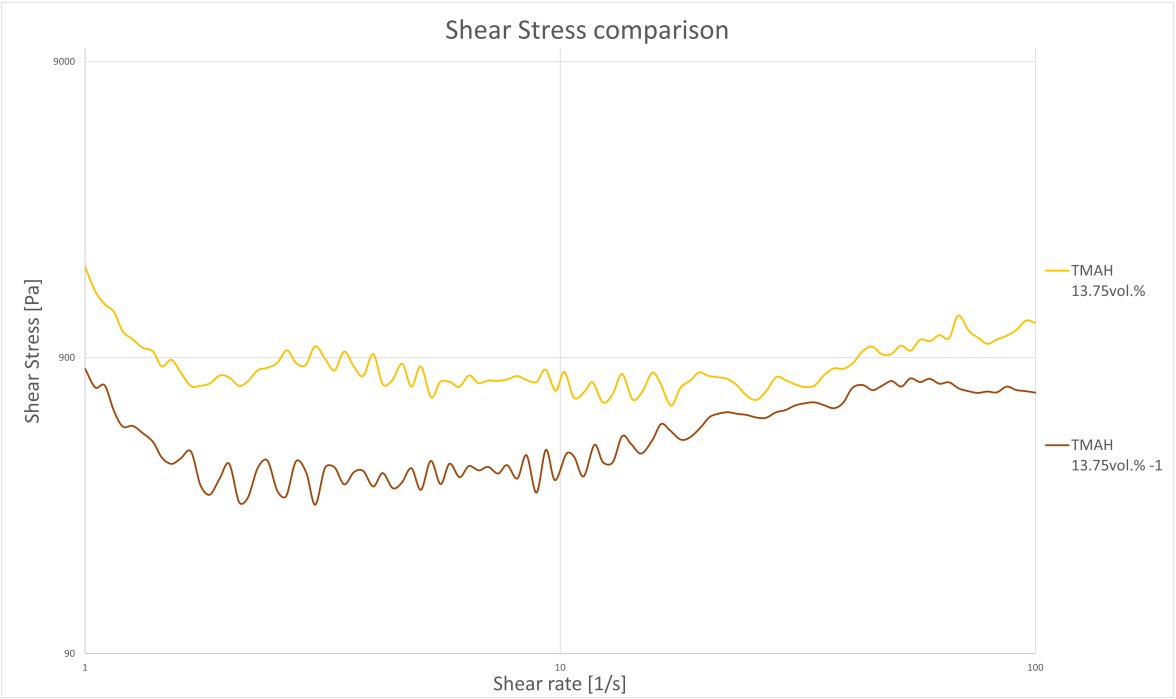

Figure 4.35: Aging effect on TMAH 13.75vol.%.

As expressed for the viscosity trend, the main change is represented by a transition in module towards lower values. This causes a decrease in module as if the initial plot is entirely moved towards

lower viscosity values.

Shear Stress Algorithm

As already explained for the SiC pure ink rheological characterization, the same data collection has been maintained in order to keep consistent results. The shear stress algorithm has the characteristic to allows us to evaluate the behaviour response of the ink wen it is loaded with a shear stress. By comparing a general SiC pure ink result plot of the shear stress algorithm previously explained, it is obvious to obtain some differences in the output plot shape and order of magnitude. By considering the usual rule expressed by del Manzo et al., it will give the possibility to understand when the ink is printable in terms of stress [30]. So the shear stress applied by the screw present into the printer head can be tuned to avoid excessive loads and excessive shear stresses and shear rates to decrease the viscosity.

As a general overview, it can be seen that the average order of magnitude of the TMAH inks keep the pure SiC ink order of magnitude. Moreover, by increasing the content of TMAH, a light decrease in modulus happens, shifting the curves towards lower G' and G" moduli. Another visible characteristic is the loss of plot shape by increasing shear stress at high concentrations of binder. It can be seen that by proceeding with the tests the curves become disordered without respecting the previous shape and proportionality with the previous ink plots.

As mentioned for the pure SiC inks, the G' modulus starts as greater than the G", meaning that a solid behaviour is dominating. However the yield stress is reached and the G" becomes greater than G', causing also the change in state, moving towards the liquid state. As a consequence, the main ink behaviour is comparable to the pure ink, even if being more variable in the modulus range and shape of the final part of the plot.

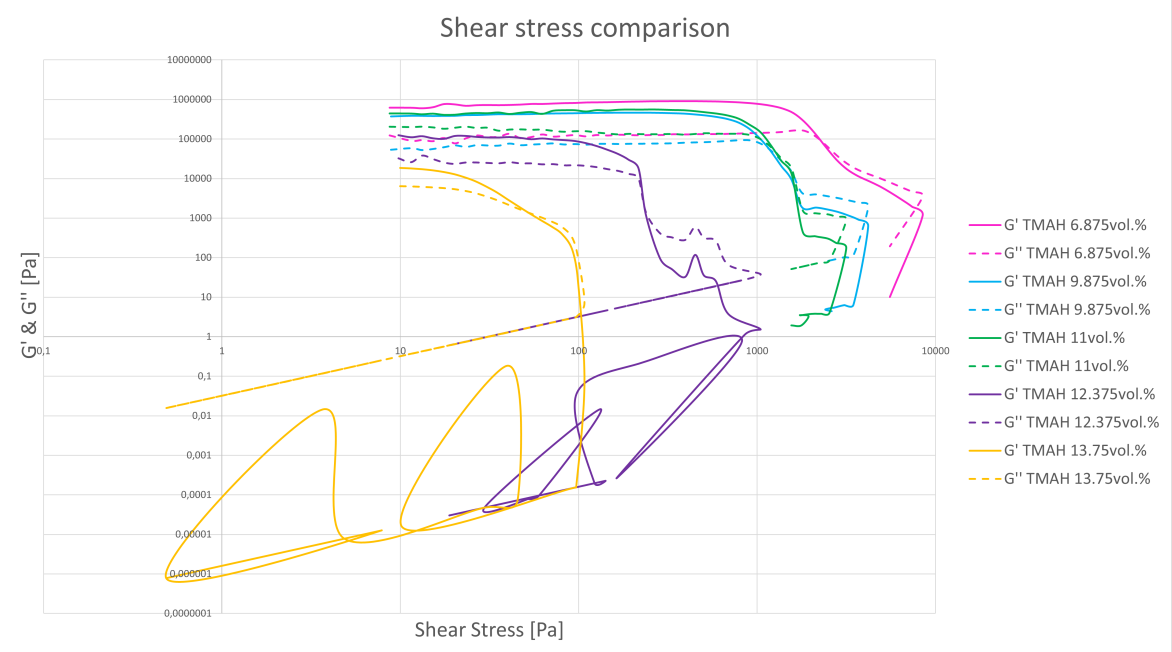

Figure 4.36: Shear Stress output.

The plots have the same shape of the pure SiC inks. However, one main characteristic distinguishes them as a cause of the TMAH addition. By looking the plots tail, the inks are characterised by a shorter concluding part being however more variable. An apparent decrease in shear stress leads to lower G' and G" values. It must be said that since the test considers a constantly increasing shear stress, there is no possibility that the rheometer loads the ink with a decreasing shear stress.

The plots that present a change in shape are represented by the TMAH 12.375vol.% and TMAH 13.75vol.%, which have the two highest TMAH concentrations. The final part of the plots have the largest module variability being however not stable. G" in both the inks after a first abrupt decrease in module respectively at 216Pa and 91Pa, they follow a linear trend at constant inclination.

G' represents the parameter mostly affected by variability. The G' plots at high TMAH concentration move up and down in module, being affected by the increase and decrease of the shear stress. The lowest G' values detected vary form 10^{-2}Pa to 10^{-5}Pa.

For the Shear Stress algorithm, no aging effect has been detected.

Frequency Sweep Algorithm

For the same reason explained in the Frequency Sweep algorithm results in the pure SiC ink section, the same test has been done on the ink with TMAH content.

By considering the variability of the results obtained, the same shape is maintained. A slight increase in module by reaching the highest frequency is detected. A more visible variation in module can be seen by increasing the TMAH content, so by liquifying the solution the viscosity decreases for the whole frequency sweep algorithm.

Despite the Shear Rate algorithm, in all the ink alternatives the main viscosity trend follows an increasing trend. As already expressed for the SiC ink, the opposite viscosity behaviour is strictly related to the action of a stress on the sample surface. By avoiding an imposed shear stress, the viscosity of the ink tends to increase.

The maximum plot values are measured when the frequency reaches its maximum values.

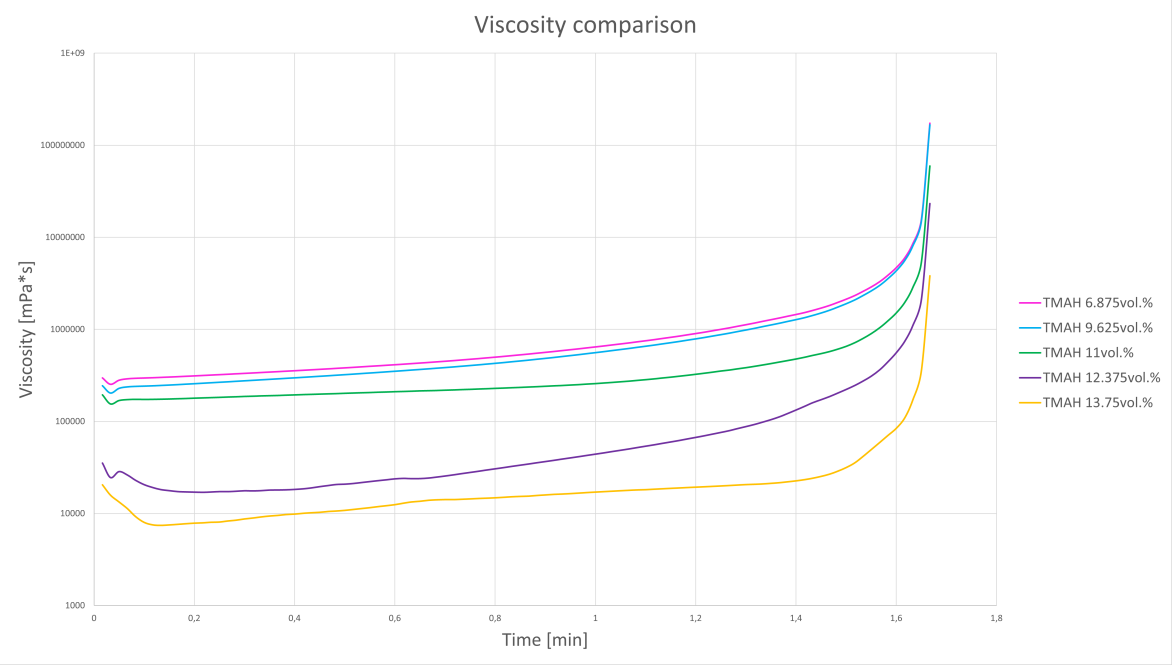

Figure 4.37: Frequency Sweep output.

Moreover, it can be seen that the TMAH 6.875vol.% behaves as SiC 40vol.%. By increasing the TMAH content the module shift is not linear but exponential, reaching he lowest values of TMAH 12.375vol.% and TMAH 13.75vol.% an order of magnitude lower than TMAH 6.875vol.%. In addition, the TMAH 13.75vol.% and TMAH 12.375vol.% linearity is lost by reaching the frequency mean value.

Similarly to the Shear Stress algorithm, even in the Frequency Sweep algorithm the aging effect is not visible.

4.4 PRINTING

To obtain the best printer definition, the smallest nozzle diameter that works for our setup has been found through iteration, by trying with the same setting and the same ink until no flow was reached. The diameter chosen was 0.41mm.

4.4.1 Parameter setting

One of the most useful parameter to control is the extruder multiplier, that controls the amount of ink extruded and the spinning speed of the printing screw. By controlling the extruder multiplier and the layer height the ink can be used to obtain the best printed structure. More in detail by considering the nozzle diameter, several iterations has been done for the SiC ink treated with TMAH. The first tries used an extrusion multiplier level around 1 to 5. These settings was discovered as non sufficient to allow the ink extrusion. The maximum levels used were up to 1000 of extrusion multiplier, causing an excessively long extrusion. Software limitations were the main limit considering excessive setting values.

The suitable extrude multiplier order of magnitude has been discovered to be lower than 50, causing error in the code only depending on the layer height.

As a consequence, by controlling the layer height the printer performance was affected. By increasing the layer height, the extrusion in some cases was not reached due a too small speed setting for the ink viscosity and need to have friction in the ink to allow a better ink outlet. By considering a not enough height, the deposited ink layers may be difficult to attach one to the other. In some cases, a too low position of the nozzle caused the collision in between the already printed parts and the nozzle while moving.

The next figures represent the tries done on a printable sample that is composed only by a line, whose thickness has been increased in order to see the behaviour of the ceramic ink while being deposited over itself.

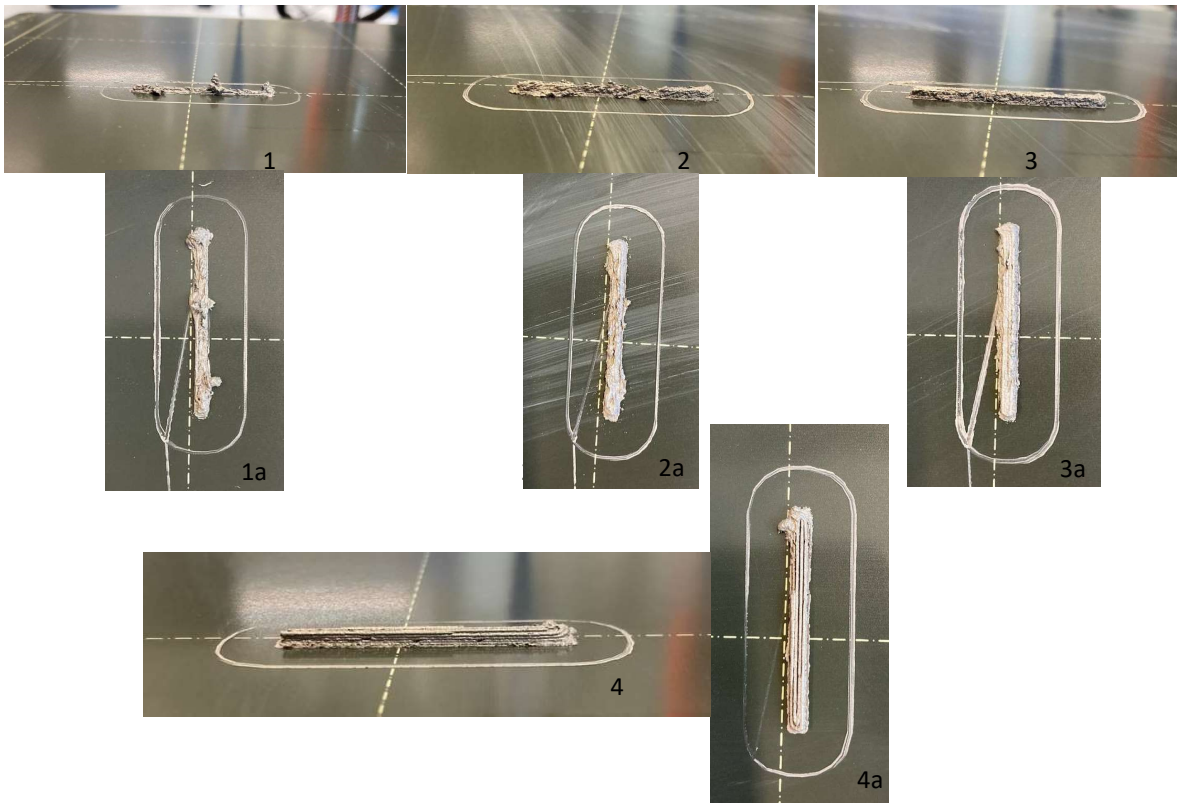

Figure 4.38: Printing tries with SiC 45vol.% TMAH 9.625vol.%.

Printing try 1 and 1a represent one of the firsts successing attempts. The first layer measured 0.5mm and the others 0.3mm. By using a sufficient extrusion multiplier around 20 but not sufficient nozzle distance from the plate the printed sample completely loss the structure. The nozzle, colliding against the already deposited ink, removed the ceramic paste. The non-sufficient calibration of the printing head height avoided the printing of different layers.

2 and 2a used the same extrusion multiplier of the sample 1. The nozzle was moved to a a higher position, 1mm more than the previous one. However the layer thickness has been decreased from 0.3mm to 0.1mm while the first layer has been kept constant. By considering these setting changes, the printer was able to print the first layer without collisions. For additional layers the nozzle height was not sufficient to avoid ink removal from the already printed layers. In fact some accumulations on the layers can be seen.

The third printing try represented in the Figure 4.38 3 and 3a represented a step forward the final settings. Several layers could be obtained. In this sample the extrusion multiplier has been increased from 20 to 40, allowing a greater amount of ceramic ink to be extruded, therefore a faster screw spinning. In addition the layer thickness has been changed: the first layer measured 0.4mm while the others 0.2mm. In this situation the ink extruded showed a successful print. In some borders it is possible to detect a non sufficient precision in the printing.

The ink try represented in Figures 4.38 4 and 4a used 0.4mm of first layer thickness and 0.2mm of first layer. The extrusion multiplier has been reduced from 40 to 30, in order to avoid an excessive extrusion of the ink and a non satisfying accuracy during the printing. As a consequence, the layers can be distinguished. The deposited lines are accumulated reaching the final sample height of 0.5cm.

4.4.2 Printing Outcome

The final set of settings used to print the test lines has been considered to be sufficient to print more complex structures. The aim of this thesis is the printing of a heat exchanger able to be used in CSP applications. The structure proposed by Du et al. and Thomas et al. represented already in Chapter 2 Figure 2.3 represents a simple geometry obtainable by DIW. The structure proposed is already been tested to be used in CSP applications [1, 3].

The same design proposed by literature has been used as a sample proof of printability of the ink produced. The same structure has been kept equal to the designed one, assuming the same size and geometry. In order to avoid excessive printing times, a section of the heat exchanger proposed by Du et al. has been printed [1, 3]. Moreover a greater printer should be used to produce the complete structure, involving larger volumes.

The dimensions used for the printing are the ones reported in Figure 4.40, representing the heat exchanger proposed by Du et al. in Figure 2.3 [1]. The small dimensions of the holes was proven to allow the sCO_2 flow, improving the heat exchange in between the two HTFs [1, 3]. The small distance between the channels is due to heat exchange maximization.

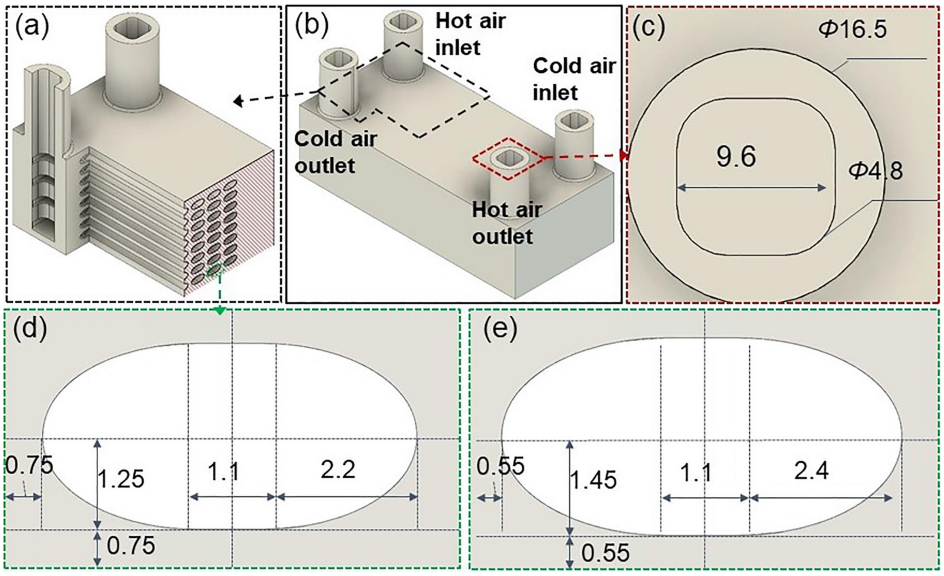

Figure 4.39: Heat exchanger dimensions proposed by Du et al. [1].

For the section realization, only nine holes were considered. Some thicker edges have been designed in order to contain the structure and decrease the printing time, which would be greater if some curved parts were considered on the edges. In the next Figure, a rendering of the section considered for the printing is considered.

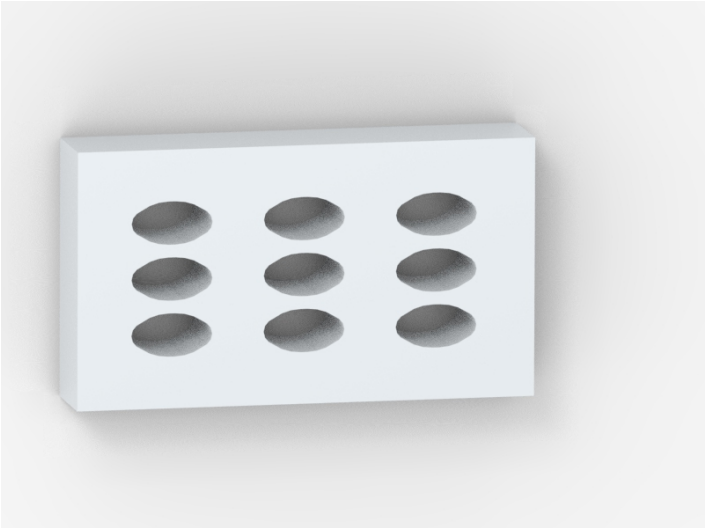

Figure 4.40: Heat exchanger section rendering with Keyshot (Siemens PLM, Germany).

The printing produced by using the settings reported in the previous section and a nozzle of 0.41mm and 0.61mm have allowed to print the structure. The ink used are SiC 36vol.% and SiC 45vol.% with TMAH 9.625vol.%. The infill density was kept constant to 200%. The first printing tries allowed to produce the outcome showed in the next Figure.

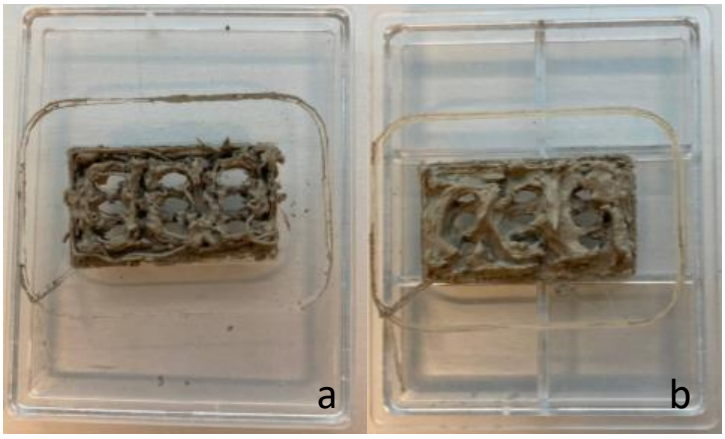

Figure 4.41: Heat exchanger printing comparison: a) SiC 45vol.% and TMAH 9.625vol.%, b) SiC 36vol.%.

As it can be seen, the printings present the same design but different outcome. The ink made of SiC 45vol.% and TMAH 9.625vol.% in Figure 4.41 a) allows to print a more defined structure, producing a distinguishable filament that due to a non correct profile definition it was not able to stand on the already printed parts. By looking at Figure 4.41 b) the first layer printed allows to distinguish the first printed layer in which the design is still visible while the next layers lose the geometry.

By focusing on the performance improving of the printed heat exchanger section, only the TMAH 9.625vol.% ink has been considered. In the subsequent Figure the outcomes can be seen.

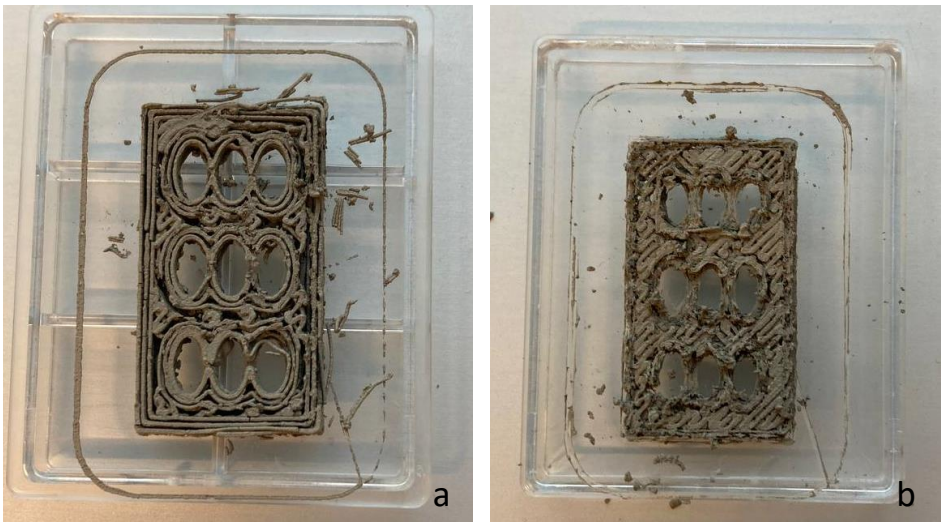

Figure 4.42: Heat exchanger printing: a) performed with a nozzle of 0.61mm diameter, b) performed with a nozzle of 0.41mm diameter.

The filling structure could be enhanced trough a change in the nozzle dimension, increasing the printed density. The quality of the print was strongly affected by the excessive drying of the first layers. This effect has caused the detachment of some printed parts that can be seen on the plastic plate, no longer belonging to the printing structure. The nozzle by printing accumulated some dirt on the nozzle tip that scratched the already printed parts compromising the final shape. In Figure 4.42 a) it can be seen that the voids present in the main structure compose a large fraction of the overall volume. by decreasing the nozzle dimensions, the Figure 4.42 b) represents a more dense printed structure. The motions of the nozzle on the printing bed can be distinguished among the various layers, actually changing direction to fill the voids left. The small parts between the holes was not obtained due to a non correct design, causing the consequent rupture of the connections. In Figure 4.42 a) the channels are left open on one border due to a non correct dimensioning of nozzle on the proposed design.

For sake of efficiency improvement and increase in the heat exchange, a different structure has been chosen to be printed. The gyroid structure is retained to be the next frontier of the heat exchanger structure, improving the contact surface with a complex structure. The gyroid represents a three-dimensionally repeated structure inspired by biological systems. It was developed by organisms and it can be found in skeletons and scaffolds [5]. This new structure is not possible to be obtained through common manufacturing technologies since its shape can be represented by the mathematical formula [5]:

$$cos(x)cos(y) + cos(y)sin(z) + cos(z)sin(x) = 0 \tag{4.1}$$

By considering the Thomas et al. and Du et al. outcomes concerning the heat exchanger printing with the inks proposed but considering the new structure proposed, the different final heat exchanger was used as sample to print. In the following figure a rendering of the .stl file provided for the printing is reported.

Figure 4.43: Printable structure.

As it can be seen, the shape proposes a different design than the one already reported. The Gyroid structure represents a contact area maximization for the heat exchange improvement. Microchannels are present allowing a differentiation between the two thermal fluids that should flow through. The vertical channels allow the different HTFs to move through the different levels while still flowing horizontally. This design can be compared to the already proposed one by Du et al. [1, 3]. The gyroid structure could be substituted to the horizontal channels considered, implying greater printing times but a more complex geometry.

The initial structure considers a length of 25mm and width of 25mm while the height is of 6mm. Each channel diameter measures 2mm. The structure represents a sample for testing phase a not for a final heat exchanger assembly, therefore the dimensions could be scaled in order to achieve the design needed.

By printing the gyroid structure, the results are conseqeuntly shown. It has been an iteration process in which after each change a print of a simplified structure was started. The gyroid structure has been reserved for the final setting optimization. By considering previous shown samples, the printing has been accelerated so to find the best setting is in the shortest time, to find the best settings to obtain the highest definition possible of the printed ink and the most complex structures.

The final prints represent the best outcomes obtained at the end of the iteration. Different calibration have been performed, considering also manual changes in the starting height of the nozzle. By iteration the best height has been obtained and kept constant. The nozzle height is part of the calibration process that should be done at the beginning of each print. However, due to the 3D printer modifications a correct position of nozzle and sensor was not possible since the interface in between the printing head and the printer support does not allow the correct positioning of the sensor proposed by the PRUSA manufacturers. Therefore it is fundamental to do the first extrusion tries by finding the best relative position of the two.

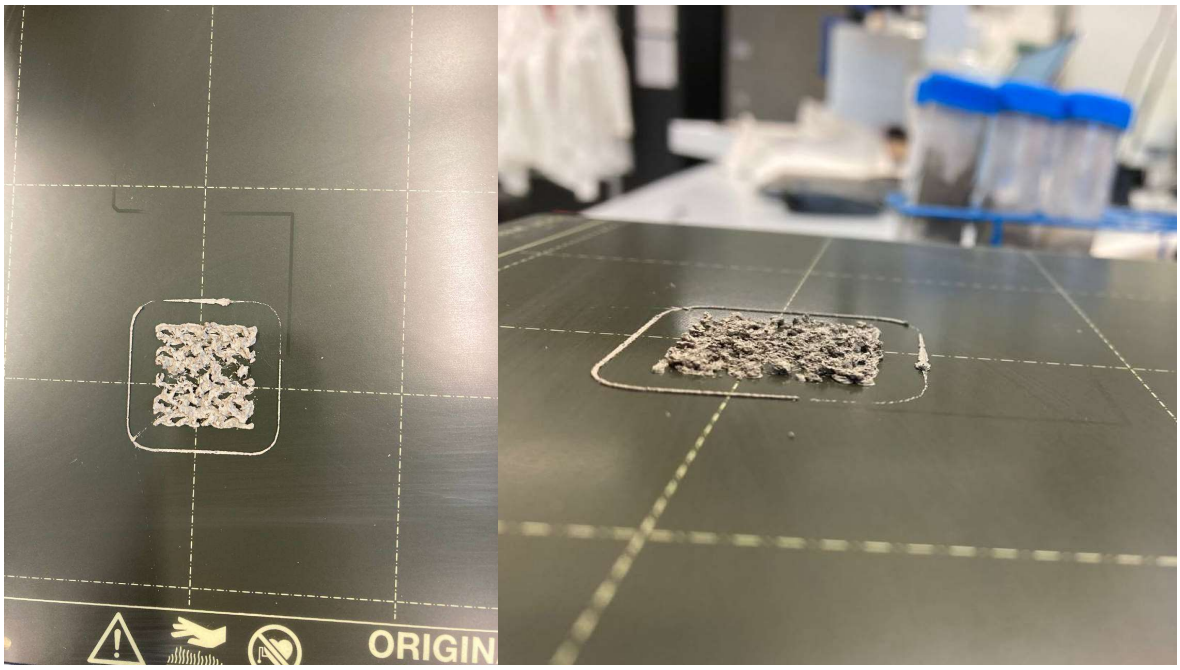

Figure 4.44: Gyroid try using SiC 45vol.% and TMAH 9.625vol.%.

By considering the previous image, the printed sample has been performed by considering subsequent iterations, with extrusion multiplier of 30, 0.2mm of layer height and 0.4mm of first layer height. Only the first layer can be distinguished from the others. The too low height of the nozzle made impossible to print complex structures. Moreover the setting related to the path to follow while printing implied the movement over the already printed parts without highering the z coordinate. The accumulations obtained are due to the nozzle that moves ink parts not already solid enough to withstand nozzle passage without being deformed.

To solve the quality problem, a higher layer thickness has been chosen, in order to allow a better nozzle positioning, and the utilization of the movement along the z axis to remove the accumulated ink while not printing in order to avoid collision with the already printed parts.

The final settings were configured as:

- Extrusion Multiplier − 30;
- First Layer height − 0.4mm
- Layer height − 0.3mm.

The greater layer height were useful in order to allow the collision with already printed parts. Moreover by increasing the height is has been seen that the friction of the ink with the already printed parts and the deposition bed allows a continuous ink flow by pulling it out of the nozzle. By considering the new settings the next structure has been achieved:

Figure 4.45: Gyroid final structure using SiC 45vol.% and TMAH 9.625vol.%.

The final structure obtained does not consider the various bridges present into the structure. Some non printed parts caused the non possible construction of structures, causing the structure breaking and voids in the structure. During these printing losses the quality of the other printed parts is strongly effected. Moreover the speed of the nozzle should be modulated in order to avoid excessive velocity while moving during the printing.

By considering the ink proposed by Feilden et al. SiC 36vol.%, the difference in viscosity behaviour due to temperature change involves half order of magnitude during the whole temperature evolution [46]. The inks was presented as completely printable therefore it has been chosen as a benchmark for comparison to the previously reported one SiC 45vol.% and TMAH 9.625vol.%, presenting sufficient characteristics to be printed. However, by implementing the ink in the 3D printer and using it to build structures, the viscosity at ambient temperature after the extrusion was not sufficiently high to allow a well-defined structure.

Using a different ink the G-Code had to be changed. The after layer change programming has been modified to:

- G92 Z0;
- G1 Z60;
- G4 S5;
- G1 Z;
- Nozzle size: 0.61mm;
- Layer height: 0.4;
- First layer height: 0.5.

The z axis elevation used for the printing of SiC 45vol.% and TMAH 9.625vol.% was removed in order to allow the continuous printing process. The visible low viscosity produced a continuous flow, therefore the elevation along z axis could have caused alterations in the geometry.

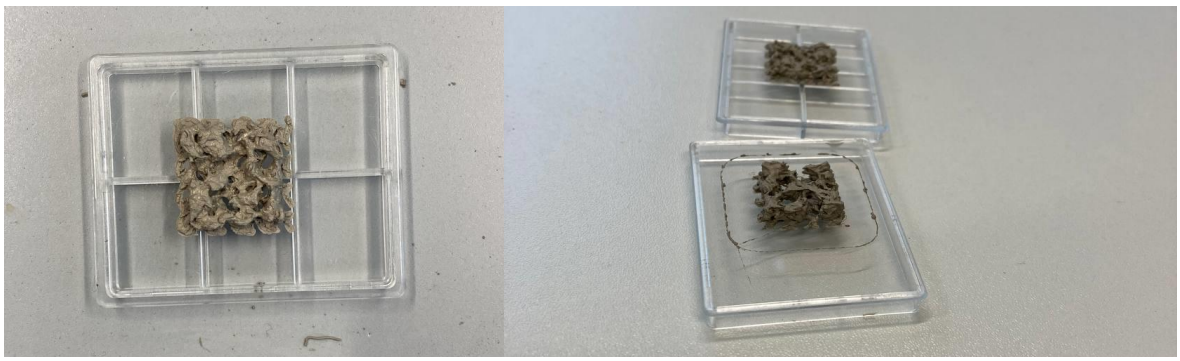

Figure 4.46: Ink SiC 36vol.% printing test of the gyroid structure.

The definition of the sinusoidal parts is lost, presenting parts with thicker walls and no geometry. The low viscosity caused the geometry walls to fall as soon as the ink was extruded, generating a confused final structure.

For the same reason, the suspended printed parts were not able to substain their weight causing the consequent collapse. The gyroid structure was printed on the first layer, while for the consequent layer deposition the weight of the other layers caused the accumulation of material in a disordered way.

4.5 MICROSTRUCTURAL CHARACTERIZATION

The SEM characterizaiton has allowed to obtain a series of pictures per type ink. Different magnifications have allowed to obtain greater zooms on the microstructure. As a consequence it was possible to analyse the porosity and the material distribution. The magnifications used were: 35 x, 50 x, 500 x, 1000 x, 5000 x. 50 x magnification was used to detect the material compositions. A greater level of magnification has been used however it caused more blurred images. As a consequence the subsequent analysis considers the magnifications already presented.

The SEM samples were taken from the printed specimens for both the ink alternatives and deposited on the surface of some plates. The breaking of the printing structure was necessary to detect the inner part of the printed samples. By covering the surfaces of the samples in Pt it has been possible to obtain more representative figure. Moreover, a thin Pt layer can be distinguished in Figure 4.48. In Figure 4.47 the platinum has been discarded by the SEM driving software.

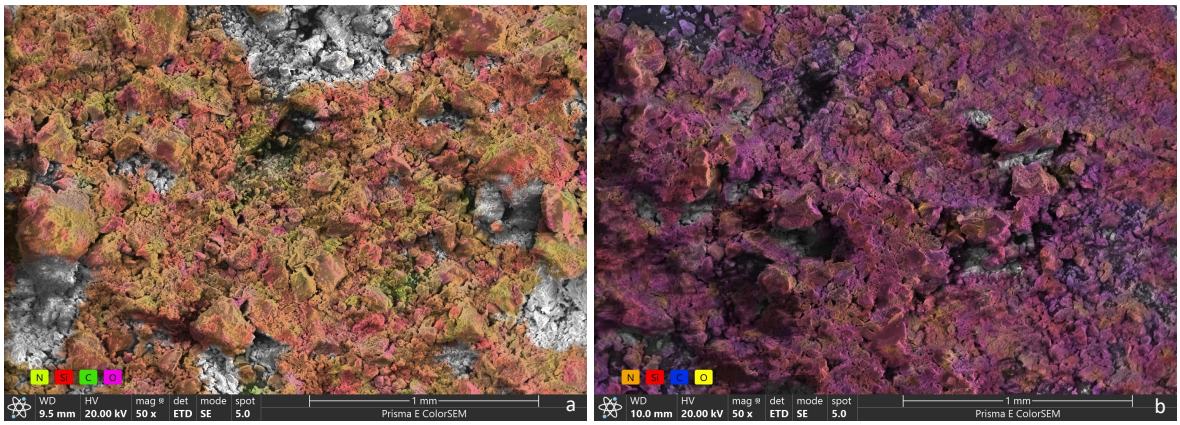

Figure 4.47: TMAH 9.625vol.% in Figure a), SiC 36vol.% in Figure b). Comparison between the material distribution in the two inks with a magnification of 50 x.

The material distribution can be analysed thanks to the various colours addressed to every chemical component. The main component, due to the vast majority of composition in the ink, in Si. C represents the second major component since contained in both Pluronic and SiC powder. Some traces of N can be detected in Figure 4.47a), however some errors in the SEM coloured solution may be present due to the similar structure of N to C. Figure 4.47b) should not present any N since not present in the ink formulation. The more clear spots may be addressed to presence of O localised in spots instead of N.

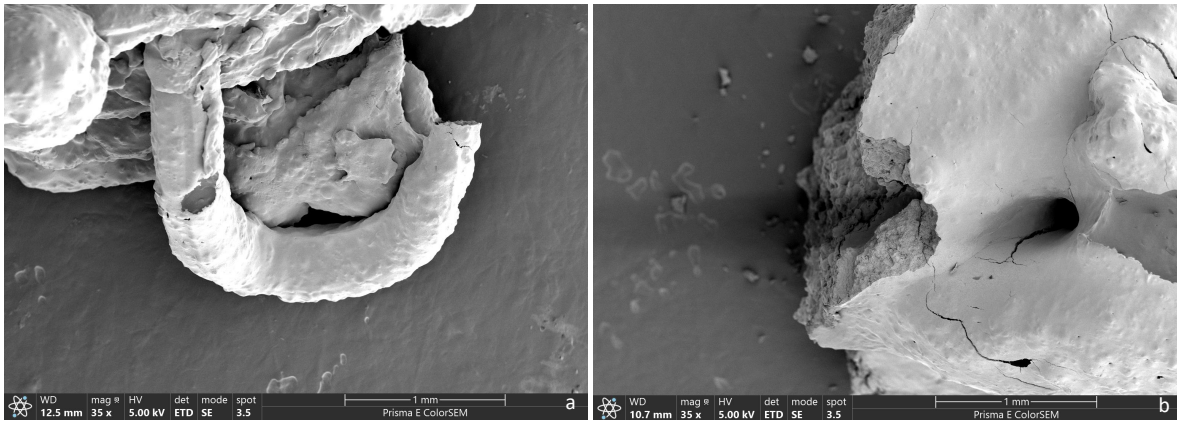

Figure 4.48: TMAH 9.625vol.% in Figure a), SiC 36vol.% in Figure b). Comparison of inks microstructure with a magnification of 35 x.

Figure 4.48a) represents an extruded filament that due to its weight and not enough structural strength has fallen from the initial position, being laid on the bed. The filament however keeps its printed dimension of 0.41mm, like the nozzle tip diameter. The surface appears as covered by a white cover which is the thin film of Pl deposited by CVD.

The bubbles present while extruding the ink are demonstrated by Figure 4.48b), in which a black dot with a diameter lower than 0.5mm has appeared. in this case also some cracks are visible on the Pt layer. However, by considering the center part of the figure the Pt crack continues in the inner part of the extruded ink.

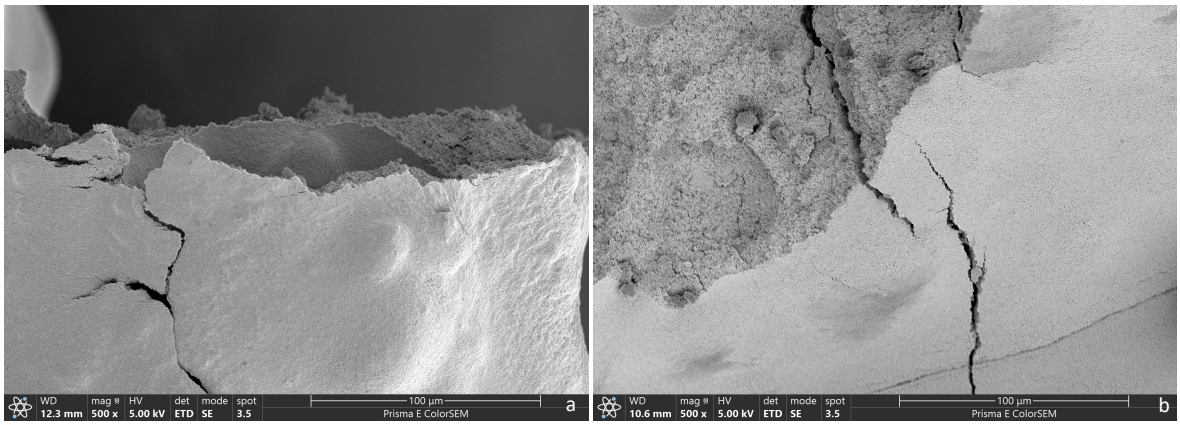

Figure 4.49: TMAH 9.625vol.% in Figure a), SiC 36vol.% in Figure b). Comparison of inks microstructure with a magnification of 500 x.

A more zoomed perspective permits to analyze the single cracks present into the printed parts and the presence of eventual agglomerations. For both the inks the printed surface does not present a planar geometry but some irregularities are present. Figure 4.49a) and Figure 4.49b) present a crack that is extended along the structure until the inner ink part can be seen. More cracks can be seen in Figure 4.49b) as well as more powder agglomerations on the inner part.

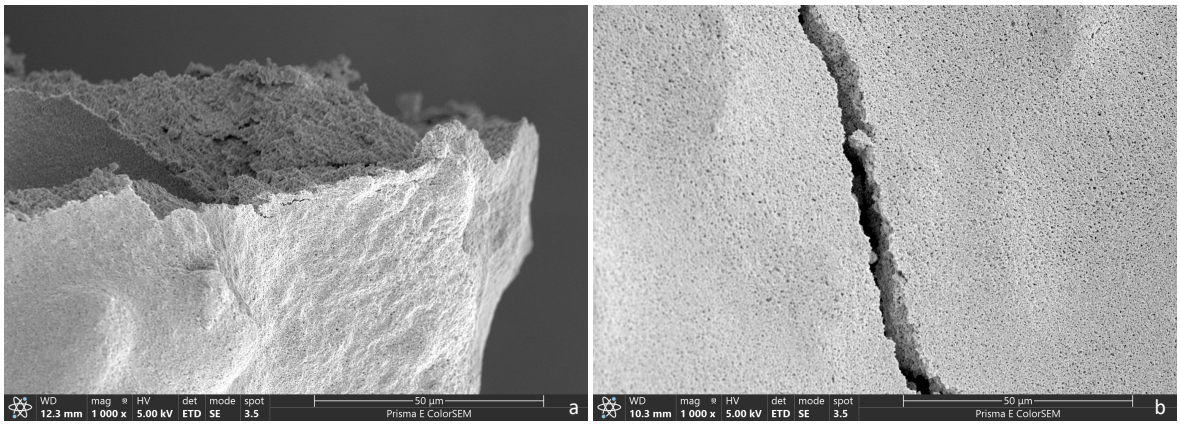

Figure 4.50: TMAH 9.625vol.% in Figure a), SiC 36vol.% in Figure b). Comparison of inks microstructure with a magnification of 1000 x.

By enlarging the magnification to 1000 x, Figure 4.50a) and Figure 4.50b) show the same previously represented structures. On the TMAH 9.625vol.% surface some smaller cracks are present where a structural break happened. However, no detectable agglomerations can be distinguished on the cross-section. The SiC 36vol.% crack follow a geometrical shape without causing other crack formation perpendicularly. the crack boundaries are not regular but assume a round shape following the pores boundaries.

As a main outcome, it is possible to visibly distinguish the pores present in SiC 36vol.%. Figure 4.50b) is characterised by a large presence of dark dots that are of different dimensions in all the structure. The pores are mainly not visible in Figure Figure 4.50a), but some dark spots can be rarely distinguished. The pores are the cause of the not complete densification of the structures and the main reason why the structure may need densification process via LSI.

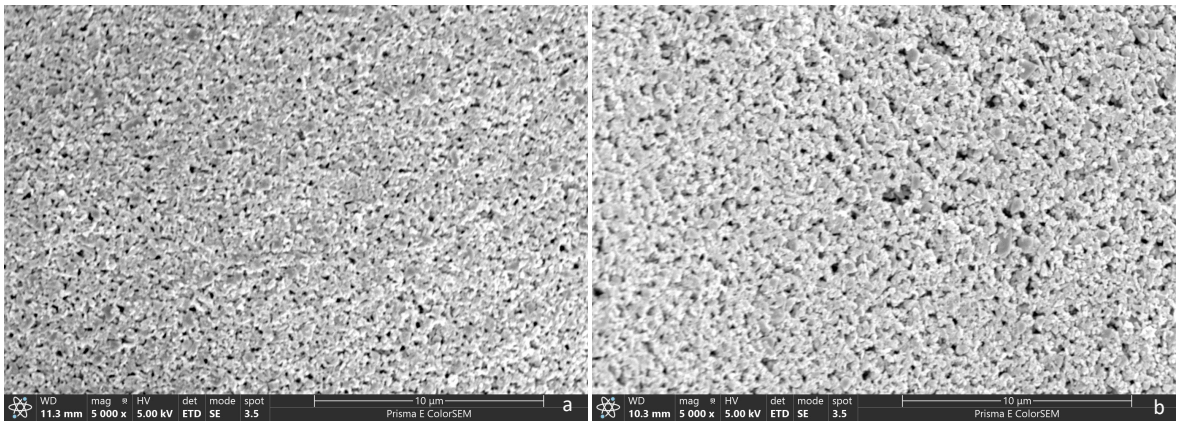

Figure 4.51: TMAH 9.625vol.% in Figure a), SiC 36vol.% in Figure b). Comparison of inks microstructure with a magnification of 5000 x.

The last two figures represent the highest magnification represented. Figure 4.51a) presents a more dispersed structure. More homogeneous dispersion can be seen with pores present. Figure 4.51b) presents a less homogenized structure in which the solid particles are visibly wider than the ones in Figure 4.51b). Wide void spots are present in between all the powder agglomeration.

DISCUSSION

5.1 PLURONIC PREPARATION

As expressed in Chapter 4.1, the Pluronic solution preparation represents a crucial step for the final ink preparation. By producing the solution sufficient care has to be taken in order to obtain the right quality. A satisfying level of quality allows a faster use of the Pluronic solution without occurring prolonged coolings.

The Pluronic powder has to be added in a step-wise manner to the deionized water to avoid accumulation. A better powder dispersion can be obtained by performing more addition steps, allowing a more homogeneous dispersion. Moreover, due to the gelation behaviour of the paste, an ice bath has to be used to avoid an excessive viscosity. By considering the different mixers, a sufficient mixing speed has to be set to avoid bubble formation.

By considering Figure 4.7, the temperature increase diagram shows the trend of the viscosities in the different Pluronic production technologies. The starting values of viscosity can be assumed equal as well as the final viscosity values. The first ramp up present in Figure 4.7 is done by the vortex mixer Pluronic solution. This could be addressed as the best quality since a transition in state from liquid to gel happens at lower temperature. This assumption is in accordance to the rheological studies done on the Pluronic solution with 25wt.%. By performing the final cooling step for a sufficient amount of time the Pluronic solutions assume a similar rheological behaviour. The solution produced by the immersion mixer caused the formation of impurities that were desegregated with a sufficiently long cooling. Therefore even though the Pluronic solution production step represents a crucial part of the ink preparation, a final cooling step may avoid presence of final inhomogeneities.

As a conclusion, the three Pluronic alternatives has been considered as equivalent for sake of research, being the primary part of the ink allowing the hydrogel structure and viscosity temperature dependent behaviour. Moreover, the Pluronic characteristics must be considered during the printing action, at ambient temperature. Here all the Pluronic solution alternatives were superimposed, highlighting the fact that no alterations in the ink should be produced by the different solutions.

5.2 SiC INK OUTCOME

The ceramic ink proposed behaves differently by considering a different solid loading. An increasing presence of ceramic particles avoid the viscous behaviour of a quasi-liquid structure, increasing the solid behaviour and tending towards a constant temperature-viscosity behaviour.

By considering Figure 4.17, the highest viscosity levels are reached by SiC 40vol.%. By increasing the volumetric solid fraction it is reasonable to assume that there is a change in the rheological behaviour that leads to a final stable trend dominated by the pure solid fraction. By considering Figure 4.17 it is possible to constant increasing trend of the inks with higher solid contents, that follows a decrease in viscosity difference in between pre-transition phase and post-transition phase.

An higher solid loading causes a shorter temperature range in which the transition phase is detected. In fact, by comparing SiC 25vol.% and SiC 40vol.% the temperature at which the solid

behaviour is detected remains 18°C while the temperature of starting transition moves toward higher temperatures.

By comparing Figure 4.17 and Figure 3.9 it can be seen that the curves are comparable. The βTCP ink behaves similarly to the SiC 40vol.%, decreasing the transition phase range and approaching a narrower change in viscosity. The presence of ceramic particles obstructs the liquidity increasing therefore the viscosity. In this situation 40vol.% of SiC is compared to 65vol.% of βTCP in 25wt.% Pluronic solution. The different proportions imply a different behaviour of the ceramic particles interacting with the hydrogel.

A small difference in viscosity module at ambient temperature is present between SiC 40vol.% and SiC 36vol.% that implies a subsequent lower ability in forming solid structures. The low viscosity values would cause a subsequent difficulty in creating suspended structures such as bridges in between two main parts. Therefore it could be possible to print with a more viscous ink such as SiC 40vol.%, tuning the printer to increase the shear stress generated by the extrusion multiplier.

In the G"/G' relationship with temperature exposed in Figure 4.18 the printable inks can be seen. However, the only theoretically printable ink should be SiC 25vol.%, which represents the lowest solid content usable for printing purposes [46]. However, SiC 25vol.% has shown a non-sufficient viscosity to be printed.

The SiC 36vol.% that was used to print has shown a sufficient viscosity to withstand on itself while printing due to a sufficient solid like behaviour. This behaviour can be expressed as the G' parameter greater than G". Referring to Chapter 3.5 in which the rheology has been explained, G'>G" means a solid like characteristic that predominates over the liquid like characteristic. However, as reported in Chapter 4.4.2 the SiC 36vol.% is not sufficient to obtain a printing quality due to the low viscosity. As reported in different papers, a solid fraction of 36vol.% of SiC represents a printable ink while effectively it should be modified in order to increase its solid like behaviour and allow the printing of solid structures.

By increasing the solid content, the crossing of G' over G" moves toward higher modules. This highlights an higher solid behaviour at the same temperatures. Moreover it implies a more difficult behaviour as hydrogel and as liquid like structure. The addition in solid content causes an increase in the rheological curves detected. The shear stress test has detected the increasing behaviour of the G' and G" by adding SiC powder. The solid particles moreover attenuate the hydrogel reversible temperature behaviour making the dominating behaviour a solid one, caused by the high concentration of powder dispersed in the paste.

During the Shear Rate algorithm the most important outcome is the relationship in between solid content and viscosity-shear rate dependence. In detail, the solid content does not cause severe changes in the viscosity behaviour . In fact, SiC 36vol.% and SiC 40vol.% do not differentiate in module during the initial and final part but just when the shear rate reaches values around 10 1/s. The similar viscosity levels among two inks such as in SiC 36vol.% and SiC 40vol.% means that by reaching sufficient values of shear rate the behaviour is the same. A high loaded ink may behave as a low loaded one, decreasing the viscosity by increasing the shear rate. This result testifies that the highly loaded ink may be printed by considering a sufficient high level of extrusion multiplier, reaching low viscosity values while it contained in the nozzle, allowing the extrusion process and assuming a solid like structure once the ink is deposited on the surface and the stresses are removed. By removing the forces, the viscoelastic behaviour comes in action, recovering the initial structure and assuming the viscosity state at which it was while being not loaded by stresses and stored at ambient temperature.

By tuning the printer setting the extrusion multiplier allows to increase the quantity of ink to be extruded through the nozzle tip. The screw moved the ink through the nozzle while spinning as if it was a liquid like structure. Therefore a sufficient viscosity was achieved by increasing the Extrusion Multiplier over the level of 20. An excessive value of Extrusion Multiplier has caused an excessive extrusion such as the one reported in Figure 4.46 representing the ink try SiC 36vol.%. The excessive Extrusion multiplier setting can be attributed to the last parts of the Shear Rate algorithm, in which an an abrupt decrease in module follows the increase in shear rate.

As reported in the Shear Stress algorithm, the G" that overcomes the G' implies a liquid like behaviour. This causes the viscosity decrease while spinning the screw. By approaching the nozzle tip the decrease in viscosity happens allowing the ink to move through the small diameter nozzle chosen. However, by removing the stress the material behaves like a viscoelastic material, therefore it goes back to the state not affected by stresses assuming a solid like structure. The deformation recovery implies the consequent recovery of the solid structure assuming the filament like behaviour after deposition. By touching the filament extruded the ink is a solid like structure, denoting the removed stress and the subsequent change in viscosity.

In Figure 4.21 the shear stress outcome of the Shear Rate algorithm can be seen. The SiC 25vol.% is characterised by the largest liquid fraction. The SiC 25vol.% ink behaviour could be assumed as the action of the liquid fraction that keeps incorporating the solid particles and counteracts the increasing applied shear stress. For SiC 30vol.% it can be said that the microstructure behaves to adapt to the increasing shear rate by applying a constant shear stress. In SiC 36vol.% the fall of an order of magnitude from the two already explained inks may be the consequence of the complete microstructure destruction. The SiC 40vol.% behaviour can be explained as a reorganization of the microstructure due to the high solid powder content by applying an increasing shear rate.

The concluding part of all the plots in Figure 4.22 is characterised by a visible deviation. This distinguished trend is a consequence of the completely destroyed inks microstructure. The liquid behaviour represents the dominant factor affecting the printability.

During the Frequency Sweep algorithm analysis of the SiC pure ink, by comparing with the shear rate viscosity outcome, the opposite viscosity behaviour is strictly related to the action of a stress on the sample surface. By avoiding an imposed shear stress, the viscosity of the ink tends to increase.

SiC 36vol.% represents a behaviour in between the highest and the lowest pure solid loaded inks SiC 40vol.% and SiC 25vol.%. By considering the plots reported in literature already explained in Chapter 3.5.2, the ink deposition behaviour should be affected by a too low viscous behaviour causing the successive ink sputtering on the surface and the non-printability of complex structures. In SiC 40vol.% the stresses caused by the high solid content could cause the impossible extrusion process requiring high levels of extrusion multipliers non reachable by the printer.

During the Frequency Sweep algorithm, by increasing the frequency the viscosity increases. However, being the ink trends completely comparable in module, it is difficult to obtain such improvements while considering different ink alternatives. Therefore, it must be said that the screw spinning should be kept in a reasonable range of values, avoiding the frequency levels around 100Hz otherwise the viscosity would increase altering the previously described liquid behaviour while spinning. 100Hz means also 100 turns per second, speed that cannot be reached by printers. Therefore such conclusions should be related to a smaller range of variation of the frequency.

5.3 INK STABILIZATION

Since one of the first aim of this study is to increase the SiC content in the paste to generate a more solid structure, the use of a solid content greater than 40vol.% of SiC is of prior importance. In this context, the TMAH has demonstrated its usefulness. By increasing the solid content an impossibility in performing the rheological measurements has been encountered. The stabilizer utilization represents a crucial step for the increase in solid content, lowering also the stresses cause by the solid accumulations.

Considering the TMAH addition, the rheological results of the ink alternatives undergo a sensible change in module by increasing the stabilizer content. Differently than the addition of solid content, the stabilizer quantity increase brings a decrease in viscosity and increase in homogeneity, distributing the powder more homogeneously and decreasing the agglomerations.

The viscosity comparison done after the Temperature Ramp algorithm, present in Figure 4.17 and Figure 4.24, shows the differentiation among a pure SiC ink and an ink including TMAH. The typical "S" shape of the temperature dependent viscosity behaviour is lost by considering a TMAH content up to 11vol.% By approaching this limit the "S" shape is preserved even if showing a transition temperature happening sooner than the pure ink. The order of magnitude of the viscosity evolution modules are kept constant.

Considering Figure 4.24, the TMAH 6.87vol.% behaviour explanation is related to the greater amount of SiC that produces a higher viscosity due to the higher solid fraction and lower possibility for the molecular motion. In TMAH 9.62vol.%, the TMAH addition allows a sooner phase transition and a different viscosity behaviour causing an apparent solid state shifted towards lower temperatures. In TMAH 12.375vol.%, the different behaviour may be a consequence of the excessive addition of TMAH causing a different behaviour acting on the molecular point of view. The 13.75vol.% TMAH behaviour can be explained as the action of TMAH to fluidize the solution, by increasing the stabilizer amount over 9.625%vol. The solution loses the hydrogel characteristic of thermal reversibility of the viscosity. By increasing the amount, the final viscosity levels that should be higher than the initial study levels decrease with a descending path down to the lowest values.

G"/G' plots represent a completely different behaviour. By increasing the temperature the usual transition phase is no more present. The TMAH inks present an almost flat evolution, highlighting the no longer temperature reversible behaviour of the hydrogel. Moreover, by increasing the TMAH content the index ratio assume similar values. Considering the printabilty index represented in Figure 4.27, the ink could potentially be always printable. Being the printabilty index of TMAH 6.87vol.% greater than one, it should behave always as a liquid like behaviour even if being visibly viscous enough to be considered as a solid. TMAH 12.37vol.% may be affected by a probable wrong formulation of the paste. As a consequence, this ink is always printable without a strong temperature effect. However, by analysing the results a new ink formulation should be made, and all the rheological analysis should be computed again in all the algorithms.

As already mentioned, the addition of TMAH causes complete changes in the molecular structure. The single G' and G" evolutions for the TMAH inks follow a trend similar to the viscosity one. By comparing the shapes shown in Figure 4.29 and Figure 4.24 it can be seen that the viscosity plot and the G' and G" moduli behave the same. As a consequence, the same conclusions done for the viscosity path depending on SiC pure ink and TMAH ink can be done on the G' and G" moduli. By increasing the TMAH content the inks lose the typical "S" shape becoming a hill like plot. A consequent increase of stabilizer causes the complete loss of module increase behaviour due to temperature increase. This last conclusion can be associated to the complete loss of the hydrogel behaviour due to the temperature evolution.

The high solid content implies a more difficult molecular mobility. Due to the already mentioned assumptions of wrong ink composition, TMAH 12.375vol.% has the lowest viscosity levels during the whole test. The Shear Rate algorithm represent the first typical ink behaviour not entirely dependent on the stabilizer content but on the viscoelastic behaviour. In fact by considering the Figure 3.11, Figure 4.20 and Figure 4.30, the same main trend can be seen. The paste viscosity is dependent on the shear rate, therefore by tuning the screw spinning, the viscolastic inks can be extruded. However, in this consideration is has to be stated that a correct nozzle diameter has to be selected in order to allow the ink flow, without causing extrusion stops and ink block. By considering the theoretical results present in Figure 3.11, the modules are of different orders of magnitude. The theoretical results consider values up to 10^4Pa while the practical ones are in the order of 10^4Pa to 10^6Pa. This difference in module can be derived to a higher solid content or complete different behaviour of the ceramic particles dispersed in the hydrogel solution due to the TMAH effect.

In Figure 4.20 it can be said that the different trends can be explained by the assumption of some impurities present in the structure. Impurities such as air bubbles in the structure may lead to a collapse in viscosity since air is less viscous than the tested ink. Another assumption could be the presence of a separation in between the solution components, so the action of Pluronic hydrogel is more marked with respect to the action of SiC powder. The most probable hypothesis is the non sufficiently accurate final ink receipt that has lead to presence of impurities, leading to a different

final behaviour. In the SiC 40vol.% it could be assumed that the action of particles are interfering more with the application of a shear stress, opposing to the deformation. This assumption could explain the first viscosity increase trend. As a consequence, this study could give an explanation of the microstructure changes when a shear rate is applied. By detecting a huge decrease in shear stress it can be assumed that the microstructure has undergone a complete reassembling.

By considering the study presented in Figure 4.32, due to the TMAH addition, the microscopic adhesion of the particles should be limited by the action of the binder. So more flattered slopes are expected as well as lower values measured. However, due to the high SiC amount a similar plot to the already shown ones for the pure SiC inks might be present. Considering high values of shear rate it may be possible to have a complete destruction of the microstructure.

In Figure 4.33, TMAH 6.875vol.%, due to a higher volumetric content, the particles are more cohesive, so the shear detected is as a consequence higher. In TMAH 12.375vol.% the lowest shear stress values have been detected, meaning that the molecules tightness is decreasing, therefore also the shear stress transmission is less effective. However, the main difference comes from the difference in concavity with respect to the other inks presented. For an increased TMAH content, the solution is differently affected in behaviour, since by increasing the stabilizer amount its effect is more efficient.

The shear stress result of the Shear Rate algorithm trend does not show different behaviour in between pure SiC inks and TMAH stabilized inks. By increasing the SiC powder the G' and G" values increase due to an increasing amount of viscosity and stresses. On contrary, by increasing the TMAH amount lower values of G' and G" are measured. By considering the highest used amount of SiC powder contained in the pure SiC inks and the lowest amounts of TMAH added to the SiC 45vol.% ink, the same ranges of variability are detected.

Figure 3.12, Figure 3.13, Figure 4.22 and Figure 4.36 show the same Shear Stress algorithm. The same order of magnitude is respected among the various ink formulations. A similar trend represents G' and G" evolution against a change in shear stress increase. By increasing the solid load the curves move toward higher values, determining a more marked solid like behaviour. On the contrary, an increase in the binder concentration causes the curves shift towards lower values. In fact by considering the SiC 4e) ink made of 6.785vol.% of TMAH and 45vol.% of SiC the G' and G" moduli are in the same order of magnitude and same shear stress evolution. The addition of SiC powder should cause the impossibility of measuring the rheological properties, however the TMAH has allowed a sufficient smoothness to be compressed to the measuring level.

Figure 3.12 shows the decrease in G' and G" moduli after the stabilizer addition. Similarly in Figure 4.36 the TMAH addition causes the decrease in G' and G" moduli. The order of magnitude is the same. The main difference with the TMAH inks is that after adding a sufficient TMAH content the typical descending trend is lost. In fact, as soon as ink TMAH 13.75vol.% and TMAH 12.375vol.% are measured the microstructure cannot withstand the shear stress. As a main consequence, the structure is lost and the G' and G' moduli tend towards 0Pa.

Figure 4.23 and Figure 4.37 show the same trend. The main ascending path is respected by adding TMAH to the SiC ink. By increasing the frequency the viscosity increases reaching the same order of magnitude of 10^8mPa*s when a frequency of 100Hz is detected. As already stated, the final part of the plot represents a non usable frequency level in the printer, therefore such range should not be considered.

The TMAH addition causes an aging effect to the SiC ink that modifies the rheological properties. Figure 4.25 and Figure 4.26 show the aging effect on TMAH 6.785vol.% and TMAH 13.75vol.% demonstrated by the Temperature Ramp algorithm during the temperature increase process. Generally the aging effect causes a faster drying of the inks causing therefore greater viscosity values at ambient temperature. The aging effect is strictly connected to the chemical reactions explained in Chapter 3.4 due to the presence of TMAH in an oxygen atmosphere.

In Figure 4.28 the TMAH 13.75vol.% is compared to TMAH 13.75vol.%-1, so the measurement of the TMAH 13.75vol.% ink done after a week, in terms of shear stress output of the Temperature

Ramp algorithm. The plot is not moved entirely towards lower values as it would be expected. In fact, due to the increased oxidized fraction, the solid behaviour should be the dominating factor while measuring G' and G" (Chapter 3.5). However, the ink presents a greater G"/G' than the TMAH 13.75vol.%, so a greater liquid behaviour is detected at the measurement beginning. Similarly at the end of the measurement, a ramp up brings the ratio towards values greater than one. This conclusion is in contrast with the previous mentioned aging effect since even if the paste is oxidized, it behaves as a fluid.

During the Shear Rate algorithm the aging effect has been detected as reported in Figure 4.31 and Figure 4.32. In this case both the SiC inks behaves similarly. A first aging effect causes the decreasing behaviour of viscosity in TMAH 6.875vol.% and TMAH 13.75vol.% while subjected to the Shear Rate increase. The aging effect causes the decrease of viscosity values moving down the curves and detecting similar irregularities in the measurement. By increasing the aging effect, the alteration is more visible and it leads to a different aging stage in which the viscosity behaviour differentiates completely from the starting one. TMAH 6.875vol.%-2 has been analysed after nine days from the first measurement. TMAH 6.875vol.%-2 undergoes a first similar trend to the original TMAH 6.875vol.% measurement, while by reaching 10Hz some more marked instabilities happen approaching an average value.

The shear stress outcome of the Shear Rate algorithm denotes a similar aging effect to the already mentioned one. In fact, by doing a first consequent analysis of the first one done one week after the first measurements, the detected shear stress is decreased in both TMAH 6.875vol.%-1 and TMAH 13.75vol.%-1. the first alteration undergoes a similar path of the original plots. The similarity in behaviour is more simple to be seen in TMAH 13.75vol.% measurement. In TMAH 6.875vol.% the transition towards lower values causes a subsequent change in behaviour after 10Hz. At 10Hz the shear stress measured stabilizes until the end of the measurement. By considering the final measurement, TMAH 6.875vol.%-2 retake the initial shear stress values of TMAH 6.875vol.%. 10Hz frequency causes a complete change in material response, producing alterations in shear stress measurement. TMAH 6.875vol.%-1 shear stress shows a first stable trend around 1790Pa, after which greater module alterations happen, showing a quasi-sinusoidal trend. The shear stress output plot reports a final confused plot in the greatest TMAH contents. A possible explanation can be the complete destruction of the ink microstructure, affected also by the presence of the binder that smooths the paste making it less viscous allowing the shear stress at high module to completely alterate the sample. As a consequence it may be said that the remaining solid parts are still detected by the rheometer and cause a resisting stress so to increase the shear stress detected and G' module.

As a consequence it can be summerised that the aging effect causes variable effects on the inks. Moreover, by considering the TMAH 6.875vol.% ink it has been proved that by doing the rheological measurements in three different episodes, the first alterations dissociates from the original one while the third one retakes similar values. Unfortunately in TMAH 13.75vol.% only two measurement episodes have been done, but it could be assumed that the behaviour could be similar to TMAH 6.875vol.% since the TMAH content is increased.

To demonstrate such theory the dependent aging effect present due to the TMAH content must be considered. A reaction of oxidation with SiC pastes is also present as expressed in Chapter 3.2 but such a reaction should have been denoted even in the pure SiC inks. This characteristic has not been detected in any of the performed measurements, therefore the TMAH can be assumed to be the main cause of the rheological characteristics change on the inks proposed.

Moreover, by looking at the general aging effect trend, a slight effect in the TMAH concentration could be to move the plot profiles towards lower viscosity levels, keeping the main rheological behaviour unaltered. The aging effect should be analysed in a longer time window so to consider a longer reaction time. The tendency to recover similar values to the original measurement highlights the fact that the aging effect could allow to homogenize the structure leading to the consideration of more stable values.

5.4 INK COMPARISON

Considerations related to the final ink viscosity and compositions should be made so to obtain a final sufficient stability of the printed parts.

The inks chosen as main representative for the ceramic structure printing are SiC 36vol.% since it is the ink proposed by del Manzo et al. and its printability has been already proved, and TMAH 9.875vol.% since characterised by a greater solid fraction (45vol.% SiC) and the lowest amount of TMAH that was sufficient to allow a successful printing (9.625vol.% TMAH) [30]. Moreover the two proposed inks behave similarly during the Shear Rate algorithm and the Shear Stress algorithm, meaning a similar viscous behaviour when a shear stress is applied and therefore a theoretical similar behaviour while being extruded by means of a screw.

9.625vol.% TMAH implies a limited risk. In fact by considering the aqueous solution in which TMAH is dissolved, the addition of Pluronic solution causes an even lower toxicity. Its utilization might be done with sufficient care to avoid any further risk for human health and environment.

The utilization of a 45vol.% SiC ink implies the use of the greatest value of solid load theoretically printable. Moreover, as expressed by Feilden et al., the solid particle loading should not overcome 45vol.% [46]. This limit has been imposed since it has been demonstrated that an excessive solid content would cause a non sufficiently low viscosity to flow through a printing head.

By performing a direct comparison of the most important results obtained in the rheological analysis, some further considerations may be done. Moreover, a possible understanding of the different printing performances can be obtained.

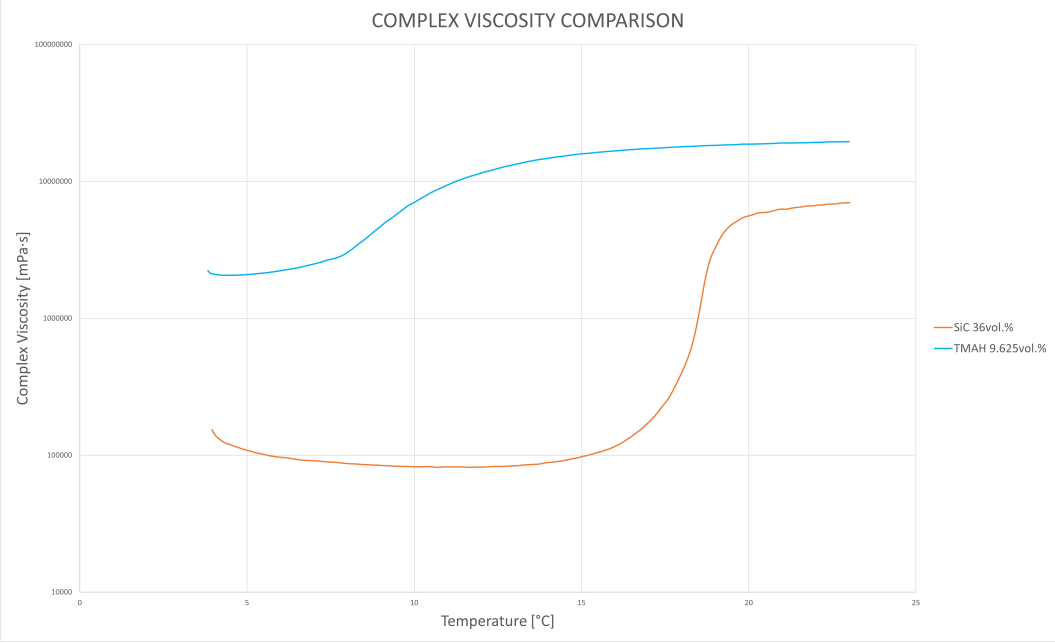

Figure 5.1: Viscosity comparison among SiC 36vol.% and TMAH 9.625vol.%.

During the Temperature Ramp algorithm represented in Figure 5.1, the viscosity output differentiate among the two inks. The viscosity at ambient temperature is the one that is shown once the ink is deposited on the printing bed. The liquid behaviour of the SiC 36vol.% extruded through the nozzle is due to the lower viscosity module with respect to TMAH 9.625vol.%. Moreover the difference in module testifies the strong behaviour of the hydrogel part still representing a huge fraction in SiC 36vol.%.

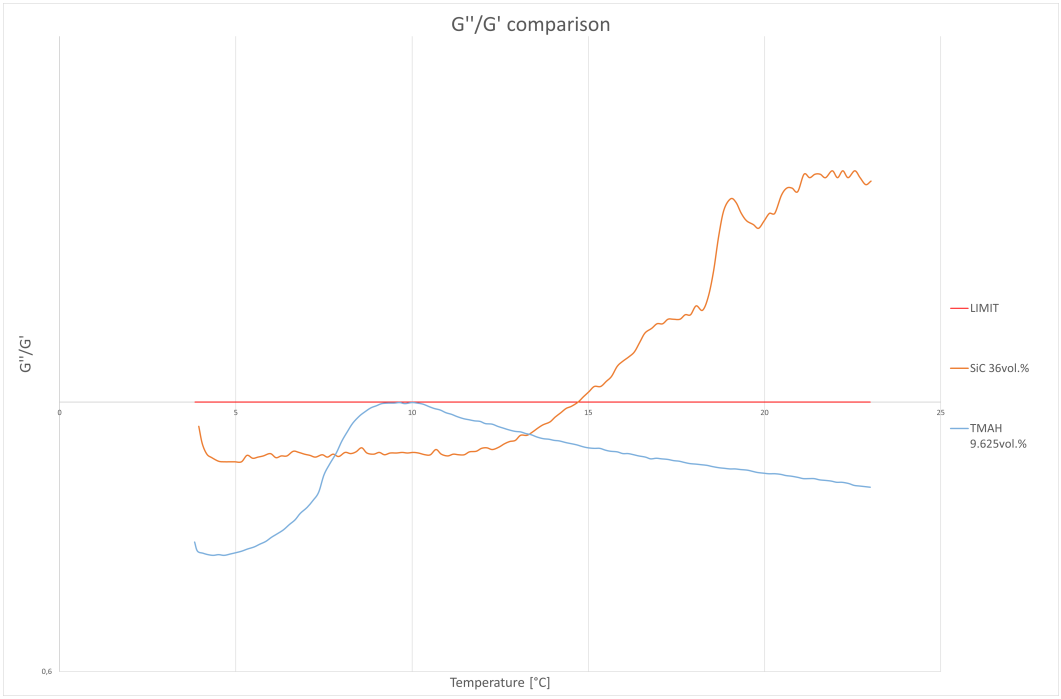

Figure 5.2: Printability index comparison among SiC 36vol.% and TMAH 9.625vol.%.

Considering the printability index (Figure 5.2), the low viscosity of SiC 36vol.% at ambient temperature causes the final printability index greater than one. In fact by assuming a G"$>$G' the dominant behaviour is a liquid one. The low viscosity causes the non sufficient external wall withstanding and loss of geometry. TMAH 9.625vol.% printability index keeps a value constantly lower than one, meaning its solid dominant behaviour. The final structural withstanding can be attributed to the greater solid loading.

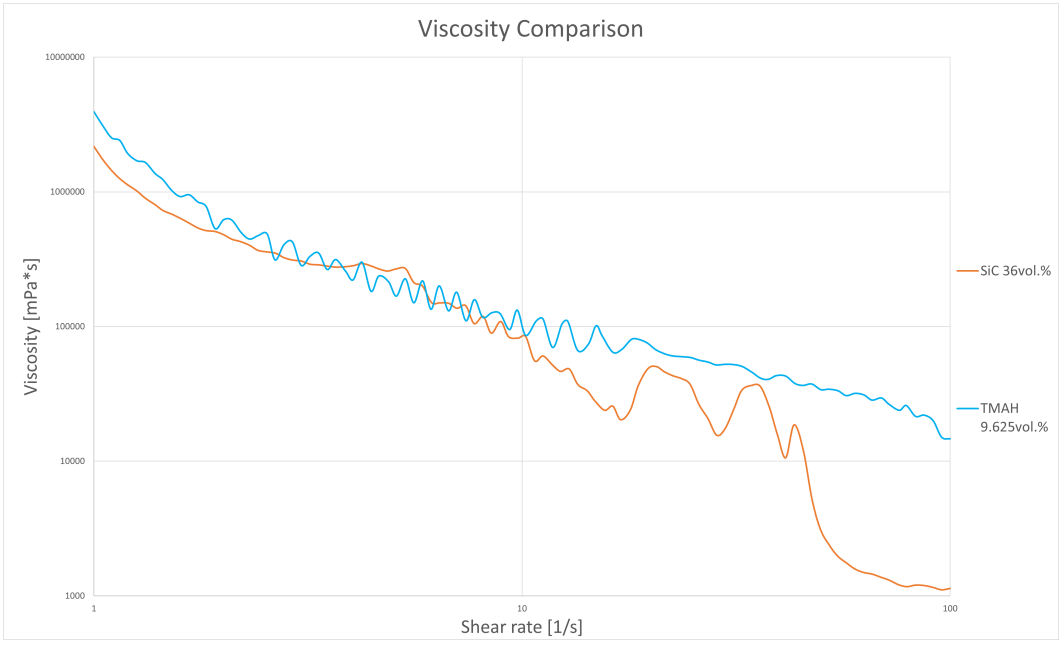

Figure 5.3: Shear thinning behaviour comparison among SiC 36vol.% and TMAH 9.625vol.%..

A shear rate value greater than 50 1/s cannot be reached with a PRUSA printer, therefore the final part for the plot can be discarded. By doing this assumption the behaviour shown by SiC 36vol.% and TMAH 9.625vol.% is similar. As a consequence an expected common extrusion attitude may be

respected while printing. As a consequence, the filament of TMAH 9.625vol.% once is extruded is attributed by an inertia and a structure similar to the one of SiC 36vol.%. However, due to the lower viscosity the extrusion of SiC 36vol.% is harder to be printed.

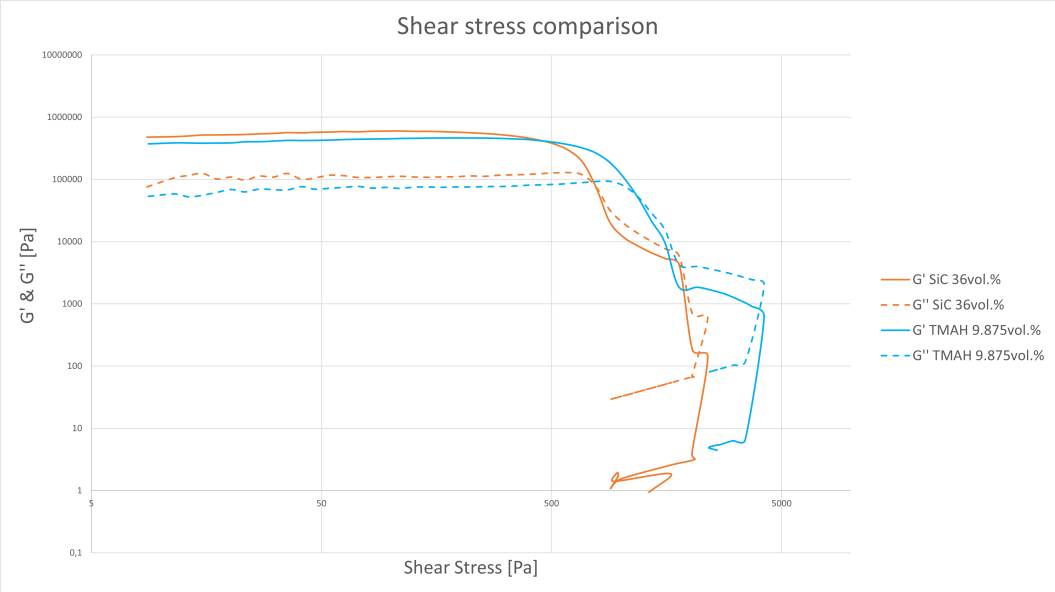

Figure 5.4: Frequency Sweep output comparison among SiC 36vol.% and TMAH 9.625vol.%.

The Shear Stress algorithm represents a very similar behaviour of the two proposed inks. The elasticity range, represented by the linear trend of G' and G", represents the common working condition until the inks are extruded by reaching the yield stress. The lower yield stress present in SiC 36vol.% should cause an easier printing with respected to the one of TMAH 9.625vol.%, requiring smaller values of extrusion multiplier.

5.5 PRINTING

By considering the previous rheological analysis, the chosen inks represent the best alternative in terms of flowability and structure withstanding. In fact, SiC 36vol.% has printable characteristics proven by Del Manzo et al. while the TMAH 9.625vol.% represents the best alternative for an ink containing a greater solid content than the usual ceramic inks and similar rheological characteristics to 36vol.% [30].

The viscosity at ambient temperature of TMAH 9.625vol.% is similar to SiC 36vol.%, being respectively $1.95*10^7$ mPa*s and $7.01*10^6$ mPa*s. A first differentiation is present in the G"/G' results, in which SiC 36vol.% shows a value greater than one, being therefore not printable. On the contrary, TMAH 9.625vol.% has a value lower than one, demonstrating the solid characteristic overcoming the liquid one. G' and G" moduli of TMAH 9.625vol.% are the double in module the SiC 36vol.% values, being 8000Pa or 9000Pa against 4000Pa of SiC 36vol.%. Greater values imply a greater effect of G', which is the characteristic parameter that indicates a greater solid like behaviour. Similar values can be noted during the Shear Rate algorithm explanation present in Figure 4.20 and Figure 4.30. Another differentiation can be noted during the final part of the shear rate algorithm in which TMAH 9.625vol.% reaches viscosity values in the order of $1.47*10^4$mPa*s while SiC 36vol.% around 10^3mPa*s. During the Shear Rate algorithm SiC 36vol.% loses the structure by approaching the 100 1/s of shear rate. A decrease in shear stress of an order of magnitude causes the collapse from 900Pa to 90Pa of the two moduli. During the Shear Stress algorithm the same range of values has been detected for G' and G" in both SiC 36vol.% and SiC TMAH 9.625vol.%. As a first conclusion, these two inks should behave similarly being characterised by similar rheological values.

During the printing procedure, the same nozzle size could not be used. The TMAH 9.625vol.%

was extrudable through a 0.41mm nozzle while the SiC 36vol.% needed a diameter of 0.61mm. This greater nozzle dimension was used due to the fact that the SiC 36vol.% could not be extruded through the nozzle, but some intermittent jets of ceramic ink were caused by accumulation on the nozzle tip.

To print the ceramic structures composed by the ink TMAH 9.625vol.% some G-Code modifications were needed and they are reported in Chapter 4. Such modifications lead to the final structure reported in Figure 4.45. SiC 36vol.% needed some modifications of the G-Code since the extruded parts was excessively liquid and not viscous enough to keep the printed structure. By moving the nozzle, it collided against the already printed parts causing geometry loss. Moreover, the nozzle cleaning has been removed since the SiC 36vol.% does not allow extrusion stops during the printing because of the inertia of the liquid ink extruded. This behaviour can be demonstrated by the final part of the plot representing the Shear Rate viscosity result in Figure 4.17. In fact the concluding part of the plot may be not an error in the algorithm, but an effective behaviour of the SiC 36vol.% microstructure if subjected to an excessive shear stress. The structure is lost, therefore the viscoelastic behaviour of stress recovery cannot be applied. As a consequence the printed structure reported in Figure 4.46 does not represent a successfull printing process and the ink composed by SiC 36vol.% cannot be considered as better performing than TMAH 9.625vol.%.

In all the inks analysed, due to the viscoelatic behaviour, it has been seen an inertia while printing that keeps the ink flowing out of the nozzle while the screw is not spinning. Due to the retraction and stop of the spinning, the viscoelastic behaviour implies the recovery of the deformation and this may be the cause of inertia.

In Figure 4.41 and Figure 4.42 the printing of a heat exchanger that can be employed into a CSP Brayton cycle was assured as feasible. in order to be effectively employed into a power cycle the printed density should be enhanced as much as possible, therefore the infill density percentage should be increased to greater levels. Moreover the design allowed to obtain the wanted structure but the channels were left opened. Therefore a further study on feasibility of the geometry respecting the details designed should be conducted. moreover, the quality of the printing obtained represent a possible improvement. The G-code has still to be improved in order to allow the best printing performances and increase the infill density up to the maximum reachable.

The TMAH 9.625vol.% created more solid structures that considered more defined architectures. The layers could accumulate considering all the different layers designed for the architecture assembly. Suspended structures were not achievable due to non sufficient paste viscosity. By increasing the solid content or reducing the TMAH concentration the sufficient viscosity could be achieved. By considering the TMAH 6.875vol.% the final viscosity could be sufficient to create sufficient strength to withstand suspended structures.

In Figure 4.45 and Figure 4.46 the two printed gyroid structures can be compared. The TMAH allows to increase the solid content into the ink. However the viscosity has still to be tuned to allow the construction of the bridges and minor details. The final gyroid structure was not obtained with any of the inks proposed. However, an enhancement is present between the two printing tries, testifying that by increasing the viscosity more complex structures can be obtained. By using less TMAH and the same SiC content the printing of gyroid structures could be done using the same settings proposed for the tries performed.

The final heat exchanger structures cannot be used or considered in CSP applications due to the poor infill density and the high porosity obtained. The process requires the sintering process to obtain the final usable structure and in order to enhance the structure filling the LSI should be used.

Moreover, similar analysis to what performed by Du et al. while measuring the effectiveness of the printed heat exchanger cannot be done due to the excessive porosity, missing LSI treatment and sintering step.

5.6 MICROSTRUCTURAL CHARACTERIZATION

Analyzing the figures reported in chapter the material distribution happened homogeneously in both the ink alternatives. However due to the action of the TMAH and the addition solid content the resulting microstructure is distinguished by porosity and presence of agglomerations. TMAH 9.625vol.% ink once extruded keeps its shape even if it has not sufficient structural strength to withstand its weight. SiC 36vol.% presents agglomerations already visible with small magnifications. Therefore, TMAH acts a crucial role in avoiding powder agglomerations in microscale.

By increasing the magnification the pores present in the structures can be distinguished. TMAH 9.625vol.% presents the most homogeneous structure, even if with some small voids present. SiC 36vol.% presents agglomerations and a less homogenous structure. Moreover the pores are visibly wider than the one present in the other ink alternative. The action of the stabilizer therefore allows to obtain a greater filling of the volume, theoretically enhancing the filled volume. As a consequence, SiC 36vol.% is addressed by a lower theoretical lower density since the same printed geometry presents wider pores than the TMAH 9.625vol.%. Density analysis should be conducted to demonstrate this.

As an outcome, the densification step should happen via LSI since liquid silicon could infiltrate inside the void parts filling the volume and increasing the final density of the green structure. Mixed powder does not represent the best alternative for densifying the ceramic structures since the powder dimension used is already one of the smallest available powder dimensions. A smaller diameter ceramic powder would cause a general increase in capital expenditures. Moreover, the powder used represents one of the smaller dimensions available. The liquid infiltration may represent therefore the best alternative, allowing the filling of the smallest pores.

CONCLUSIONS

The present thesis focuses on the process of preparation and rheological study of a ceramic ink for the extrusion printing of a heat exchanger employed in CSP applications. The need of an inert material able to work with molten salts and sCO_2 implies the use of SiC as material of choice. SiC is addressed by some of the most suitable physical, chemical and thermal properties necessary for a heat exchanger to withstand high temperatures. Up to now several studies have been directed on the properties discovery of this ceramic material, presenting it as one of the main materials useful for the improvement of the energy field.

A heat exchanger for CSP must be addressed by some features that make it suitable to work without causing material degradation and being chemically eroded. Moreover, in order to enhance the thermal exchange, the contact surface in between heat exchanger and thermal fluids has to be improved. To enlarge the contact area some complex geometries can be adopted, requiring some particular production technologies. Usual industrial manufacturing technologies for the ceramics are limited by the impossibility to obtain certain features in geometries always more demanding. As a consequence the use of a 3D printer might solve the technological issue.

Among the various 3D printing technologies, binder jetting represents the most used to work with SiC. Binder jetting can print large volumes by using a technology that is able to print with a high definition any printable geometry. The main limits are represented by material waste due to the layer deposition and high capital expenditures for the 3D printer components. Robocasting represents a possible solution for both the issues since no material waste is associated to the printing process and it can be purchased without large investments. The DIW is another name for Robocasting and expresses the main process by which the ink is extruded on the printing surface. The extrusion process requires the deep analysis of the rheological properties to allow a continuous flow of the paste through the printer nozzle. A suitable ink for the DIW should be characterised by rheological values to accomplish the designed printing process, leading to the final printed structure.

By performing the ink production, several attempts have been made. The first step was the production of an hydrogel suitable to embed ceramic particles. Pluronic was discovered as good gelation agent for ceramic particles, already fully studied in many researches. The gelation process of the Pluronic hydrogel causes a thermoreversible behaviour, leading to a complete change in the paste viscosity. A transition temperature has been found to be the cause why the hydrogel state changes from liquid to gel. 17°C represents the transition temperature of the Pluronic hydrogel produced by dissolving 25wt.% of Pluronic powder in deionized water. Different production technologies were tested to understand if the manufacturing could affect the purity of the solution. To understand the differences between the various production technologies, the rhelogical properties of all the hydrogels produced have been studied. By considering the main hydrogel utilization as ink binder, the most important algorithm used was the Temperature Ramp algorithm during both temperature increase and temperature decrease. For both the temperature evolution, a temperature from 4°C to 23°C was used. The viscosity represented the main outcome of quality comparison. Because of the powder addition in steps or in a single step, no significant changes have been discovered in between but a more difficult mixing process in the single step Pluronic addition solution. During the temperature increase from 4°C to 17°C the solution was in liquid state and the viscosity followed a plateau. When temperature approached the transition temperature the viscosity undergo a rapid increase reaching the solid state and maximum viscosity. The last viscosity value laid on a plateau. During the temperature decrease the trend was symmetrical. In the rheological analysis conducted in between the

three mixing technologies involved, as main outcome it has been discovered that there are not serious alteration in the hydrogel solution viscosity. Viscosity has been compared among the entire temperature evolution range detecting small changes during the transition phase. During the liquid phase the Pluronic solution were addressed by the same viscosity. In gel state the viscosity increased up to a unique plateau value, that can be named as the final hydrogel viscosity considering a Pluronic load of 25wt.%.

As a second phase, the SiC ink was produced by considering different solid loading from 10vol.% to 50vol.%. Due to the Pluronic rheological results, the vortex mixer was used to prepare all the pastes. By increasing the solid load, the mixing efficiency decreased. As soon as the amount of SiC exceeded 36vol.% the some agglomeration balls appeared due to the increased ink viscosity. Inks with an amount of ceramic powder greater than 50vol.% were not possible to be obtained due to impossible mixing. The agglomeration balls problem has been solved by using a final cooling at 4°C for 24h. The cooling process was sufficient to demolish agglomerations and increase the ink homogeneity. From this first thermal treatment the first outcome of the SiC can be noted. The SiC ink keeps thermal reversible behaviour of the Pluronic paste, but the ability to change the viscosity decreases by increasing the solid load. The powder addition was performed both in step-wise or in a single episode. As a consequence, the ink quality was strongly affected by generating bubbles and powder agglomerations. A final cooling down was not sufficient to solve the bubble formation and the agglomerations. However, a final mixing at a sufficient speed and time to solve the low homogeneity issue might be used. The rheological analysis has been conducted by using all the four algorithms programmed. During the Temperature Ramp algorithm, plots similar to the Pluronic ones were obtained. This similar trend stands for the similarity in behaviour when the solid load is small and the hydrogel effect is still dominant. By increasing the solid amount the typical trend is lost, increasing the liquid state viscosity plateau, smoothing the transition phase. In the G"/G' comparison the theoretically printable inks were the one with the lowest solid amount, 25vol.% SiC. The Shear Rate algorithm represented a fundamental study since it was discovered the direct relation in between shear rate increase and the viscosity decrease. In fact, all the tested ink viscosities followed a similar fashion down to the final minimum value. Concerning the shear stress detected on the sample, the trends changed by increasing the SiC amount following at first a linear trend and than a sinusoidal one. The shear stress algorithm detected the G and G" of all the tested inks that increased by rising the solid load. A direct consequence of the viscosity increase is the enhancement in the G' and G" moduli, testifying a stronger paste behaviour when the volumetric solid amount increased. As a final rheology study the Frequency Sweep algorithm has been used in which the viscosity follows an exponential rise with the frequency boosting.

For SiC fraction over 40vol.% the rheological analysis were not possible to be conducted since too high stresses were originated on the rheometer components. In order to decrease the viscosity and reduce the loads generated by the paste, TMAH has been added. TMAH works as a stabilizer for the SiC paste. By considering previous works done on the ceramic pastes, a solid loading of 45vol.% has been used as standard value. 45vol.% represents the maximum theoretical value of SiC that can be embedded in a Pluronic hydrogel. Similarly than what was done for the SiC pure ink, TMAH addition has been done from a concentration of 0.06875vol.% to 13.75vol.%. After the TMAH addition a mixing was performed to allow the complete distribution of the stabilizer. No cooling was needed. The same studies done for the pure SiC ink have been done for the TMAH + SiC ink. During the Temperature Ramp algorithm a differentiation from the previously tested SiC rheological properties happened by increasing the TMAH content. A concavity change in the viscosity trend appeared by approaching the highest stabilizer concentrations. Considering the G"/G' result, all the inks produced after TMAH 6.875vol.% were categorized as theoretically printable. The Shear Rate algorithm showed similar trends than the pure ink results, decreasing the viscosity by increasing the shear rate. However, some variations in the viscosity trend were more marked than in the pure SiC ink. The shear stress caused by the Shear Rate increase followed a similar trend to the SiC. During the Shear Stress algorithm the addition of TMAH to the SiC paste caused the decrease in module of the output plots. By approaching the greatest TMAH amount the G' ad G" undergone a decrease in module around two orders of magnitude, meaning a smooth structure. The final frequency plot showed the same output of the pure SiC ink, decreasing the viscosity by increasing the TMAH amount. As a main outcome, the aging effect of the final ink has been discovered. By increasing the TMAH concentration the paste was more inclined to completely lose the typical resulting trend. However the aging effect was discovered to be not only dependent on the TMAH content but also on the time. By performing

the analysis in different episodes the resulting plots reported a inclination of the deviations caused by the first aging effect to recover the original trends.

For the printing process two inks were chosen: SiC 2) representing an ink composed by 36vol.% of SiC (Table 3.1) and SiC 4edd) composed by 45vol.% of SiC and 9.625vol.% of TMAH (Table 3.2). The rheological values of these two inks was characterised by similar ranges. SiC 2) has been used as a reference since its receipt was described in literature. SiC 4edd) represent the ink proposed for the heat exchanger printing.

The 3D printer was modified to allow the printing of ceramic pastes. A new nozzle was installed implying the ink extrusion via a screw motion. To perform the printing the G-Code of the 3D printer has been manipulated considering the ink extrusion and the printing efficiency maximization. The currents were lowered to 150mA in order to avoid printing interruptions. Moreover, due to the limited volume of the cartridge, only small geometries can be printed. A further enhancement could be obtained by using a greater volume to fill the nozzle while extruding, allowing a continuous flow of the paste.

The printing of the two inks was successful even if the printing quality was not sufficient to produce the geometries chosen. The pastes were too poorly viscous to print with a sufficient precision the structures. The SiC 36vol.% created wider structures losing the geometry from the firsts layers. Moreover a nozzle tip of 0.61mm was used. A nozzle tip of 0.41mm allowed the extrusion printing of SiC 45vol.% and TMAH 9.625vol.%, obtaining a sufficient quality to print some layers. However due to the poor viscosity the suspended parts were not possible to be obtained.

In order to improve the printing process and extrude a more defined geometry, a higher viscosity may be used. A more viscous paste could allow to obtain more solid parts able to withstand their weight while being printed and build suspended structures. Bridges were not possible to be obtained since the structures were excessively smooth causing also an excessive spreading of the paste on the surface. The extrusion process during the suspended printing phases stopped, creating accumulations on the nozzle tip. By increasing the solid content the ink deposition should be granted on the already deposited layers improving also the adhesion in between the different layers.

The ink receipts could be improved to limit the environmental risk and health risk caused by the TMAH addition. The various risks associated to the TMAH addition have been reported and care has been taken to produce the pastes. However, the use of TMAH implies the utilization of a non renewable solution that affects severely the environment. As a possible improvement, TMAH could be substituted with a more sustainable stabilizer, which could produce similar results even if being not so efficient.

An observed electrostaticity seen by approaching the extruded filament with a sputter could be used to improve the attachment of the printed ink to the bed, helping the extrusion of the ink through the nozzle to be faster. Such an advantage can be obtained by the aim of a non coated-metallic bed.

A density measurement was not performed due to not suitable instrumentation. For both the ink alternatives, a calculation attempt was done by measuring volume and mass of the ink contained into a syringe before and after the drying. However, due to a not perfect filling of the volume such result was not considered. A suitable density measurement must be done to allow further studies to come. To solve the theoretically described low density problem, the densification step could be done. It represents a process that has to be performed before the sintering. The densification represents a crucial step for the final utilization of the printed ceramics. A greater density would allow the maximization of the mechanical and thermal properties. By using the LSI the voids present the printed parts may disappear. A comparison between the LSI treated structures and the normal one could allow to understand the improvements.

For the heat exchanger production conclusion the sintering must be done. Sintering allows to obtain the final ceramic properties, obtaining the solid structures made of SiC (SiC 36vol.%) and in case of SiC 45vol.% and TMAH 9.625vol.% TMAH residuals. Due to the sintering process, the C present in the Pluronic may stay trapped inside the structure, representing a possible resource for the particle

treatment and possible resource for density improvement. Thanks to the pure liquid Si present in the main SiC matrix and the high temperatures involved, a formation of new SiC structures composed by the pure C and pure Si may take place.

As a final step, the thermo-mechanical properties may be compared between the two inks considering both the not densified samples and the LSI treated samples. It is expected that the best properties are held by the LSI treated printed samples since more dense and already tested by many literature studies.

To conclude, the SiC 45vol.% and TMAH 9.625vol.% may represent the best alternative for a heat exchanger printing due to its formulation composed by 45vol.% of SiC in the hydrogel paste. The volumetric load proposed represents the largest theoretically usable solid amount for the extrusion printing. A high solid content implies high viscosity values and poor printablity. However, by using the stabilizer its printing represented a successful approach. The thermal and mechanical properties are expected to be outstanding compared to the proposed inks with 36vol.% SiC. Moreover the utilization of AM may lead to geometries improving. By enlarging the contact area using more complex geometries the heat exchange may be boosted. Using the DIW as extrusion printing technology, the costs of production may decrease concretely if compared to the usually considered ones with binder jetting. Moreover, the DIW process may be considered to print structures that are bigger than the ones considered in this thesis, so to successfully print a complete heat exchanger for CSP applications.

The G-Code should be manipulated in order to allow a more suitable printing while considering as ink a SiC paste, avoiding collisions in between the already printed parts and the nozzle. The inertia discovered while printing makes the interruption of the printing difficult. To avoid such problem, it may be considered a sooner stop of the screw while printing the structures, calculating the amount of ink that is extruded and finding the volume that can be printed.

Bibliography

[1] W. Du, W. Yu, D. M. France, M. Singh, and D. Singh, "Additive manufacturing and testing of a ceramic heat exchanger for high-temperature and high-pressure applications for concentrating solar power," *Solar Energy*, vol. 236, pp. 654–665, 4 2022.

[2] C. M. Mendez and G. Rochau, "sCO_2 brayton cycle: Roadmap to sCO_2 power cycles NE commercial applications," *Sandia National Laboratories*, 2018.

[3] J. Thomas, M. Banda, W. Du, W. Yu, A. Chuang, D. M. France, and D. Singh, "Development of a silicon carbide ceramic based counter-flow heat exchanger by binder jetting and liquid silicon infiltration for concentrating solar power," *Ceramics International*, vol. 48, pp. 22975–22984, 8 2022.

[4] T. Fend, W. Völker, R. Miebach, O. Smirnova, D. Gonsior, D. Schöllgen, and P. Rietbrock, "Experimental investigation of compact silicon carbide heat exchangers for high temperatures," *International Journal of Heat and Mass Transfer*, vol. 54, pp. 4175–4181, 9 2011.

[5] W. Li, G. Yu, and Z. Yu, "Bioinspired heat exchangers based on triply periodic minimal surfaces for supercritical co2 cycles," *Applied Thermal Engineering*, vol. 179, p. 115686, 10 2020.

[6] S. Chen, "Practical electrochemical cells," *Handbook of Electrochemistry*, pp. 33–56, 1 2007.

[7] C. L. Cramer, A. M. Elliott, E. Lara-Curzio, A. Flores-Betancourt, M. J. Lance, L. Han, J. Blacker, A. A. Trofimov, H. Wang, E. Cakmak, and K. Nawaz, "Properties of sic-si made via binder jet 3d printing of sic powder, carbon addition, and silicon melt infiltration," *Journal of the American Ceramic Society*, vol. 104, pp. 5467–5478, 2021.

[8] K. Cai, B. Román-Manso, J. Smay, J. Zhou, M. Osendi, M. Belmonte, and P. Miranzo, "Geometrically complex silicon carbide structures fabricated by robocasting," *J. Am. Ceram. Soc.*, vol. 95, pp. 2660–2666, 2012.

[9] S. Lamnini, H. Elsayed, Y. Lakhdar, F. Baino, F. Smeacetto, and E. Bernardo, "Robocasting of advanced ceramics: ink optimization and protocol to predict the printing parameters - a review," *Heliyon*, vol. 8, p. e10651, 9 2022.

[10] H. Xia, J. Wang, J. Lin, and G. Quiao, "Thermal conductivity of sic ceramic fabricated by liquid infiltrating molten si into mesocarbon microbeads-based preform," *Mater. Char.*, vol. 82, pp. 1–8, 2013.

[11] R. Pachaiyappan, R. Gopinath, and S. Gopalakannan, "Processing techniques of a silicon carbide heat exchanger and its capable properties – a review," vol. 787, pp. 513–517, Trans Tech Publications Ltd, 1 2015.

[12] S. Somiya and Y. Inomata, "Carbide ceramics - 1: Fundamental and solid reaction," *Elsevier Science Publishers LTD*, 2012.

[13] N. Shahrubudin, L. Te Chuan, and R. Ramlan, "An overview on 3d printing technology: Technological, materials, and applications," vol. 35, pp. 1286–1296, 08 2019.

[14] Y. Zhang, W. Jarosinski, Y. G. Jung, and J. Zhang, "Additive manufacturing processes and equipment," *Additive Manufacturing: Materials, Processes, Quantifications and Applications*, pp. 39–51, 1 2018.

[15] E. Garcia-Tunon, S. Barg, J. Franco, R. Bell, S. Eslava, E. D'Elia, R. C. Maher, F. Guitian, and E. Saiz, "Printing in three dimensions with graphene," *Advanced Materials*, pp. 1688–1693, 2015.

[16] Y. Lakhdar, C. Tuck, A. Terry, C. Spadaccini, and R. Goodridge, "Direct ink writing of boron carbide monoliths," *J. Eur. Ceram. Soc.*, vol. 41, pp. 76–92, 2021.

[17] B. Nan, X. Yin, L. Zhang, and L. Cheng, "Three-dimensional printing of ti3sic2-based ceramics," *J. Am. Ceram. Soc.*, vol. 94, pp. 969–972, 2011.

[18] S. Mrityunjay, H. M. C, and G. J. E, "Additive manufacturing of light weight ceramic matrix composites for gas turbine engine application," *Ceram. Eng. Sci. Proc*, vol. 36, pp. 145–150, 2015.

[19] X. Du, X. Ren, Y. Chen, C. Ma, M. Radovic, and Z. Pei, "Model guided mixing of ceramic powders with graded particle sizes in binder jetting additive manufacturing," *American Society of Mechanical Engineers Digital Collection*, 2018.

[20] A. Zocca, P. Lima, and J. Gunster, "Lsd-based 3d printing of alumina ceramics," *J. Ceran. Sci. Technol.*, vol. 8, pp. 141–148, 2017.

[21] X. Du, M. Singh, and D. Singh, "Binder jetting addtive manufacturing of silicon carbide ceramics: development of bimodal powder feedstock by modelling and experimental methods," *Ceram. Int.*, vol. 46, pp. 19701–19707, 2020.

[22] J. A. Gonzalez, J. Mireles, Y. Lin, and R. Wicker, "Characterization of ceramic components fabricated using binder jetting additive manufacturing technology," *Ceram. Int.*, vol. 42, pp. 10559–10564, 2016.

[23] D. Solis, A. Silva, N. Volpato, and L. Berti, "Reaction bonding of aluminum oxide processed by binder jetting," *J. Manuf. Process.*, vol. 41, pp. 267–272, 2019.

[24] F. H. Gern and R. Kochendörfer, "Liquid silicon infiltration: description of infiltration dynamics and silicon carbide formation," *Composites Part A: Applied Science and Manufacturing*, vol. 28, pp. 355–364, 1 1997.

[25] Q. Li, Y. Yin, L. Kong, and L. Qiao, "Enhancing heat transfer in the heat exchange medium of energy piles," *Journal of Building Engineering*, vol. 40, p. 102375, 8 2021.

[26] D. Lavric, H. Weyten, J. De Ruyck, P. Valentin, and V. Lavric, "Delocalized organic pollutant destruction through a self-sustaining supercritical water oxidation process," *Energy Conversion and Management*, vol. 46, pp. 1345–1364, 06 2005.

[27] U. D. of Energy, "sco_2 power cycles," *U.S. Department of Energy*.

[28] K. Sridharan and T. R. Allen, "Corrosion in molten salts," *Molten Salts Chemistry*, pp. 241–267, 1 2013.

[29] M. Belmonte, "Advanced ceramic materials for high temperature applications," *Adv. Eng. Mater.*, vol. 8, pp. 693–703, 2006.

[30] L. del Mazo-Barbara and M. P. Ginebra, "Rheological characterisation of ceramic inks for 3d direct ink writing: A review," *Journal of the European Ceramic Society*, vol. 41, pp. 18–33, 12 2021.

[31] A. Knop, V. Böhmer, and L. A. Pilato, "Phenol–formaldehyde polymers," *Comprehensive Polymer Science and Supplements*, pp. 611–647, 1 1989.

[32] C. R. Corporation, "Properties and uses of phenolic resins," *Capital Resin Corporation*, 2020.

[33] T. S. P.-R. Rodriguez, L. Cesari, C. Castel, E. Favre, V. Fierro, and A. Celzard, "Review on the preparation of carbon membranes derived from phenolic resisns for gas separation: from petrochemical precursors to bioresources," *Carbon*, vol. 183, pp. 12–33, 2021.

[34] W. Yang, J. Liang, X. Wang, H. Lian, and H. Dai, "Formaldehyde-free self-polymerization of lignin-derived monomers for synthesis of renewable phenolic resin," *International Journal of Biological Macromolecules*, vol. 166, pp. 1312–1319, 2021.

[35] Q. Wang, Y. Wang, J. Ding, C. Wang, X. Zhou, W. Gao, H. Huang, F. Shao, and Z. Liu, "A biorthogonal system reveals antitumor immune function of phyroptosis," *Nature*, vol. 579, pp. 421–426, 2020.

[36] C. R. Thompson, C. Moore, F. V. Saal, and S. Swan, "Plastics, the environmental and human health: current consensus and future trends," *Philos. Trans. R. Soc. B.*, vol. 364, pp. 2153–2166, 2009.

[37] M. Xu, Y. R. Girish, K. P. Rakesh, P. Wu, H. M. Manukumar, S. M. Byrappa, Udayabhanu, and K. Byrappa, "Recent advances and challenges in silicon carbide (sic) ceramic nanoarchitectures and their applications," *Materials Today Communications*, vol. 28, p. 102533, 2021.

[38] J. Lewis, "Colloidal processing of ceramics," *J. Am. Ceram. Soc.*, vol. 83, pp. 2341–2359, 2000.

[39] P. Greil, "Advanced engineering ceramics," *Adv. Eng. Mater.*, vol. 4, pp. 247–254, 2002.

[40] H. Abe, Y. Miyamoto, M. Umetsu, T. Uchikoshi, T. Okubo, M. Naito, Y. Hotta, T. Kasuga, A. Suda, H. Mori, R. Mezaki, T. Morimoto, A. Azushima, K. Kondou, K. Uematsu, T. Takada, K. Nogi, H. Fujii, J. Akedo, Y. Kinemuchi, Y. Sakka, Y. Yamaguchi, Y. Masuda, and S. Inagaki, "Control of nanostructure of materials," *Nanoparticle Technology Handbook*, pp. 177–265, 1 2008.

[41] R. A. Kepekçi, B. Y. İlçe, and S. D. Kanmazalp, "Plant-derived biomaterials for wound healing," *Studies in Natural Products Chemistry*, vol. 70, pp. 227–264, 1 2021.

[42] C. Gutiérrez and R. Moreno, "Interparticle potentials in nonaqueous silicon nitride suspension," *J. Am. Ceram. Sci.*, vol. 86, pp. 59–64, 2003.

[43] P. Tartaj, M. Reece, and J. Moya, "Electrokinetic behaviour and stability of silicon carbine nanoparticulate dispersions," *J. Am. Ceram. Sci.*, vol. 81, pp. 389–403, 1998.

[44] W. Li, P. Chen, M. Gu, and Y. Jin, "Effect of tmah on rheological behavior of sic aqueous suspension," *Journal of the European Ceramic Society*, vol. 24, pp. 3679–3684, 11 2004.

[45] M. Toofan and J. Toofan, "A brief review of the cleaning process for electronic device fabrication," *Developments in Surface Contamination and Cleaning*, pp. 185–212, 1 2015.

[46] E. Feilden, E. G. T. Blanca, F. Giuliani, E. Saiz, and L. Vandeperre, "Robocasting of structural ceramic parts with hydrogel inks," *Journal of the European Ceramic Society*, vol. 36, pp. 2525–2533, 8 2016.

[47] C. Ferraro, E. Garcia-Tunon, S. Barg, M. Miranda, N. Ni, R. Bell, and E. Saiz, "Sic porous structures obtained with innovative shaping technologies," *Journal of the European Ceramic Society*, vol. 38, pp. 823–835, 3 2018.

[48] R. Ergun, J. Guo, and B. Huebner-Keese, "Cellulose," *Encyclopedia of Food and Health*, pp. 694–702, 1 2016.

[49] Q. Fu, E. Saiz, and A. Tomsia, "Direct ink writing of highly porous and strong glass scaffolds for load bearing bone defects repair and regeneration," *Acta Biomater.*, vol. 7, pp. 3547–3554, 2011.

[50] X. Liu, M. Rahaman, G. Hilmas, and B. Bal, "Mechanical properties of bioactive glass (13-93) caffolds fabricated by robotic deposition for structural bone repair," *Acta Biomater.*, vol. 9, pp. 7025–7034, 2013.

[51] B. Nan, F. Galindo-Rosales, and J. Ferreira, "3d printing vertically: direct ink writing free pillar arrays," *Mater. Today*, vol. 35, pp. 16–24, 5 2020.

[52] A. M'Barki, L. Bocquet, and A. Stevenson, "Linking rheology and printability for dense and strong ceramics by direct ink writing," *Scientific Reports*, vol. 7, p. 6017, 2017.

[53] T. E. Gould, M. Jesunathadas, S. Nazarenko, and S. G. Piland, "Mouth protection in sports," *Materials in Sports Equipment*, pp. 199–231, 1 2019.

[54] R. A. Shirwaiker, M. F. Purser, and R. A. Wysk, "Scaffolding hydrogels for rapid prototyping based tissue engineering," *Rapid Prototyping of Biomaterials: Principles and Applications*, pp. 176–200, 1 2014.

[55] V. Lenaerts, C. Triqueneaux, M. Quartern, F. Rieg-Falson, and P. Couvreur, "Temperature-dependent rheological behavior of pluronic f-127 aqueous solutions," *International Journal of Pharmaceutics*, vol. 39, pp. 121–127, 9 1987.

[56] N. C. for Biotechnology Information, "Pluronic f-127," *PubCHem Compound Summary for CID 10154203*.

[57] M. Vadnere, G. Amidon, S. Lidenbaum, and J. Haslam, "Thermodynamic studies on the gel-sol transition of some pluronic polyols," *Int. J. Pharm.*, pp. 207–218, 1984.

[58] B. Pradines, M. Djabourov, C. Vauthier, P. M. Loiseau, G. Ponchel, and K. Bouchemal, "Gelation and micellization behaviors of pluronic® f127 hydrogel containing poly(isobutylcyanoacrylate) nanoparticles specifically designed for mucosal application," *Colloids and Surfaces B: Biointerfaces*, vol. 135, pp. 669–676, 11 2015.

[59] W. Wang, R. Narain, and H. Zeng, "Hydrogels," *Polymer Science and Nanotechnology: Fundamentals and Applications*, pp. 203–244, 1 2020.

[60] N. A. Peppas and A. S. Hoffman, "Hydrogels," *Biomaterials Science: An Introduction to Materials in Medicine*, pp. 153–166, 1 2020.

[61] M. Jalaal, G. Cottrell, N. Balmforth, and B. Stoeber, "On the rheology of pluronic f-127 aqueous solutions," *J. Rheol.*, p. 139, 2017.

[62] F. Álvarez, A. Cifuentes, I. Serrano, L. Franco, G. Fargas, F. Fenollosa, R. Uceda, L. Llanes, C. Tardivat, J. Llorca, and J. J. Roa, "Optimization of the sintering thermal treatment and the ceramic ink used in direct ink writing of α-al2o3: Characterization and catalytic application," *Journal of the European Ceramic Society*, vol. 42, pp. 2921–2930, 6 2022.

[63] J. Franco, P. Hunger, M. E. Launey, A. P. Tomsia, and E. Saiz, "Direct write assembly of calcium phosphate scaffolds using a water-based hydrogel," *Acta Biomaterialia*, vol. 6, pp. 218–228, 1 2010.

[64] H. Almashhadani, *Corrosion and Corrosion Protection Studies of Carbon Steel alloy in Seawater using; Zirconia, Silicon Carbide and Alumina Nanoparticles*. PhD thesis, 10 2014.

[65] AZoM.com, "Silicon carbide (sic) properties and applications," *www.azom.com*, 2001.

[66] K. Watari and S. Shinde, "High thermal conductivity materials," *MRS Bull.*, vol. 26, pp. 440–444, 2001.

[67] Z. Li and R. Brandt, "Thermal expansion and thermal expansion anisotropy of sic polytypes," *J. Am. Ceram. Soc.*, vol. 70, pp. 445–448, 1987.

[68] A. S. Mukasyan, "Silicon carbide," *Concise Encyclopedia of Self-Propagating High-Temperature Synthesis*, pp. 336–338, 1 2017.

[69] S. Logothetidis, H. Polatoglou, J. Petalas, D. Fuchs, and R. Johnson, "Investigation of the electronic transitions of cubic sic," *Wide-Band-Gap Semiconductors*, pp. 389–393, 1 1993.

[70] G. Pensl and W. Choyke, "Electrical and optical characterization of sic," *Physica B Codens. Matter.*, vol. 185, pp. 264–283, 1993.

[71] R. Stein, P. Lanig, and S. Leinbenzeder, "Influence of surface energy on the growth of 6h-and 4h-sic polytypes by sublimation," *Mater. Sci. Eng. B Solid State Mater. Adv. Technol*, vol. 11, pp. 69–71, 1992.

[72] C. Coletti, M. Jaroszeski, A. Pallaoro, A. Hoff, S. Iannotta, and S. Saddow, "Biocompatibility and wettability of crystaline sic and si surfaces," *29th Annual International Conference of the IEEE Enginering in Medicine and Biology Society*, pp. 5849–5852, 2007.

[73] M. Dudley, B. Raghothamachar, H. Wang, F. Wu, S. Byrappa, G. Chung, E. Sanchez, S. Mueller, D. Hansen, and M. Loboda, "Synchrotron x-ray topography studies of the evolution of the defect microstructure in physical capor transport growth 4h-sic single crystals," *ECS Trans*, vol. 58, pp. 315–324, 2013.

[74] S. Byrappa, "Defect studies in 4h-silicon carbide pvt growth bulk crystals, cvd grown epilayers and devices," *Stony Brook University*, 2013.

[75] G. Harris, "Properties of silicon carbide," *London: INSPEC, Institution of Electrical Engineering*, 1995.

[76] A. Zocca, P. Colombo, C. Gomes, and J. Gunster, "Additive manufacturing of ceramics: issues, potentialities and opportunitues," *J. Am. Ceram. Soc.*, vol. 98, pp. 1983–2001, 2015.

[77] Z. Chen, Z. Li, J. Li, C. Liu, C. Lao, Y. Fu, and et al., "3d printing of ceramics: a review," *J. Eur. Ceram. Soc*, vol. 39, pp. 661–687, 2019.

[78] D. Kopeliovich, "Advances in the manufacture of ceramic matrix composites using infiltration techniques," *Advances in Ceramic Matrix Composites*, pp. 79–108, 1 2014.

[79] N. Radhika and M. Sathish, "A review on si-based ceramic matrix composites and their infiltration based techniques," *Silicon*, vol. 14, pp. 10141–10171, 2022.

[80] G. Shim, S.-H. Kim, I.-S. Han, H.-J. Bang, Y.-H. Seong, S. Lee, W. Kim, and K. Shin, "Influence of pyrolysis and melt infiltration temperatures on the mechanical properties of sicf/sic composites," *Ceram. Int.*, vol. 48, pp. 1532–1541, 2022.

[81] J. Kriegesmann, "Processing of silicon carbide-based ceramics," *Comprehensive Hard Materials*, vol. 2, pp. 89–175, 1 2014.

[82] R. Naslain, "Ceramic matrix composites: Matrices and processing," *Encyclopedia of Materials: Science and Technology*, pp. 1060–1066, 1 2001.

[83] C. M. Carney, "5.10 ultra-high temperature ceramic-based composites," *Comprehensive Composite Materials II*, pp. 281–292, 1 2018.

[84] J. Cesarano, "A review on robocasting technology," *MRS Online Proceeding Library (OPL)*, vol. 542, 1998.

[85] J. Lewis, "Direct ink writing of 3d funtional materials," *Adv. Funct. Mater.*, vol. 16, pp. 2193–2204, 2006.

[86] E. Munch, J. Franco, S. Deville, P. Hunger, E. Saiz, and A. P. Tomsia, "Porous ceramic scaffolds with complex architectures," *JOM*, vol. 60, pp. 54–58, 2008.

[87] S. Shin, S. Suh, and I. Stroud, "Reincarnation of g-code based pat programs into step-nc for turning applications," *Comput. Aided Des.*, vol. 39, pp. 1–16, 2007.

[88] I. S. O. I.S.O., "Automation system and integration - numerical control of machines - program format and definitions of address words - part 1: Data format and positioning, line motion and contouring control system," *International Standards Organization I.S.O. 6983*, 2005.

[89] E. Garcia-Tunon, E. Feilden, H. Zheng, E. D'elia, A. Leong, and E. Saiz, "Graphene oxide: An al-in-one processing additive for 3d printing," *American Chemical Society*, vol. 9, pp. 32977–32989, 10 2017.

[90] N. C. for Biotechnology Information, "Tetramethylammonium hydroxide," *PubChem Compound Summary for CID 60966, https://pubchem.ncbi.nlm.nih.gov/compound/Tetramethylammonium-hydroxide*, 2023.

[91] O. Tabata, R. Asahi, H. Funabashi, K. Shimaoka, and S. Sugiyama, "Anisotropic etching of silicon in tmah solutions," *Sensors and Actuators A: Physical*, vol. 34, pp. 51–57, 1992.

[92] K. Sato and M. Shikida, "Wet etching," *Comprehensive Microsystems*, vol. 1, pp. 183–215, 1 2008.

[93] A. Oliveira, P. Sepulveda, and V. Pandolfelli, "Deflocculation of al2o3-sic suspensions," *Am. Ceram. Soc. Bull.*, vol. 80, pp. 47–53, 2001.

[94] S. Pattnaik and K. Swain, "Mesoporous nanomaterials as carriers in drug delivery," *Applications of Nanocomposite Materials in Drug Delivery*, pp. 589–604, 1 2018.

[95] Q. Huang, M. Gu, K. Sun, and Y. Jin, "Effect of pretreatment on the properties of silicon carbide aqueous suspensions," *Ceram. Int.*, vol. 28, pp. 747–754, 2002.

[96] Sigma-Aldrich, "Tmah datasheet,"

[97] I. Widyatmoko, "14 - sustainability of bituminous materials," in *Sustainability of Construction Materials (Second Edition)* (J. M. Khatib, ed.), Woodhead Publishing Series in Civil and Structural Engineering, pp. 343–370, Woodhead Publishing, second edition ed., 2016.

[98] R. S. Teixeira, L. Bufalino, G. H. D. Tonoli, S. F. D. Santos, and H. S. Junior, "Coir fiber as reinforcement in cement-based materials," *Advances in Bio-Based Fiber: Moving Towards a Green Society*, pp. 707–739, 1 2022.

[99] G. Papanicolau and S. Zaoutsos, "Viscelastic constitutive modeling of creep and stress relaxation in polymers and polymer matrix composites,"

[100] W. Herschel and R. Bulkley, "Konsistenzmessungen vom gummi-benzollosungen kolloid zeitschrift," pp. 291–300, 1926.

[101] A. P. Desphane, "Rheology of complex fluids,"

[102] D. A. Zaidel, N. Chin, and Y. Yusof, "A review on rheological propeties and measurements of dough and gluten," *J.Appl. Sci.*, vol. 10, pp. 2478–2490, 2010.

[103] A. Schwab, R. Levato, M. Este, S. Piluso, D. Eglin, and J. Malda, "Printability and shape fidelity of bioinks in 3d bioprinting," *Chem. Rev.*, vol. 120, pp. 11028–11055, 2020.

[104] J. Kutin and I. Bajsic, "Fluid-dynamic loadin of pipes conveying fluid with a laminar mean-flow velocity profile,"

[105] C. Minas, D. Carnelli, E. Tervoort, and A. Studart, "3d printing of emulsions and foams into hierarchical porous ceramics," *Adv. Mater.*, vol. 28, pp. 9993–9999, 2016.

[106] Q. Liu and W. Zhai, "Hierarchical porous ceramics with distinctive microstructure by emulsion-based direct ink writing," *Am. Chem. Soc.*, 2022.

[107] L. Goyos-Ball, E. García-Tuñón, E. Fernández-García, R. Díaz, A. Fernández, C. Prado, E. Saiz, and R. Torrecillas, "Mechanical and biological evaluation of 3d printed 10cetzp-al2o3 structures," *Journal of the European Ceramic Society*, vol. 37, pp. 3151–3158, 8 2017.

[108] H. Elsayed, A. Chmielarz, M. Potoczek, T. Fey, and P. Colombo, "Direct ink writig of three dimensional ti2alc porous structures," *Addit. Manuf.*, pp. 365–372, 5 2019.

[109] H. Jin, D. Jia, and Y. Zhou, "Direct ink writing of si2n2o porous ceramics strenghtened by directional β-si3n4 grains," *Ceram. Int.*, vol. 46, pp. 15709–15713, 2020.

[110] P. Diloksumpan and et al., "Combining multi-scale 3d printing technologies to engineer hydrogel-ceramic interfaces," *Biofabrication*, vol. 12, 2020.

[111] T. Mezger, "The rheology handbook, 2nd edition," *Vincentz Publishings*, 2006.

[112] J. Smay, C. Joseph, and J. Lewis, "Colloidal inks for directed assembly of 3-d periodic structures," *Langmuir*, vol. 84, pp. 5429–5437, 2002.

[113] I. Krieger and T. Dougherty, "A mechanis of non-newtonian flow in suspensions of rigid spheres," *J. Rheol.*, p. 137, 1959.

[114] T. K. Kim, T. Kim, I. Lee, K. Choi, and K. D. Zoh, "Removal of tetramethylammonium hydroxide (tmah) in semiconductor wastewater using the nano-ozone h2o2 process," *Journal of Hazardous Materials*, vol. 409, p. 123759, 5 2021.

[115] J. Liu, C. Tian, H. Xiao, W. Guo, P. Gao, and J. Liang, "Effect of b4c on co-sintering of sic ceramic membrane," *Ceram. Int.*, pp. 3921–3929, 2019.

[116] J. Huang, K.-S. Wang, and C. Liang, "Oxidative degradation of tetramethylammonium hydroxide (tmah) by uv/persulfate and associated acute toxicity assessment," *J. Environ. Sci. Health A Tox. Hazard Subst. Environ. Eng.*, 2017.

[117] E. Eray, V. M. Candelario, V. Boffa, H. Safafar, D. N. Østedgaard Munck, N. Zahrtmann, H. Kadrispahic, and M. K. Jørgensen, "A roadmap for the development and applications of silicon carbide membranes for liquid filtration: Recent advancements, challenges, and perspectives," *Chemical Engineering Journal*, vol. 414, p. 128826, 6 2021.

[118] Puredyne, "Puredyne kit b - operation and maintenance manual," *www.puredyne.com/en/resources*, 2021.

[119] P. R. by Joseph Prusa, "Original prusa 3d printer i3 mk3s," *www.prusa3d.com.*

[120] P. R. by Joseph Prusa, "Superpinda sensor testing," *https://help.prusa3d.com/article*, 2021.

[121] Marlin, "G-code," *Marlinfw.org.*

[122] Adobe, "Stl files explained," *www.adobe.com.*

[123] P. R. by Joseph Prusa, "Prusaslicer," *www.github.com/prusa3d.*

[124] M. de Assumpcão Pereira-da Silva and F. A. Ferri, "Scanning electron microscopy," *Nanocharacterization Techniques*, pp. 1–35, 1 2017.

[125] Y. Yan, "Tribology and tribocorrosion testing and analysis of metallic biomaterials," *Metals for Biomedical Devices*, pp. 213–234, 1 2019.

[126] "Deposition technologies: An overview," *Handbook of Deposition Technologies for Films and Coatings: Science, Applications and Technology*, pp. 1–31, 1 2010.

[127] A. Behera, P. Mallick, and S. Mohapatra, "Nanocoatings for anticorrosion: An introduction," *Corrosion Protection at the Nanoscale*, pp. 227–243, 1 2020.